



Norwegian University of  
Science and Technology

# Processing and Characterisation of Diatoms for Light Harvesting Materials in Solar Cells

**Petter Ottesen**

Materials Science and Engineering

Submission date: June 2011

Supervisor: Gabriella Tranell, IMTE

Co-supervisor: Ingeborg Kaus, SINTEF  
Mari Juel, SINTEF



---

## Problem Description

In the last decade there have been parallel research on different topics which might be interconnected. The work of reducing the losses in solar cells is a never-ending process, and at the same time diatom frustules have been investigated for their optical properties. In addition diatom frustules have been tested with regards of using them as templates for reproducing the structure. In 2008 a scientific report were published where diatom frustules had been used as electrode material in dye-sensitised solar cells.

At the Norwegian University of Science and Technology (NUST) solar cell research has been a focus area since the start of the solar cell industry in Norway in the mid nineties. As collaboration between NUST and the research fundation SINTEF, SOLBIOPTA, a project with with main goal of incorporating diatom frustules into solar cells, were started last year. The problem given in this thesis was drafted together by the student and the supervisor.

The task were divided into 4 parts:

- Part I: Characterisation of Diatom Frustules and Their Pore Structure.
- Part II: Manufacturing and Characterisation of Gold for Use as Templates in Solar Cell Industry.
- Part III: Deposition and Characterisation of Amorphous Silicon and Silicon Nitride on diatom frustules.
- Part IV: Manufacturing and Characterisation of Structures similar to Solar Cells.

The tasks were conducted with several different deposition and characterisation methods used in the solar cell industry and regular characterisation methods in material science like light microscopy, SEM and FIB. This thesis is supposed to give an overview over the challenges which will might be met when attempting to incorporate diatom frustules into solar cells.

---

## Declaration

I hereby confirm that this work has been done in accordance with the laws of the Master of Science in Architecture and Engineering exam at the Norwegian University of Science and Technology.

30th June 2011

---

Petter Ottesen

---

## Preface

This master thesis came to be as an initiative from SOLBIOPTA, and the problems to be addressed were discussed with Associate Professor Gabriella Tranell (NTNU), Ph.D. Ingeborg Kaus (SINTEF), Ph.D. Mari Juel and the author. SOLBIOPTA is a project lasting for 4 years with a main target to incorporate diatoms or structures derived from diatoms into photovoltaic solar cells. The work itself is of scientific value to SOLBIOPTA, as processes to transfer the diatoms structure over to metallic and ceramic surfaces might be essential for future use of diatoms for templating in solar cells. The diatoms were produced by researchers at the Department of Biotechnology at NTNU, while the experimental work has been done in collaboration with SINTEF Materials and Chemistry in Trondheim. The majority of the experimental work has been carried out by the author alone at the NTNU Nanolab, during 20 weeks in the spring of 2011.

At the Department of Materials Science and Engineering the author has been surrounded by and benefitted from people with knowledge about solar cells, electron microscopy, and nanoscale properties of metals and oxides, some of them employees at SINTEF. First of all, I would like to acknowledge Associate Professor Gabriella Tranell for inspiring confidence and being supportive through the entire thesis. Scientists Mari Juel and Ingeborg Kaus at SINTEF must be thanked for being helpful with feedback and sharing their theoretical and experimental knowledge. Further I would like to acknowledge my two fellow master students from the SOLBIOPTA project, Anne K. Noren and Lotte Skolem for giving me input about their research. Research scientist Per Erik Vullum has been very helpful with the use of his skills, time and knowledge during characterisation with FIB. Other people who might be mentioned are Matilde S. Chauton and Lasse Olsen, they prepared the diatoms for my project. Øystein Dahl must be acknowledged for the advice and insight he gave about PECVD deposition. Torill Krogstad gave assistance during the HF etching done with the gold template.

---

## Abstract

By applying a texture to the front surface of solar cells, less light may be reflected and the incoming light may be given a longer path length inside the solar cell causing a better light absorbance for the solar cell. The textured layer is today made by etching with an acidic etch with a large part hydrogen fluoride. In the future a more environmental approach for creating textured solar cells may be favoured. There are many ways of creating textured surfaces, one of them are by imprinting the surface by a template, and remove the template when the process is completed.

In this project the diatom species *Coscinodiscus walesii* and an undefined *Coscinodiscus species* were cleaned and processed for investigation. The work done can be divided into four tasks. The first was characterisation and investigation of the pore structure. The second were manufacturing and characterisation of gold for use as templates. The third were deposition and characterisation of thin films of silicon and silicon nitride on diatom frustules. The last part were to make structures are very similar to solar cells with diatom frustules incorporated into them.

The diatom frustules were characterised by SEM and the pore structure were cut through with FIB to characterise the structure. There were structural differences between the two species. The *Coscinodiscus walesii* was grown in a cultivation chamber, and lacked the circular inner pore structure which the undefined *Coscinodiscus species* had. This was the only real difference between the two species. On the cultivated species were deposited a gold film, which a small rectangle were lifted off by a tungsten needle in FIB. The small rectangle were characterised with the SEM-column in a dual beam FIB. Pore structures down to 40 nm were replicated by the gold film lifted off the frustule. By depositing a relatively thick film of gold on a glass substrate covered with diatom frustules and dissolving the glass substrate and diatom frustules with hydrogen fluoride, a template were made with a replication of the diatom frustule pore structure.

Silicon and silicon nitride were deposited on diatom frustules and characterised with FIB to investigate how those materials followed the frustule topography. A good conformity of films made of those materials was confirmed, and 4 different samples which were similar to solar cells were manufactured and characterised by light microscopy, SEM and FIB. Two samples were made to be similar to crystalline silicon solar cells. One had dried frustules on top of a silicon surface and the entire surface of the sample were coated with silicon nitride, a blue colour were observed in the entire surface and the silicon nitride had also been deposited on the diatom frustules. For the other sample similar to crystalline silicon solar cells another layer were deposited between the frustule and the silicon substrate. The double silicon layer made the sample surface yellow, the diatom frustules did not get darker due to a layer above and a layer beneath them. Only in some places where the frustules had loosened from the sample the sample were blue as the silicon nitride layer were the same as a single layer of silicon nitride. For the last two samples, thin film solar cell structures based on amorphous silicon deposited with

---

PECVD were made. A sample there a aluminum coating were deposited on a glass substrate and diatom frustules were dried on top of the aluminum coating, afterwards a 5  $\mu\text{m}$  thick film of amorphous silicon were deposited. SEM images showed that the film were distributed even across a diatom frustule and a light microscopy investigation showed that light were spread when it hit the diatom frustules, hence creating a longer mean path through the solar cell.

---

## List of Abbreviations and Acronyms

<b>Shortened form</b>	<b>Full text</b>
ALD	Atomic Layer Deposition
BaSIC	Bioclastic and Shape Preserving Inorganic Conversions
CVD	Chemical Vapour Deposition
EBE	Electronic Beam Evaporator
EDTA	Ethylene Diamine Tetraacetic
FEG	Field Emission Gun
FIB	Focused Ion Beam
HDPCVD	High-density Plasma Chemical Vapour Deposition
HIT	Heterojunction with Intrinsic Thin Layer
ISE	Ion-induced Secondary Electron
ITO	Indium Tin Oxide
LMIS	Liquid Metal Ion Source
PECVD	Plasma-Enhanced Chemical Vapour Deposition
PV	Photovoltaic
PVD	Physical Vapour Deposition
PVSC	Photovoltaic Solar Cell
SDS	Sodium Dedecyl Sulfate
SE	Secondary Electron
SEM	Scanning Electron Microscope
SIMS	Secondary Ion Mass Spectroscopy

# Contents

<b>1</b>	<b>Introduction</b>	<b>1</b>
<b>2</b>	<b>Theoretical Background</b>	<b>3</b>
2.1	Structure of Diatom Frustules . . . . .	3
2.2	Template Technology . . . . .	5
2.2.1	Diatoms in Template Technology . . . . .	6
2.2.2	Gold as Material for Nano-Prototypes . . . . .	10
2.2.3	Thin Films and Their Usage . . . . .	16
2.3	Templating . . . . .	17
2.3.1	Deposition with Electron-Beam Evaporator . . . . .	17
2.3.2	Plasma-Enhanced Chemical Vapour Deposition . . . . .	19
2.4	Characterisation . . . . .	21
2.4.1	Characterisation by Scanning Electron Microscopy . . . . .	21
2.4.2	Focused Ion Beam (FIB) . . . . .	23
<b>3</b>	<b>Experimental Details</b>	<b>27</b>
3.1	Harvesting and Cleaning of Diatoms . . . . .	27
3.1.1	Harvesting of Cultivated Plankton . . . . .	27
3.1.2	Harvesting Net Plankton . . . . .	30
3.1.3	Cleaning of Diatoms . . . . .	30
3.2	Part I: Characterisation of Diatom Frustules and Their Pore Structure	31
3.2.1	SEM-characterisation of Diatom Frustules . . . . .	31
3.2.2	FIB-characterisation of Diatom Frustules . . . . .	31
3.3	Part II: Manufacturing and Characterisation of Gold for Use as Tem- plates in Solar Cell Industry . . . . .	32
3.3.1	Deposited Gold Film Characterised by FIB and SEM . . . . .	32
3.3.2	Manufacturing and Characterisation of Gold Film Templates	35
3.4	Part III: Deposition and Characterisation of Amorphous Silicon and Silicon Nitride on diatom frustules . . . . .	37
3.4.1	Characterisation of Amorphous Silicon Film Deposited on Frustules by SEM and FIB . . . . .	37
3.4.2	SEM and FIB Characterisation of Silicon Nitride Film De- posited on Frustules . . . . .	39
3.4.3	Sample Preparation . . . . .	39

3.5	Part IV: Manufacturing and Characterisation of Structures similar to Solar Cells . . . . .	41
3.5.1	Sample Preparation . . . . .	41
3.5.2	Analysis of Solar Cell Structures . . . . .	45
<b>4</b>	<b>Results</b>	<b>47</b>
4.1	Part I: Characterisation of Diatom Frustules and Their Pore Structure	47
4.1.1	SEM-characterisation of <i>Coscinodiscus walesii</i> . . . . .	47
4.1.2	SEM-Characterisation of the <i>Coscinodiscus sp.</i> . . . . .	48
4.2	Part II: Manufacturing and Characterisation of Gold for Use as Templates in Solar Cell Industry . . . . .	52
4.2.1	Deposited Gold Film Characterised by FIB and SEM . . . . .	52
4.2.2	Manufacturing and Characterisation of Gold Film Templates	56
4.3	Part III: Deposition and Characterisation of Amorphous Silicon and Silicon Nitride on diatom frustules . . . . .	61
4.3.1	Characterisation of Amorphous Silicon Film Deposited on Frustules by SEM and FIB . . . . .	61
4.3.2	SEM and FIB Characterisation of Silicon Nitride Film Deposited on Frustules . . . . .	61
4.4	Part IV: Manufacturing and Characterisation of Structures similar to Solar Cells . . . . .	63
4.4.1	Characterisation by Light Microscope . . . . .	63
4.4.2	Characterisation by FIB and SEM . . . . .	70
<b>5</b>	<b>Discussion</b>	<b>75</b>
5.1	Part I: Characterisation of Diatom Frustules and Their Pore Structure	75
5.2	Part II: Manufacturing and Characterisation of Gold for Use as Templates in Solar Cell Industry . . . . .	77
5.2.1	Deposited Gold Film Characterised by FIB and SEM . . . . .	77
5.2.2	Characterisation of Gold Film Templates . . . . .	78
5.3	Part III: Deposition and Characterisation of Amorphous Silicon and Silicon Nitride on diatom frustules . . . . .	80
5.3.1	Characterisation of Amorphous Silicon Film Deposited on Frustules by SEM and FIB . . . . .	80
5.3.2	SEM and FIB Characterisation of Silicon Nitride Film Deposited on Frustules . . . . .	81
5.4	Part IV: Manufacturing and Characterisation of Structures similar to Solar Cells . . . . .	81
5.4.1	Crystalline Silicon Solar Cell Samples . . . . .	82
5.4.2	Thin Film Cell Samples . . . . .	82
<b>6</b>	<b>Conclusion</b>	<b>85</b>
6.1	Part I: Characterisation of Diatom Frustules and Their Pore Structure	85
6.2	Part II: Manufacturing and Characterisation of Gold for Use as Templates in Solar Cell Industry . . . . .	86

6.3	Part III: Deposition and Characterisation of Amorphous Silicon and Silicon Nitride on diatom frustules . . . . .	86
6.4	Part IV: Manufacturing and Characterisation of Structures similar to Solar Cells . . . . .	86
<b>7</b>	<b>Future Work</b>	<b>87</b>
	<b>Bibliography</b>	<b>89</b>



---

# 1. Introduction

Since the start of the solar cell industry in the late fifties and early sixties, there has been one relation of particular interest, namely the ratio between the effect and cost of the photovoltaic cell. This ratio will decide whether or not the solar cells produced are able to compete with electrical power produced from other sources (i.e. coal, gas, fission, hydro, wind). The development has gone through improvement of existing technology and evolution of new technology, and by that mentality the ratio of effect divided by cost has increased over time. The industry will need new ways to produce the solar cell material and find new ways to improve the efficiency of the cells.

There are three methods of improving the solar cell efficiency of an already produced wafer. First there is the possibility of using tandem cells. They are multilayered cells where each layer has a unique band gap filtering out all photons with that and higher energy, while the rest of the photons pass through the layer, and each subsequent layer absorb photons between its band gap to the band gap for the cell in front of it. The last method of enhancing solar cell efficiency is called “to increase light harvesting”. The other two are up- and down-conversion of solar light. Up-conversion is two low energy photons are combined by an intermediate energy band into a high energy photon. These methods reduce the loss mechanisms of solar cells. When looking at the loss mechanisms of a solar cell, it is easy to understand why improved light harvesting has a great potential if utilised properly.

In nature there are known structures that possess promising features which are similar to already known light harvesting structures. The porous silica shell, frustule, of a group of phytoplankton called diatoms have shown the same effects as photonic crystals. [Fuhrmann et al., 2004] While there has been research to an extent on these small organisms, there have been no attempts so far to incorporate them into up- or down-converting layers for solar cells. Even though the porous silica of diatoms have large potential it might be necessary to convert the porous structure into other materials to be able to use it for light harvesting in solar cells.

When manufacturing solar cells it is common to etch the cells with an acidic mixture to gain a structure with good antireflective properties, this process is harmful to the environment as hydrogen fluoride (HF) is very corrosive and may cause damage and harm to plants and animals. [MacDonald et al., 2003] It is also very costly to cleanse the water of HF before it is allowed back in the

nature. The porous structure of diatom frustules have a low reflectivity of incident light, if properly investigated it may cause the etching process in solar cells to become obsolete. If frustules could be converted into another material with similar properties, it would have a great potential for replacing the etching process as the leading process to create antireflective structures.

The possibility to transfer the structure of the frustule into other materials than silica is investigated by several research groups. Reduction of frustules with gaseous magnesium and dissolving of the magnesia formed in the process by HF was carried out by Bao et al. [2007]. Templating of diatoms with gold has been conducted by Losic et al. [2005, 2006a] and Yu et al. [2010], but their intent has been to show that it is possible to deposit gold onto diatom frustules.

In the author's specialisation project replicas of the surface of a diatom were made. [Ottesen, 2010] These were the first attempts to replicate diatom structures for using them in photovoltaic devices. This master thesis will attempt to continue the work of the specialisation project, by making a template out of a gold film shaped by diatom frustules. This were done with the the following well explored deposition methods like plasma-enhanced chemical vapour deposition to test whether or not diatoms can be covered and used as texturation for anti-reflection purposes, and characterisation methods like scanning electron microscopy, focused ion beam and light microscopy. In addition, structures similar to solar cells will be manufactured and characterised by the same methods. Diatoms have potential use as the base of templates for texturation or directly into solar cells as texturation. This thesis will investigate both possibilities.

---

## 2. Theoretical Background

For material scientists in general, the relevancy for diatoms has up to today been peripheral. In the last decade the interest has increased, and many articles have been published about diatoms and their possible applications in material science, electronic engineering and medical technology. [Losic et al., 2009]

The diatoms have a shell, frustule, made of silicon dioxide which has a nanocrystalline structure. With nanocrystalline structures there are certain size-dependent effects which may change the properties of the silica, like electrical conductivity, optical properties and more. A brief survey of the structure of the diatom frustule will be given in this section. In addition to the structure, there will be an introduction to templating and why the different materials are used in this project.

### 2.1 Structure of Diatom Frustules

This subsection will give a brief survey of the diatom's structure, and explain why frustules have the functional properties they do. The shell of a diatom consist of two overlapping valves joined together with girdle bands. [Gordon et al., 2008] The frustules have high mechanical strength and are biocompatible with humans and other species. [Kröger and Poulsen, 2008; Stefano et al., 2008]

Gordon et al. [2008] and Hildebrand et al. [2009] state that there is not a proper group symmetry in diatoms, but it is common to divide diatom species into pennate and centric diatoms. Pennate diatoms are elongated, usually with bilateral symmetry. Centric diatoms have a radial symmetry, but are not necessarily circular. They could be said to have an  $n$ -fold symmetry axis. Kröger and Poulsen [2008] divide each of these two groups into two new subgroups. The centric class is divided into radial centrics and polar centrics. The radial centrics have a Petri dish-like shape, more or less like a cylinder. Polar centrics are not circular but still have a rotational symmetry axis, where  $n \geq 3$ .

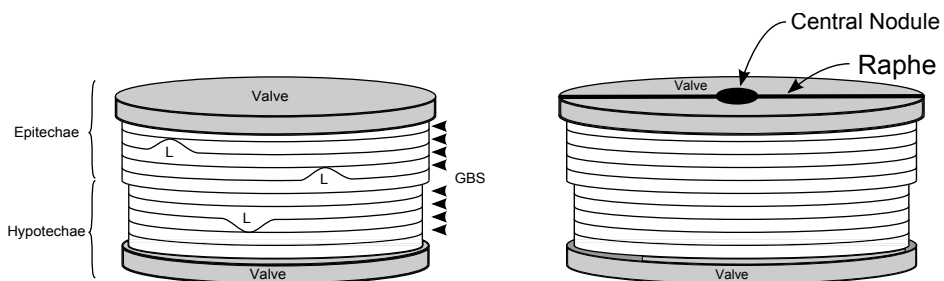
While the frustule gives some diatom species the possibility to move around, it will in *Thalassiosira weissflogii* act as a proton buffer, this is believed to enhance the  $\text{CO}_2$  aquisition. [Drum and Hopkins, 1966; Edgar and Pickett-Heaps, 1983; Milligan and Morel, 2002] For *Coscinodiscus grantii* the girdle band acts as a photonic crystal, and it may aid in light harvesting for the photosynthesis. [Fuhrmann et al., 2004]

The girdle bands are the sides of the diatom and have a high amount of porosity compared to the theca. While the girdle band production process will be inside the cell, the new girdle bands will form right on the inside of the existing girdle bands and connect to the hypotheca. The shape and porosity are different from species to species of diatoms. For a specified shape and size the appropriate species have to be chosen, this can be crucial for certain applications. What species chosen for different applications will then be important, and only a handful of the  $10^5$  species of diatoms have been tested for certain applications, the large number of untested diatom species give large potential for new discoveries in diatom properties and possible applications.

The theca is the name of the two halves the frustule consist of, the epitheca is the larger of the two, and the hypotheca the smaller. Each theca has a valve and these make up the top and bottom of the frustule and side walls, girdle bands. The hypotheca will grow out of the epitheca, and will be much easier than the epitheca to modify by metabolic consumption with other elements than Si.

Valves are the top and bottom parts of the frustules. Although the diatoms become smaller for every generation, the pore size stays the same. This means that the pores will be more dominant on the surface as the diatoms get smaller and smaller. To say that the pore size is the same overall is at best inaccurate, because there are normally three layers of pores in the valves. [Kröger and Poulsen, 2008] Valves also consist of raphae and central nodule, these are a part of the valves in pennate diatoms (for more information see Figure 2.1(b)). [Kröger and Poulsen, 2008]

The girdle band structure is the part of the frustule that connects



(a) Schematic diagram of diatom cell wall structure. A diagram of centric diatom cell wall features. Valves at top and bottom are labeled, and the epitheca and hypotheca are labeled, as are the girdle bands (*GBS*), which are located by arrows head. The bell-shaped structures of girdle bands called the ligula vare labeled *L*.

(b) Diagram of pennate diatom cell wall features. Valves and girdle bands are labeled as in (a). On the upper valve are denoted the central nodule (*CN*) and raphe.

Figure 2.1: These schemes show the most common structure of a diatom, there are a number of species that differ from this representation, and that must be taken to consideration when investigating diatoms.

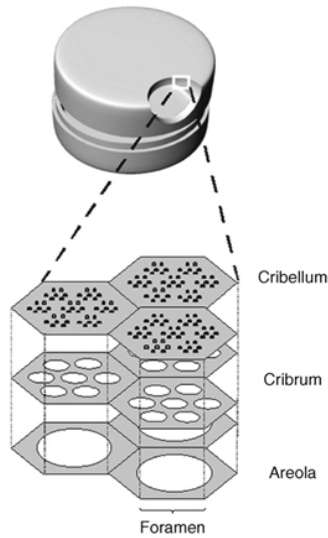


Figure 2.2: Schematic of a centric diatom frustule with cross-sectional three-dimensional (3D) profile of the silica wall based on SEM data. Source: [Gordon et al., 2008].

the two valves together. The girdle bands are thin overlapping strips of silica that encircle the cell and also provide overlap between the epitheca and hypotheca. The structure is different from species to species, not all species have complete circles of girdle bands, instead some have broken bands that become narrower close to the points of break.

Diatoms have large species-specific variations in shape, size, geometry, organization, and density of pore structures represent subtle changes in the material structure to optimise it for a given condition and environment. [Losic et al., 2009] For more information see Pappas [2005] and Losic et al. [2009] The structure of a diatom is essential for what kind of properties it has. Only by selecting a good species and proper morphology for the given application, will the diatom give such good properties that it may be used for commercial products.

## 2.2 Template Technology

To manufacture materials with specific shapes and features, template technology is used. Template technology is the common term for all manufacturing processes which require moulds, dies and masks to shape and make materials with specific shapes and features. In nanotechnology there has been much research

in making effective templates for producing self-assembled metal nanowires.[Brust et al., 2002] It is especially for the miniaturisation of electronic devices such templates are interesting, current technologies for lithographic fabrication are pushed towards their size resolution limits, and that is generating a need for research into alternative fabrication strategies.

If a cheap or recyclable template could be developed for deposition of a functional material, and at the same time could replace an existing technology, i.e. texturing with acids or coating with  $\text{SiN}_x$ , it would have great possibilities to gain ground in the PV industry. There are a large number of diatom species, each with its own unique shape and structure. That combined with their low cost and low nutrient requirements, and the large amount of promising properties build up under the potential of diatoms as a base for manufacturing applicable templates.

This subsection will investigate the potential for diatoms as base when converting their frustules into new structures and materials. There are many possible routes that may be used when some or all features of the frustule are desired. To gain certain properties a specific route have to be chosen, while there for some may be many different routes giving about the same product. This will be discussed further in subsection 2.2.1.

The features of gold and other materials will be described in this subsection, and the reason for using gold as a template for further manufacturing will be made clear. For further testing it will be necessary to make prototypes of other materials, so it must be kept clear that gold is only used as first prototype to prove concept of deposition on diatom frustules. Not all materials are suitable for deposition through vapor, so some materials might be deposited through other methods, i.e. liquid-solid deposition, spin coating, dip coating, plasma enhanced chemical vapour deposition (PECVD).

### **2.2.1 Diatoms in Template Technology**

As diatoms have grown to be a focus in nanotechnology, there have been a large amount of research about them and their properties. Many different kinds of processes have proven to give possibilities to use diatoms as templates for new materials with similar properties. An outline of the different processes used when manufacturing new 3D materials is shown in Figure 2.3. A wide range of those processes require multiple process steps and can be complicated to execute properly.

There have been reported attempts on using diatoms as templates for producing zeolites. Both hydrothermal growth and vapor-phase transport have been tried and reported with success. [Anderson et al., 2000; Wang et al., 2002] Anderson et al. used diatomeous earth to produce a material which grew inside the frustule, and gained the porosity of the frustules and also kept a small particle size and shown features with porosity stretching from 5.5 Å to 80 nm, over 3 orders of magnitude. The process was mostly done by hydrothermalisation in an autoclave, and even the starting material was dominated by macroporosity, zeolite crystal growth introduced a well defined secondary structure that contained both mesopores and micropores.

Wang et al. did not use ‘fresh’ frustules, but used a kind of rock with a high amount of fossilised frustules called diatomite. [Wang et al., 2002] The vapor phase transport process is a process closely related to the hydrothermal growth process. An autoclave is used, but the medium which is put into the autoclave together with the diatomite is a mixture of ethyleneamine, triethylamine and water. This charge was then heated for several days at 550°C. Wang et al. stated in their article that this process is environmentally friendly and economical.

Another material of interest is carbon, as porous carbon has many applications, it would be of great interest to produce carbon in a cheap way by the way of using diatoms. Holmes et al. produced carbon by using diatom frustules as templates by filling the void space inside the frustules with a sucrose solution. The sucrose is then polymerised by sulfuric acid and carbonised in a reducing atmosphere, and the frustule is at last dissolved by sodium hydroxide solution. [Holmes et al., 2006] Holmes et al. also state that diatomaceous earth are environmentally friendly and a cheap material with a combination of being abundant, so the process has potential of being utilised as a profitable product. An issue with this process is that the structure is not of the ordered kind which is grown around latex spheres, but hopefully the low cost of diatoms makes up for the poorer structure ordering. [Holmes et al., 2006] Losic et al. stated that the pores produced from this method are one order of magnitude smaller than the porous carbon utilised in polymer electrolyte membranes used in fuel cells. [Losic et al., 2009]

Zinc silicate and powders based on zinc silicate are materials with shape and size dependent properties, which may be produced by solution coating and annealing. [Cai and Sandhage, 2005] According to Cai and Sandhage there is no three-dimensional microscale self-assembly which is man-made that can compete with diatom frustules. They deposited a thin conformal layer of zinc silicate on the surface of diatom frustules while they preserved the frustule shape. Experimentally Cai and Sandhage exposed the frustules to precursors for zinc oxide which they

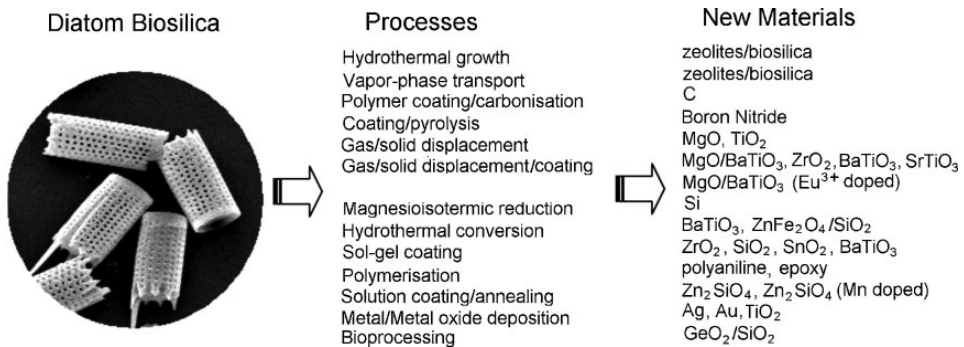


Figure 2.3: Schematic of processes for engineering 3D nanostructured materials using diatom biosilica. Source: [Losic et al., 2009].

warmed up to form zinc oxide, the frustule with coating was then heat treated to let the zinc oxide and silica react and form zinc silicate.

When using the gas-silica displacement, magnesium gas is put into a process chamber together with frustules and heated to 900°C, then the magnesium reacted with the silica, and made a mixture of magnesia, silicon and silica. There were also some Mg<sub>2</sub>Si present as a byproduct of the reduction reaction between magnesium and silicon. The solidified Mg-Si did not adhere strongly to the replica, and when cooled down it was removed with a needle. Not only the micro porosity and shape of the diatom remained, but also the micropores and the nanoscale features. Magnesium gas is only one of many gases which may be used as reducing agents. [Sandhage et al., 2002]

The new structure had a much larger surface area than normal diatom frustules, as it was hollowed out by the dissolution of magnesia. This was tested by seeing how much nitrogen that was able to be adsorbed by the replica, as a gas sensor was made of their replica. [Bao et al., 2007] This product had the shape of the frustule used as template to produce it, but the product will be even more porous than the template, and the main three-dimensional features of the frustule will be contained in the replica. Such a structure will have potential for photoluminescent properties, this was tested by Bao et al., the replicas was first partially oxidised by immersion in water, and this enhanced the photoluminescent properties of the replicas. [Bao et al., 2007] Bao et al. did not provide any measurement of the photoluminescence and it is not possible to say whether or not it is applicable as a luminescent layer in solar cells.

Titania, as a material, has been used as anti-reflective coating in solar cells, and a porous structure was produced by the use of reduction by titanium fluoride. [Unocic et al., 2004] Such porous structure have a lower reflectivity than the same material with a less porous structure. If such a porous material can be produced on larger scale it might lead to more effective solar cells. Unocic et al. made two different experiments to synthesise titania, first they tried a high temperature approach with a high excess of titanium fluoride compared to the amount of silica in the frustule ( $\geq 4.9 : 1$ ). [Unocic et al., 2004] This gave coarse plates of titanium dioxide, so the original diatom shape was not preserved. The other experiment done by Unocic et al. was to try to lower the temperature and have a more even distribution of titanium fluoride and silica. SEM pictures revealed that this approach have similar features as the original frustule. Although an energy-dispersive X-ray (EDS) analysis showed that a majority of the silica was replaced with titanium oxide difluoride (TiOF<sub>2</sub>), but there were also small amounts of the anatase polymorph of titanium dioxide in the frustule. Then the frustule was warmed up to 350 °C and placed in an oxygen-rich atmosphere for some time before a new EDS analysis was done. The new EDS analysis showed high amounts of anatase present, a transmission electron microscope (TEM) image showed that the new particles formed had sizes below 100 nm. [Unocic et al., 2004]

Unocic et al. are not the only scientists who have produced titania by using diatoms as template, Losic et al. produced titanium dioxide by atomic layer deposition (ALD). The frustules were exposed to a volatilised titanium tetrachloride

Table 2.1: The pore size reduction of diatom frustules *Coscinodiscus sp.* and *T. eccentrica* before and after ALD of  $\text{TiO}_2$ . Average  $\pm$  error is obtained from the least of 100 measurement and 3 samples. Source: [Losic et al., 2006b]

	Pore size [nm] <i>Coscinodiscus sp.</i> (external)	Pore size [nm] <i>T. eccentrica</i> (external)	Pore size [nm] <i>T. eccentrica</i> (internal)
Uncoated	192 $\pm$ 25	770 $\pm$ 30	43 $\pm$ 6
Coated, 250 cycles	178 $\pm$ 23	760 $\pm$ 27	32 $\pm$ 4
Coated, 500 cycles	170 $\pm$ 19	749 $\pm$ 23	21 $\pm$ 4
Coated, 1000 cycles	146 $\pm$ 21	725 $\pm$ 26	< 5

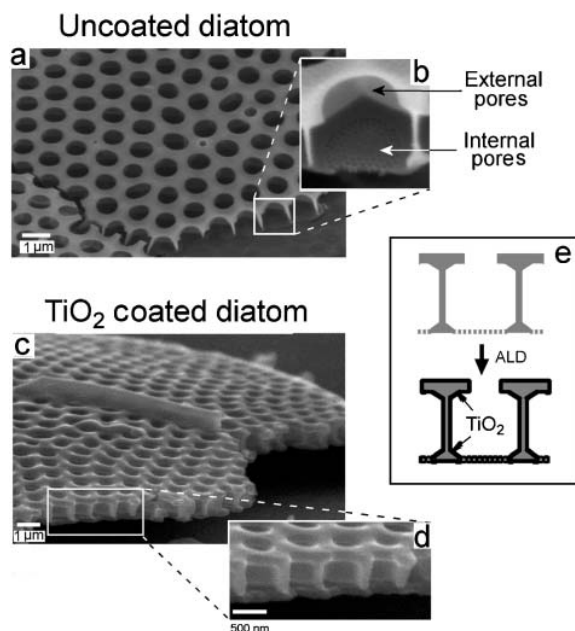


Figure 2.4: (a) and (b) SEM images of uncoated frustules of *T. eccentrica* with profiles of the pore structure. (c) and (d) SEM images of fractured frustule after  $\text{TiO}_2$  coating (500 cycles). (e) Scheme of formation of conformal  $\text{TiO}_2$  inside a pore. Source: [Losic et al., 2006a].

and water, the gas was introduced in pulses to assure an even distribution in the chamber. The EDS analysis of the coated frustules showed a presence of silicon, titanium and oxygen, but Secondary Ion Mass Spectroscopy (SIMS) revealed that the surface had a relative high concentration of titanium, oxygen and chlorine when the surface was coated. For an uncoated diatom the amount was much lower, and

probably only present as impurities in the frustule. Another effect of this is that the pore size changes as more cycles are added to the process. Losic et al. did test with up to 1000 cycles and over 100 measurements on 3 different samples, the results from this experiment is shown in Table 2.1. The SEM images shown in Figure 2.4 visualise clearly that there have been built up a layer during the deposition, and that the layer is conformal. Another quality of the ALD is that more materials than titanium oxide can be deposited, materials like alumina, zirconia, tin dioxide, vanadia, zinc oxide and titanium nitride. [Losic et al., 2006b] These are materials that have potential to give new properties to diatom frustules.

## 2.2.2 Gold as Material for Nano-Prototypes

Gold has been in special interest due to its application in catalysts, sensors and possibly in new generations of optical, electronic and magnetic devices. Fabrication of nanostructured gold has mostly been applied by methods like electron beam lithography, laser ablation, electrochemical deposition, etching, template synthesis and scanning probe microscopy. There have been reports of fabrication of nanostructured gold substrates with nanoscale geometries that include wires, rods, rings and hollow structure by the use of templates.

Even though gold has several promising properties, gold is not applicable in all products. As a material to produce prototypes, gold may be used as it is stable and easy to handle. Gold does not corrode and is only dissolved by very reactive acids (i.e. nitro-hydrochloric acid), gold does also have the ability of being stable with small dimensions, all this makes gold a good material for making nano-prototypes. There have also been reported attempts of coating diatom frustules with gold reported by Losic et al. [2005], Losic et al. [2006a] and Yu et al. [2010]

By evaporating a thin layer ( $<1 \mu\text{m}$ ) of gold onto cleaned diatom and choosing a diatom species with a relative coarse pore structure, namely the *Coscinodiscus sp.* [Losic et al., 2005] The large frustule diameter and flat valve surface make this a good diatom frustule to test this kind of deposition the first time. Losic et al. did succeed on making good replicas which followed the diatom topology very well. Their successful attempts of making replicas of frustules in gold were the first successful templates of diatoms with deposition of metal directly on the surface.

In the latest paper about gold deposition onto frustules, Yu et al. used electroless deposition of gold to produce self-supporting replicas of the frustules. This created gold structures which were good replicas of the frustule, and the frustule was dissolved by a 6% HF solution, this procedure gave the self-supporting replicas. An interesting feature with the electroless deposition, is that the gold is deposited both on the inside and outside of the frustule. Once the frustule is removed, the gold replica would be a double cylinder which is interconnected where the pores of the original frustule would be.

In the paper from 2006, Losic et al. continued their work on producing nanostructures of gold by using diatoms as templates. Thermal evaporation of gold onto a diatom frustule was used to gain different shapes of nanostructured materials. By depositing gold and stripping off the gold film afterwards, as shown in Figure 2.5, a self supporting replica was made. To strip the gold film of and

keeping it intact, a certain thickness is needed. Losic et al. deposited a continuous film close to a thickness of 1000 nm to gain enough thickness to mechanically remove the gold film. AFM and SEM imaging was conducted to see to what extent the topography of the frustule was replicated. The process kept the features of the areola intact, and also gave good replicas of the cribellum and cribrum. There a difference in the number of pores in the diatom and the number dots in the gold replica was observed, this reduction is interesting as a conformal layer would be expected. For more information about this see Losic et al. [2006a].

Although gold is a stable, ductile and noble with regards to its properties, there are certain aspects that have to be considered when trying to manufacture dimensions in the nanometer range. As the dimensions are getting smaller, properties like melting temperature and phase transitions occur at a lower temperature. [Bertolini and Rousset, 2006] There will also be specific particle shapes that are dominant, when the gold particles are larger than 8 nm across different planes will become dominant, and the planes will shape the particles into different polyhedrons depending on diameter and temperature. These properties may affect the way gold will behave in the pores of the diatom frustule, as the diameter of the pores is about 40 nm.

As the gold films become thinner than 5 nm, there is an increasing chance they will crumble into small particles; due to a thin layer having a large curvature, which will cause the film to have physical properties like smaller particles. When the particle size is reduced, the melting point of gold changes drastically,

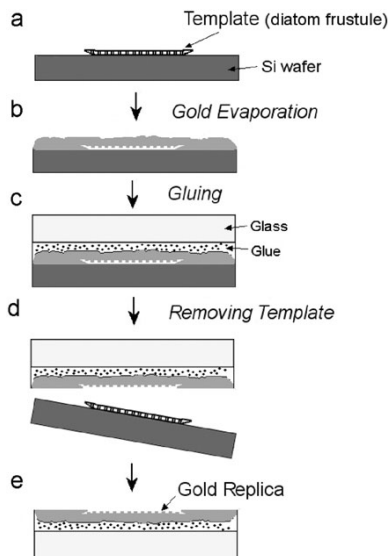
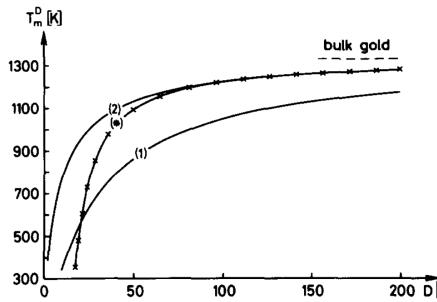
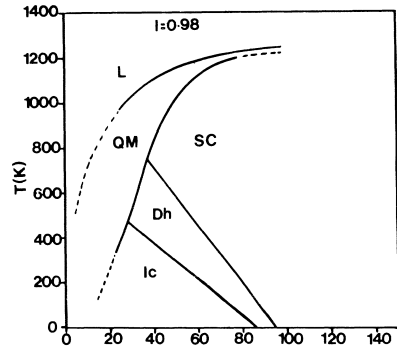


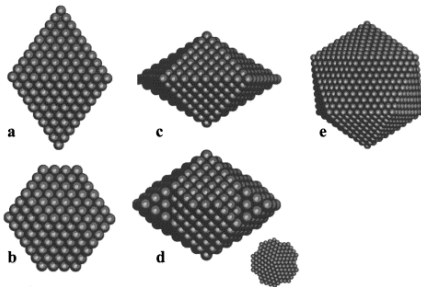
Figure 2.5: Schematic for fabrication of gold nanostructures using diatom frustules as templates. Source: [Losic et al., 2006b].



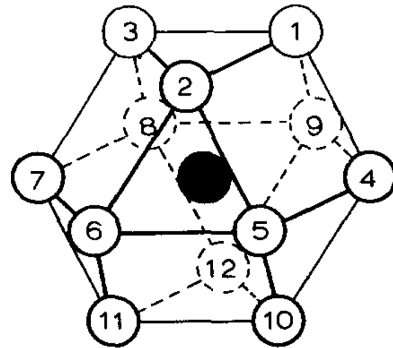
(a) Size effect on the melting temperature of small gold particles. Curve (\*) corresponds to the experimental results of Buffat. Curves (1) and (2) are the predictions obtained with Lindemann's melting criterion. Source: [Solliard, 1984].



(b) Structural phase diagram over gold with regards of temperature and particle diameter in Å. Liquid (L). Quasi-melt (QM). Single Crystal (SC). Truncated decahedron (Dh). Icosahedron (Ic). Source: [Ajayan and Marks, 1988]



(c) A schematic presentation of different particle shapes. (a) The fcc octahedron. (b) The truncated octahedron. (c) The regular decahedron. (d) The truncated decahedron. (e) The icosahedron structure. Source: [Ascencio et al., 2000]



(d) Atom in a fcc structure with numbering of nearest neighbours. Source: [Pérez et al., 1982]

Figure 2.6: The structural and morphological properties of gold nanoparticles are presented in these figures.

the melting point drops rapidly below room temperature when the features are between 1 and 2 nm. For sputter coater processing used to coat sample before SEM imaging, this can be critical for operation in SEM after sputtering. Figure 2.6(a) gives a graphic presentation of the melting temperature as a function of particle size. While Lindemann's melting criterion is theoretical, the experimental results of Buffat and Borel show a more realistic approach to the melting point of gold as a function of particle size. [Buffat and Borel, 1976]

Another size effect is the domination of different surface orientation. As the particle size changes, the particle structure changes with it to minimise the surface energy, Figure 2.6(b) shows which shapes are stable in the specific areas. Particles larger than around 7 nm at room temperature will not have clearly defined dominating planes and are looked at as a single bulk crystal, if the expression 'bulk' can be used about 7 nm large particles. As particle size becomes smaller, certain planes are more stable than others and it will tend to form truncated dodecahedrons, dodecahedrons will form in the range 5 – 7 nm. The smallest particles will form icosahedrons, but only down to 2 nm. [Bertolini and Rousset, 2006] Particles less than 2 nm will not form any stable interfaces, but will change between numerous different shapes. [Iijima and Ichihashi, 1986] This phenomenon is what Bertolini and Rousset refer to as quasi-melt. The melting point of gold will also lower drastically with regards to smaller particle size as shown by Figure 2.6(b). The shapes of the different crystals can be studied further in Figure 2.6(c).

Another property that is size dependent is the morphology of the particles. As a particle changes size, the plane(s) which are most stable would change, this would happen to reduce the number of surface atoms, and increase the total

Table 2.2: Numbers of atoms in different positions in a truncated octohedron particle and considering successive filled shells, according to Hardeveld and Hartog [1969]. Z is the coordination number of the atoms under consideration.

Total number of atoms	Number of surface atoms	Number of corner atoms Z = 6	Number of edge atoms Z = 7	Number of atoms of type (100) Z = 8	Number of atoms of type (111) Z = 9
38	32	24	0	0	8
201	122	24	36	6	56
586	272	24	72	24	152
1289	482	24	108	54	296
2406	752	24	144	96	488
4033	1082	24	180	150	728
6266	1472	24	216	216	1016
9201	1922	24	252	294	1352
12234	2432	24	288	384	1736
27534	3632	24	360	600	2648
46929	5882	24	468	1014	4376

coordination number of the particle. By coordination number is meant the number of other atoms which every single atom are in contact with. For a graphic presentation see Figure 2.6(d). A bulk atom would have a coordination number ( $Z$ ) which is 12, atoms in a surface plane of (111) would have a  $Z = 9$ , boundary planes with of (100) have  $Z = 8$ , edge atoms  $Z = 7$  and corner atoms  $Z = 6$ . These numbers are for fcc materials only. [Bertolini and Rousset, 2006] To see how the particle size affect the number of surface atoms it is best to present these in a table as given in Table 2.2. A particle in this dimension will be susceptible to temperature changes, and if a process step require a high temperature, some of the smallest features might be lost during heating and cooling of the sample.

Even though gold is a good material for a proof of concept, other materials will be required to gain good properties for light harvesting or antireflexive coatings for solar cells. Interesting materials already used by the solar cell industry will be investigated in the following subsection together with thin films.

### **2.2.2.1 Elements and Compounds Used in the Solar Cell Industry**

There is a whole range of materials which may be deposited by either PVD or CVD. The number of materials with a potential use in the solar cell in the solar cell industry are fewer, but there are still a large number. In this subsection the materials which have been used in this thesis will be investigated to show the versatility of templating for solar cells. The experimental techniques of the different materials will not be disussed here, as they may vary due to different requirements and specifications for functional properties in the range of applications, for further information references can be investigated. The focus of this part will mainly be on applications of materials for solar cells.

## **Silicon**

Silicon is the most used material in the electronics industry, and as a abundant and relatively cheap material it has been the material of choice for the PVSC industry as well. The main goals of researchers in the industry is to get as high effect out of every cell at the lowest price possible. This can be done by either increasing the effect or by lowering the costs, new production methods for solar grade silicon have been developed. [Wærnes et al., 2005; Yuge et al., 2001] There have also been a number of methods to increase the efficiency further, including tandem cells, up- and downconverting cells and cells with heterojunctions, but these methods are more costly than the production of regular PVSC of silicon.

Although silicon is mostly used in its crystalline form in regular mono and poly crystalline, silicon has other possibilities when used as an amorphous material in thin film solar cells. By the use of plasma enhanced chemical vapour deposition (PECVD), amorphous silicon can be deposited with or without dopants to make a cell with two different semiconductors on a substrate, called Heterojunction with Intrinsic Thin Layer (HIT) cell. [Green, 2004; Peike et al., 2009] A schematic figure of a HIT cell is shown in Figure 2.7(a). This kind of thin film cells do not have any kerf loss or loss due to cut-off when the pulled crystal is cut

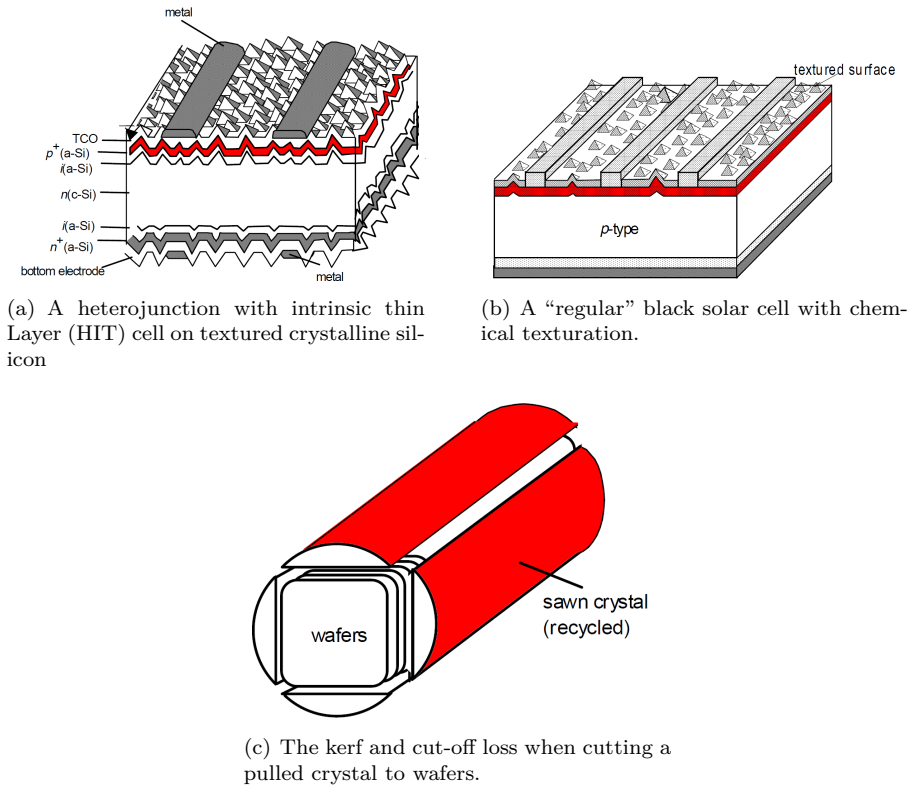


Figure 2.7: Figures are borrowed from Green [2004]. Figures are not in scale.

to ingot shape, as seen in Figure 2.7(c), which may give HIT cells the advantage they need to be competitive with crystalline silicon solar cells. HIT cells made of amorphous and crystalline silicon have an intrinsic layer between the positive and negative doped layers. As an intrinsic semiconductor material has rather poor conductivity this layer will allow recombination to take place, and therefore HIT cells manufactured this way will have a large loss. [Peike et al., 2009]

While the HIT cells have a large loss due to the intrinsic layers between the different doped layers, the "regular" black solar cell has a different design and a quasi-neutral zone between the p- and n-doped layers. In Figure 2.7(b) the beams on top are the metal contacts, the grey layer on top are the antireflection coating. The red layer is the n-doped layer. The dotted zone near the bottom of the cell is the  $p^+$ -doped area, an area with a stronger doping than the rest of the p-doped area due to heat-treatment after depositing an aluminum layer as a back contact. Aluminum will diffuse into the cell and act as a strong dopant.

While crystalline silicon has been the leading material for producing solar cells, HIT cells have shown great potential with a maximum efficiency above

21 %. [Peike et al., 2009] These results give high hopes that HIT cells based on amorphous silicon can be utilised. If deposited by PECVD, it should be possible to deposit the amorphous silicon onto a dense monolayer of diatom frustules, and that way create a porous and rough surface, which may not need texturing to act as an antireflective surface.

Diatom frustules have proven to have light focusing effects, and given the optical properties of silicon, a texture made by frustules might have the right properties for a solar cell. The present technique used to gain the texture in front of solar cells is to etch the front with an acidic mix which contains HF among other compounds, if this technique had been replaced by texturation by deposition, the use of acids in the PV industry could have been reduced by large amounts.

### **Silicon Nitride**

In addition the silicon has to be passivated and covered by an antireflective coating of silicon dioxide or silicon nitride. If the antireflective coating is deposited between the silicon and the frustule shaped substrate, the antireflective coating will obtain a surface texture close to or similar as the frustule shape. The diatom frustule has dimensions in the same range as the texturation made by the etching process by HF, and it might be possible to texturise the solar cells by depositing silicon nitride into shapes similar to diatom frustules.

One of the methods used to gain an antireflective coating is to deposit the silicon nitride from a gas mix of silane ( $\text{SH}_4$ ) and ammonia ( $\text{NH}_3$ ) with PECVD, and that way create a layer of silicon nitride ( $\text{Si}_3\text{N}_4$ ). Silicon nitride actually have two purposes, in addition to be applied as an antireflective coating, it also passivates the surface of the silicon cell. [Lipinski et al., 2006] The passivation of the silicon surface will increase the lifetime of the charge carriers, the charge carriers will then gain a longer path of diffusion and increase the chance of any of the charge carriers to reaching of the contacts at the surface of the cell.

Another way of producing the silicon nitride surface is to heat the silicon cell and expose one side to nitrogen gas. Silicon and nitrogen then react to form silicon nitride. The original topography of the silicon would stay the same, and the cell might have better light absorbing properties than a smooth silicon nitride surface. The silicon nitride produced this way will not have the same properties to passivate the surface of silicon cells, but might have other advantages. Silicon nitride have possibility to vary the refractive index by changing production variables and methods. [Aberle, 2000] By adjusting the refractive index of the material, it can be adjusted for specific applications and environments.

### **2.2.3 Thin Films and Their Usage**

Crystalline solar cells have a huge kerf loss during manufacturing, silicon thin films made by amorphous silicon have the advantage that they have no kerf loss (silicon cut away during sawing from ingot to wafer). While crystalline solar cells are texturated after they are cut into wafers, the amorphous silicon cells gain their texturation when they are deposited on a already existing substrate.

Normally the texture is gained through etching a transparent conducting oxide with HF, and then deposit amorphous silicon in the structure which have been made by the etch. [Roca et al., 1997]

By using a ductile template of gold which has the pattern of diatoms imprinted, another way of creating these textured surfaces may be utilised. Environmental aspects are in consideration as hydrogen fluoride is a toxic and corrosive substance and always has to be rinsed before disposed of. Thin film cells are based on many different materials, and if an environmental-friendly method like diatom templating could be used as texturation method for this kind of cells, there would be a potential for large improvements with regards of environmental issues.

Another way the diatoms could be utilised by thin film solar cells are to use them as a backscattering layer in solar cells, by spreading the light rays and increase the mean path for the rays in the solar cells, the amount of light the thin films absorb will increase as well. [Gjessing et al., 2010] According to Gjessing et al. [2010] small rough particles of silicon dioxide would be good for such purpose. Such particles could be gained by filling the inside of each theca with glass and placing the thecas with the valve away from the substrate in the back. and by reversing the deposition process the rear surface can work as a texturation to spread the incoming light rays. Due to thin films are just what the name says, thin, the texturation from the rear may be present at the front, creating both front and rear texturation and laying the foundations for a good PV cell. The utilisations mentioned for HIT cells in the section are only a few of many possible applications for diatoms in solar cells.

## 2.3 Templating

### 2.3.1 Deposition with Electron-Beam Evaporator

The electron-beam evaporation (EBE) method is a simple, reliable method for deposition of metals and oxides. A substrate is placed on a supporting wafer, and slid into a vacuum chamber. The first thing done during deposition is heating a tungsten filament until it emits electrons. Then accelerate the electrons and targeting them towards the material chosen for deposition. The target will start to melt and eventually evaporate. As the process chamber is held in a high vacuum (around  $10^{-6}$  mbar) no polluting elements or compounds will be present, the film deposited will hence have the same composition as the target.

It is important to remember that the evaporation is done in high vacuum, and hence the target material have a much lower evaporation temperature than in atmospheric pressure, due to the low evaporation temperature the electron beam moves across the target surface to heat up a larger area of the target. In this way the material rather steam off than going into rapid boiling, this help to enhance lifetime for targets. It also confers the conformal thin film known to be deposited by EBE.

EBE has a very small quantity of ionised target atoms compared to the other PVD processes described by Lugschreider et al.. The E-beam evaporation has

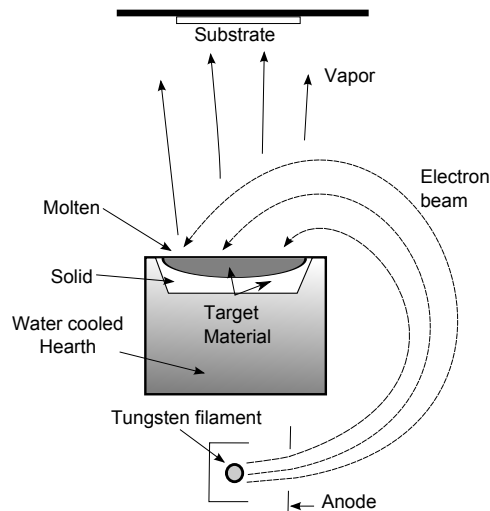


Figure 2.8: Schematic of electron beam evaporator. Electrons are extracted from a heated wire of tungsten. The electrons are accelerated by an electric field and guided by a magnetic field perpendicular to the plane of diagram to hit and heat the target material. The target material will melt and evaporate by the electron beam, and the atoms from the target material will form a solid thin film on the substrate.

less than 1 percentage of ionised atoms, compared to magnetron sputtering which have between one and five percentage of ionised target material while the rest is argon and nitrogen ions. [Lugschreider et al., 1996] For anodic and cathodic arc ion plating between 5 and 40 percent (anodic) and 50 and 100 percent (cathodic) are ionised, and for these depositions are there normally sublimation from solid directly to vapour which are the vapourisation process. [Lugschreider et al., 1996] Another positive effect of the low ionisation quantity in the e-beam evaporation is the low energy requirement for deposition, this means a lower temperature in the substrate and reduces the risk of thermal stresses and cracks as a result from the thermal stresses. [Lugschreider et al., 1996] The high vacuum in the EBE process removes most contaminating species, this assures a thin film with the same composition as the target material. It is also possible to add reactive gases to form complex products like CrN from Cr<sub>2</sub>N and N<sub>2</sub>(g). [Lugschreider et al., 1996] All materials which can be melted and evaporated in vacuum have the potential of being used in an EBE, the only challenge is the stability of different materials as they are heated till they come close to their evaporation temperature.

Silicon is one example of materials which have easy to get unstable, and targets of silicon have been witnessed to explode. [Graper, 1987] The work of Graper shows that gold is a good material for deposition by forming a stable thin film. It requires little to no attention and have its only one issue regarding

instability of the target. The melt will oscillate, and the lining between hearth and target material may not be made of carbon. [Graper, 1987]

The EBE was used to deposit gold films for the experiments conducted in this thesis. The evaporation technique has no limitation with regards of the thickness it can deposit. Hence films from 1 nm up to several  $\mu\text{m}$  thick can be deposited without any major issues. Gold films for both the attempt with lifting of parts of the film deposited on the frustule and the gold film deposited on the glass substrate which were later etched away were deposited by EBE.

### **2.3.2 Plasma-Enhanced Chemical Vapour Deposition**

Chemical Vapour Deposition (CVD) is the common term for thin film deposition by reaction of a gas mixture. The three aspects important are chemical action, material supply and reactants in vapour phase. Chemical action is contributed as a chemical reaction or thermal decomposition. All the materials are supplied by a gas inlet, and by the definition of CVD all reactants must start out as gas. [Quirk and Serda, 2001]

Typically the chemical processes which can happen in a CVD process are divided into five: decomposition of compounds when heated (pyrolysis), dissociation of compounds with application of radiant energy that break bonds (photolysis), chemical reaction of a molecule with hydrogen (reduction), a chemical reaction of an atom or molecule with oxygen (oxidation), and a combination of reduction and oxidation with the formation of two new compounds (reduction-oxidation (redox)). [Quirk and Serda, 2001]

There are three different kinds of CVD reactors, atmospheric pressure, low pressure and plasma-assisted CVD. Atmospheric pressure reactors are simple reactors, and give fast deposition at a low temperature which makes this process suitable for low temperature oxides. There are some disadvantages to the atmospheric pressure CVD reactor as well: poor step coverage, particle contamination and low throughput. Low pressure CVD have a excellent purity and uniformity, and a conformal step coverage and large wafer capacity which makes this process suitable for high-temperature oxides, silicon nitride and tungsten deposition. As the atmospheric pressure CVD reactor, the Low pressure CVD also has some disadvantages: high temperature, low deposition rate and requirement of a vacuum system. To be able to fill high aspect ratio gaps, deposit low temperature oxides over metals, and deposition of silicon and silicon nitride plasma-assisted CVD reactors are used. These reactors could either be built for atmospheric pressure (High-density Plasma CVD (HDPCVD)) or for low pressure (Plasma-Enhanced CVD (PECVD)). The advantages of such reactors are the low temperature needed, the fast deposition rate, good step coverage and good gap fill. To gain plasma, a RF system is required, this increase cost, stress is much higher with a tensile component, and there are risks of chemical (e.g.  $\text{H}_2$ ) and particle contamination. [Quirk and Serda, 2001]

Plasma-assisted CVD has a reactor with a heated table where the sample is placed during deposition. In addition to the heat, the process is also assisted by a plasma which is caused by RF power used to break up the gas molecules in a

vacuum. The free radicals formed by the plasma are chemically reactive species and easily bond to other atoms to form a film on the sample surface. The byproducts are gaseous and are removed by the vacuum pumping system. To remove contaminants such as hydrogen, a certain temperature is needed; the temperature also helps the reactions to form good films, as resins may cause pores or other harmful effects. The reactions forming the film at the sample surface are very complex, and the properties of a plasma-deposited film depend on many variables, such as electrode configuration and separation, power level and frequency, gas composition, pressure and flow rate, and substrate temperature. [Quirk and Serda, 2001]

PECVD uses plasma energy to create and sustain the CVD reaction, and PECVD is a development of the low pressure CVD since the system pressure of both types of CVD processes is comparable. The large advantage of PECVD compared to low pressure CVD is the lower deposition temperature needed for PECVD. PECVD reactors are cold-wall plasma reactors, with the sample heated in its chuck while the remaining parts in the reactor are unheated. The advantage of cold-wall reactors are their tendency to create less particle contamination than warm-wall reactors, and they also require less downtime for cleaning, Figure 2.9 is

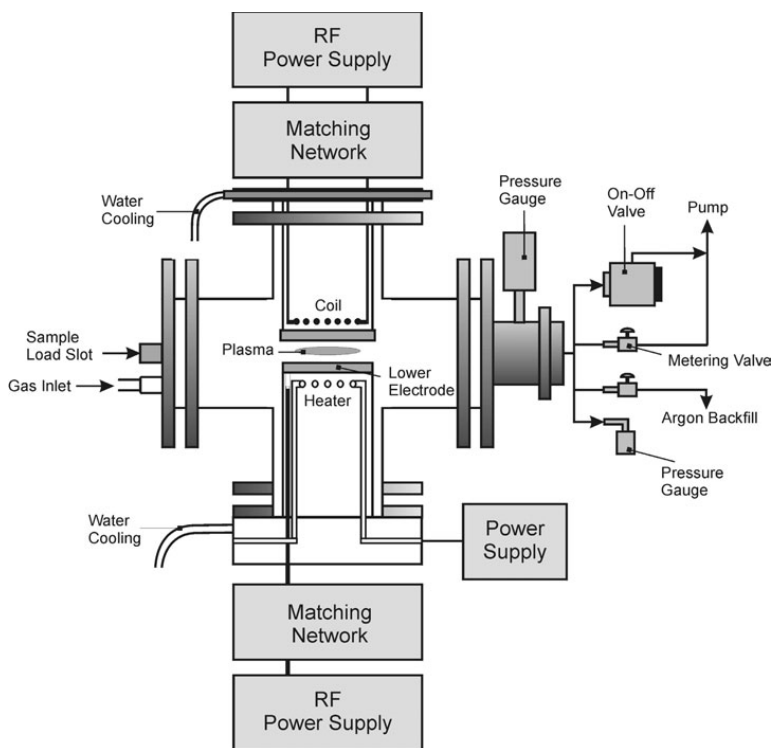


Figure 2.9: Schematic of plasma-enhanced chemical vapour deposition set-up. [Meyyappan et al., 2003]

a schematic of PECVD-system with all major parts included in the figure. [Quirk and Serda, 2001]

For small gaps ( $< 0.5 \mu\text{m}$  gap width) PECVD is not able to fill high aspect ratio gap without leaving voids. For devices using  $0.25 \mu\text{m}$  technology and below, HDPCVD has replaced PECVD due to its superior gap-fill properties. The main difference between HDPCVD and PECVD is that the plasma is much denser even at low pressures compared to PECVD. To be able to achieve the high-density plasma, two or more gases are required. Argon is often used to be able to gain the high-density plasma in addition to any reaction specific gases. To form the high-density plasma it get excited by RF power and directs the plasma regions into a dense region above the wafer surface. Another reason for the HDPCVD to be able to deposit film into high-aspect ratio geometries are the high density combined with wafer bias, which cause directionality of the plasma ions. [Quirk and Serda, 2001]

Although PECVD is more complicated and requires a better process control during deposition than EBE does, PECVD is in wide use as deposition technique in the electronics industry. In the PV industry PECVD is in use as deposition method when producing thin film cells. When manufacturing thin film silicon solar cell, a glass substrate is the foundation of the cell. A layer of transparent conducting oxide is deposited on top by PECVD to make a contact at the front of the cell. Then amorphous silicon is deposited with dopants to create a p-i-n structure in the cell. A back-surface reflector is deposited last. The reflector could either be made of a high reflectivity metal or oxide, both aluminum and silicon dioxide can be deposited by PECVD.

## 2.4 Characterisation

The experimental theory of how the characterisation is done by electron microscopy and focused ion beam is handled in this subsection.

### 2.4.1 Characterisation by Scanning Electron Microscopy

Imaging in the scanning electron microscopy is done by registering the intensity of either backscattered or secondary electrons. Both signals are monochromatic, and images are displayed in grayscale [Hjelen, 1989]. Two phases observed with different colours in light optical microscopy, will look the same in SEM if the intensities are equal. The shape is still observable though. SEM provides several other tools which make characterization possible. Atomic number contrast observed in backscatter-mode can be used to differentiate between phases as long as their average atomic number is not identical. For amorphous  $\text{SiO}_2$  and Au, substrate and film, the atomic numbers are very different and this option can be utilised.

For the purpose of using SEM as the main tool for characterising diatoms, secondary electrons are the most viable imaging to use. By having a short

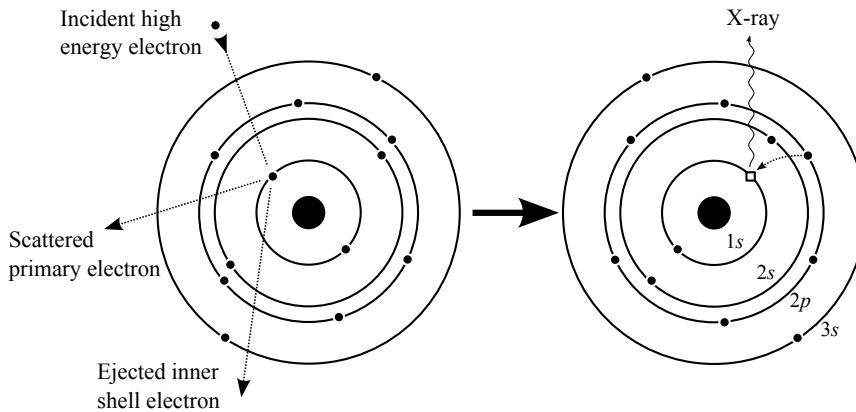


Figure 2.10: Illustration of how X-rays are generated by high energy electrons. To the left an incoming high energy electron ejects an inner shell electron which leaves behind a vacant position. To the right, an outer shell electron drops into the vacant position and liberate excess energy in the form of a  $K_{\alpha}$  X-ray. Source: [Bunkholt, 2010]

working distance and using the in-lens detector, large magnification with good resolution can be achieved. For measurement of pore sizes on the frustule surface, a distance measurement implemented in the software is the best technique, as it is fast to use and will give precise results.

The details of energy-dispersive spectroscopy (EDS) are described by both West and Hjelen, explaining how X-rays are emitted from a specimen positioned in the SEM when fired upon with electrons. [Hjelen, 1989; West, 1999] From the sharply-pointed emitter of the field emission gun (FEG), high energy electrons are accelerated towards the specimen where they interact with the atoms in two different ways. Bremsstrahlung, white radiation or continuous X-rays is the emitted X-ray signal created by decelerating or stopping high energy electrons that lose energy while penetrating the electrostatic fields around atoms in a material. In emission spectra this is considered as noise and cannot contribute to an elemental analysis. Fortunately, high energy electrons also interact directly with atoms that are heavier than Li. Depending on the energy of the electrons, they can ionise the atoms by kicking out an inner shell electron as illustrated by Figure 2.10. The atoms then return to their ground state by dropping an electron from an outer shell into the vacant position, and at the same time releases excess energy in the form of electromagnetic radiation, an X-ray. The energy of the emitted X-ray depends on how large the quantum jump is, a  $2p$  to  $1s$  jump results in so called  $K_{\alpha}$  radiation while a  $3p$  to  $1s$  jump gives  $K_{\beta}$  radiation.  $K_{\alpha}$  is more frequent and intense than  $K_{\beta}$ , but is in fact a doublet of  $K_{\alpha_1}$  and  $K_{\alpha_2}$ . Transitions or energy differences from one shell to another are unique to each element and makes quantitative and qualitative analysis possible.

By registration and plotting the intensity of emitted X-rays from a sample versus energy in a spectrum, the chemical composition of the material can be revealed. The peak position identifies the element, while the intensity is proportional to the quantity (after ZAF-corrections). To be able to detect all elements one must be sure the incoming electrons have high enough energy to eject orbital electrons, and for increasing atomic number the acceleration voltage must be increased to provide the electrons with sufficient energy. As a rule of thumb one should use an acceleration voltage twice that of the critical excitation voltage. When the acceleration voltage increases, the electrons penetrate deeper and the emission volume becomes larger. The resolution associated with X-ray radiation pictured in Figure 2.11 is, however, relatively poor and much larger than the beam diameter. The X-rays that escape the material are detected by a detector that is sensitive to the energy of the incoming radiation and connected to the SEM. A cooled Li doped silicon crystal converts the radiation to a voltage signal, and the chemical composition is readily displayed in the form of a spectrum. With EDS the sensitivity is somewhere between 500 ppm and 5000 ppm, but all detectable energies are measured simultaneously.

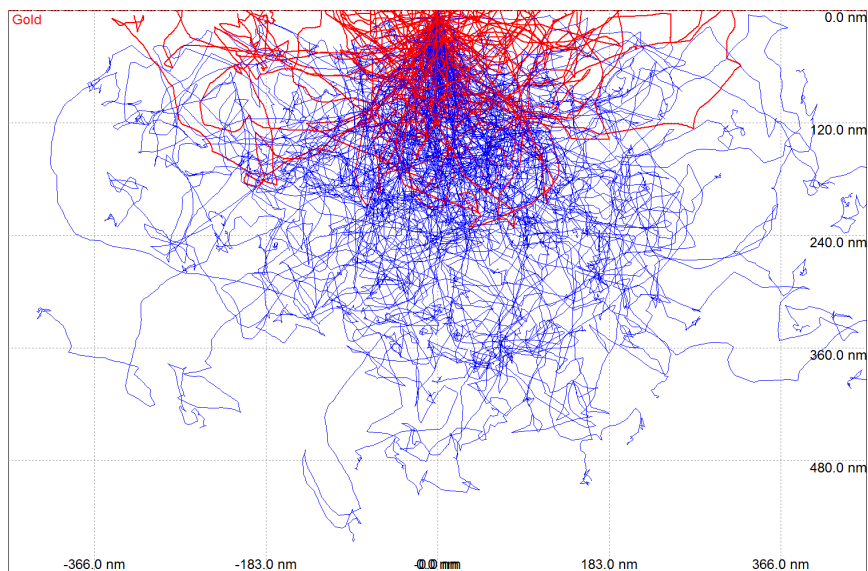


Figure 2.11: Monte Carlo simulation of X-ray emission volume in a gold matrix. Performed in Casino v2.42 software with a beam diameter of 5 nm at 20 kV. Only the red X-rays escape the material, the blue ones are all absorbed.

## 2.4.2 Focused Ion Beam (FIB)

A FIB-system is very similar to a SEM-system, the major difference is the medium which is accelerated by the column. For a FEG-SEM there are

electrons emitted by a field emission gun (FEG), for a FIB system a heated gallium needle emits  $\text{Ga}^+$  ions. As the ion hit the sample, some material are sputtered from the sample, the dislodged material may be in the form of secondary ions, atoms, and secondary electrons. All of the sputtered species can be collected and analysed as signals that can form an image on a screen as the primary beam scans the surface.

There are two basic functions of a FIB, imaging and sputtering with an ion beam, and such an ion beam requires a highly focused beam. To get a focused beam with nanometer-scale precision a liquid metal ion source (LMIS) is used. A LMIS gives the brightest and most focused ion beam. A blunt needle source of Gallium is used, the reasons Ga is used instead of other potential LMIS material, like In, Bi, Sn and Au, are the low melting temperature of gallium (30 °C), low volatility, and low vapour pressure. [Volkert and Minor, 2007] As a FIB is operated, more Ga is flowing from a reservoir to the needle where it is extracted by field

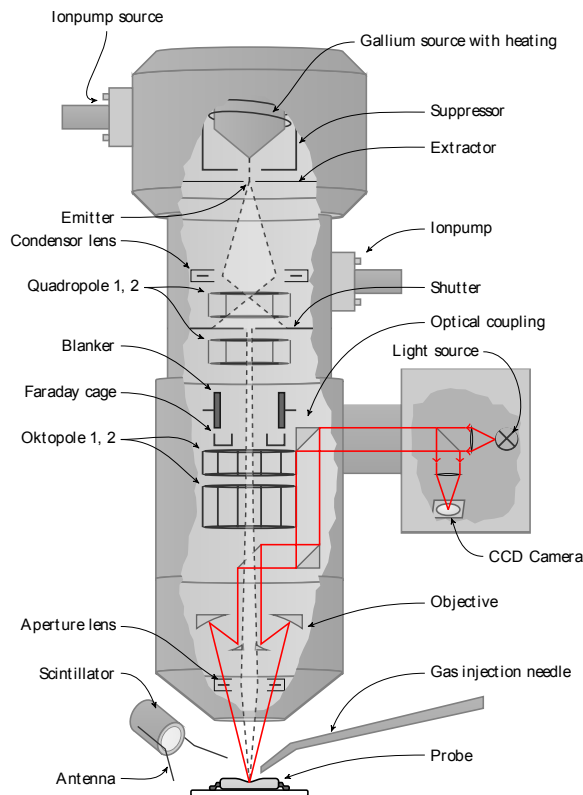


Figure 2.12: Focused ion beam system with a ccd camera attached. The optical path of the ccd system is lined in red, while the optical path of the ions are in pale grey with dotted lines around.

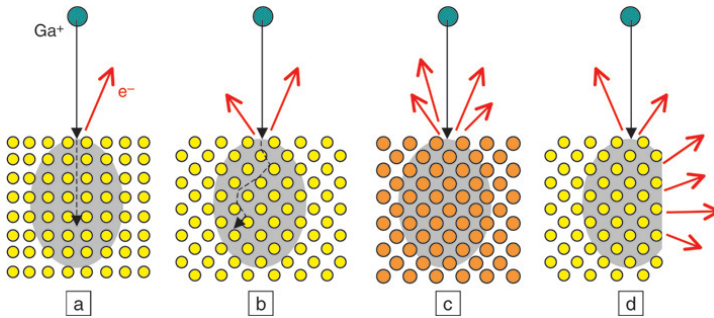


Figure 2.13: Schematics showing the influence of (a), (b) crystal orientation, (c) atomic mass, and (d) surface geometry on 30 keV  $\text{Ga}^+$  collision cascades and ISE image contrast formation. The orange atoms in (c) are more massive than the yellow atoms in (a), (b), and (d). Similar concepts influence sputtering yields. Source: [Volkert and Minor, 2007].

emission, the small radius (10 nm) of the Ga needle gives a potential of a resolution down to 5 nm. [Volkert and Minor, 2007]

The ultimate resolution for a FIB is dependent on sputtering, and because every material has different properties of sputtering, the resolution is dependent on the sample material. For modern FIB the sputter limited signal-to-noise ratio is about 10 nm. The stage of a FIB has the same properties as a SEM, it is grounded, has three axes of translation, rotation and tilt capabilities, and has an eucentric point. (i.e., a well-centered point such that the field of view is maintained when tilting the specimen) at the working distance of the ion beam. [Volkert and Minor, 2007]

A FIB may contain the same detectors as a SEM to detect the electrons or x-rays created by the interaction of the ion beam with the sample. The ions sputtered from the surface may be detected using detectors like electron multipliers and also mass spectroscopy of the sputtered ions is also possible (secondary ion mass spectroscopy (SIMS)). Another feature of the FIB system is the gas injection needle, the needle can enhance etching on specific sites, or it may result in chemical vapor deposition, depending on gas used and sample in the vacuum chamber of course. All of this results in a system that can image, analyse, sputter and deposit material all with very high spatial resolution and controlled through a single software program. [Volkert and Minor, 2007]

While the conventional SEM imaging is based on detecting the secondary electrons (SEs), most imaging in a FIB is based on detecting the low-energy electrons, often referred to as ion-induced secondary electrons (ISEs). The number of electrons with energies below 10 eV are usually 1–10 when using an acceleration voltage in the column of 30 keV or below for the gallium ions. These electrons are created in the top atomic layers where the primary ion impacts the solid as well as where backscattered or sputtered particles leave the sample.

Different mechanisms of contrast is illustrated in Figure 2.13. It is clear by comparing Figure 2.13(a) and (b) to each other, that the crystal will emit more electrons due to a higher number of collisions when orientated so the ion does not channel along crystal planes. Figure 2.13(c) illustrates that heavier samples typically result in more ISEs and SEs. Figure 2.13(d) shows that surface topography can lead to increases in the number of ISEs and SEs, because of the increase in the number of ion-solid interactions near the sample surface. The SE and ISE images are also often distinguished by the amount of charging generated in insulating samples. [Volkert and Minor, 2007] In insulating samples it is for SEM required to coat them to gain a good resolution, for FIB this is not required as Ga will make a thin conducting layer at the sample surface due to implantation of ions. [Volkert and Minor, 2007]

A major drawback of FIB imaging and machining is the damage created by the ion beam. If the sample is exposed to prolonged times of the ion beam, a number of disordered cascade regions may start to overlap and a damaged surface layer is formed. For  $\text{SiO}_2$  this will come in the form of sample surface amorphisation, but for other materials the damage can come in the form of point defect creation, dislocation formation, phase formation, grain modification, or other unusual effects. [Volkert and Minor, 2007]

---

## 3. Experimental Details

This chapter will explain more in detail how the experimental part of this project was carried out, and this chapter will go through the experimental set-ups in detail. In this survey harvesting and cleaning of diatoms will be covered, together with deposition and the characterisation. All together every single experiment and action leading to the results will be explained. In chapter 3 and 3 an overview of the experimental work is presented.

### 3.1 Harvesting and Cleaning of Diatoms

The diatoms used in this thesis originate from two different sources, net plankton and diatom culture grown in a laboratory. The quality of the two samples were different as they were cleaned at different occasions, and the net plankton also had some particles from the seawater. Most of these particles dissolved in the cleaning process. Both the net plankton and the culture diatom sample had to be filtered and centrifuged before being cleaned to remove any fixative and salt, which could pollute the sample, and make any characterisation harder to carry out with good results. This subsection will go through the harvesting and cultivation of the diatom, and finish with the cleaning and removal of organic material from the diatom frustules.

#### 3.1.1 Harvesting of Cultivated Plankton

The diatom species *Coscinodiscus walesii* was cultivated in freshwater saturated on  $\text{Si(OH)}_4$  and other vitamins so it would have good growth conditions. The amount of  $\text{Si(OH)}_4$  and vitamins in the medium were monitored, and these resources were added to the medium from time to time to keep the nutrient level high, and hence keep the culture growing. When a high concentration of *Coscinodiscus walesii* was obtained, a small portion (25 ml) of the culture was removed from the cultivation chambers to be cleaned. After the 25 ml were centrifuged, a few cubic millimeters of a green-brownish powder was at the bottom of the tube used in the centrifuge. These few cubic millimeters with diatoms are to be cleaned and used further in the experimental work of this thesis.

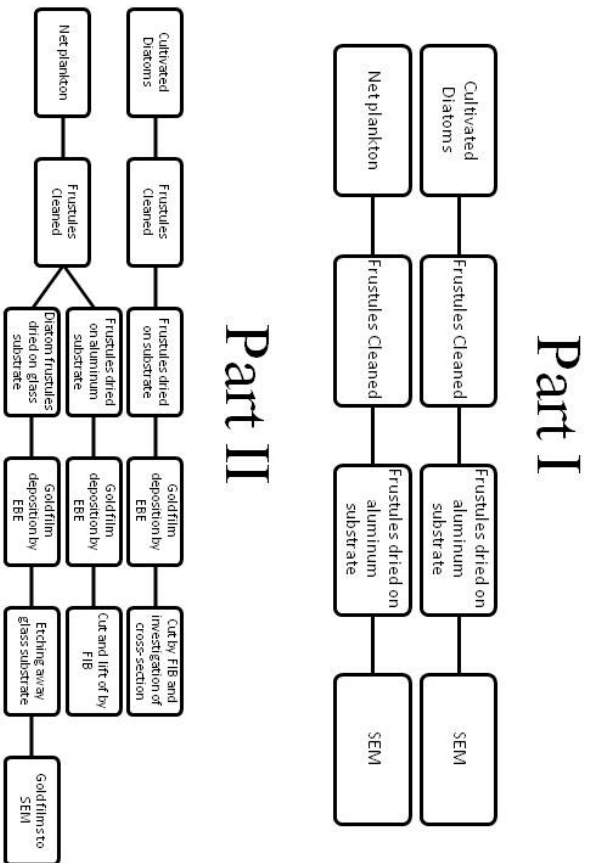


Figure 3.1: A schematic overview of the experimental work done in the two first parts in this thesis.

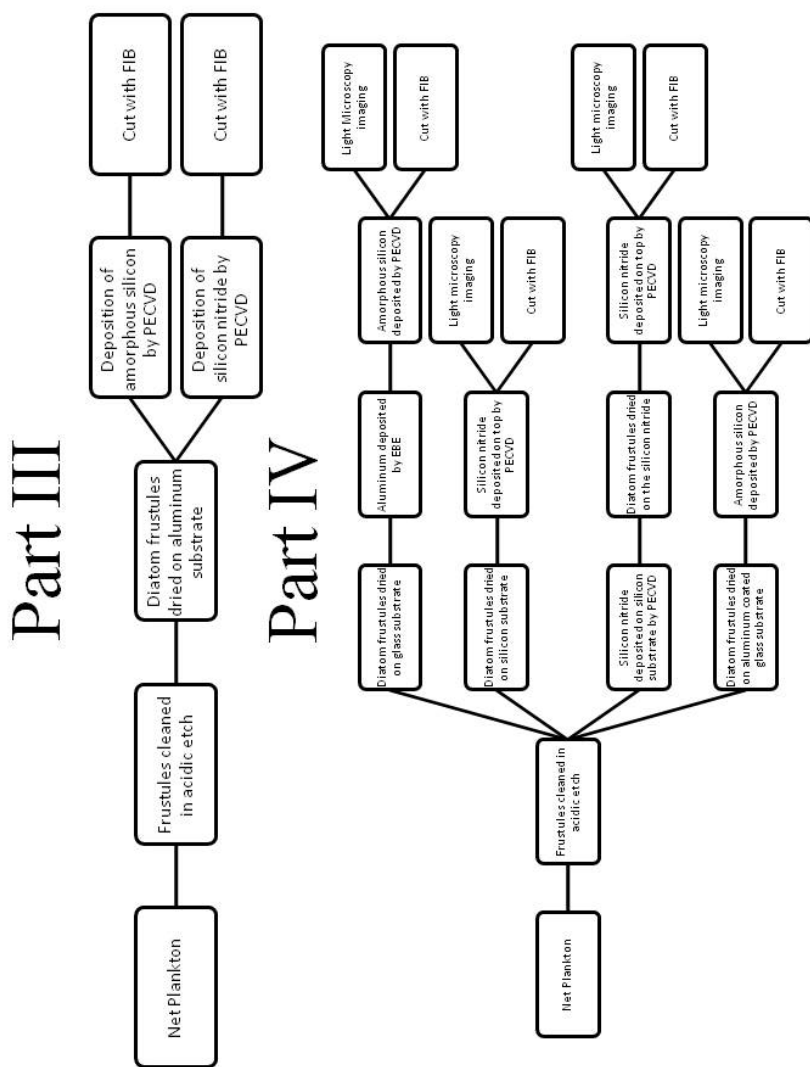


Figure 3.2: A schematic overview of the experimental work done in part III & IV in this thesis.

### 3.1.2 Harvesting Net Plankton

As diatoms are naturally abundant in all places where liquid water and moisture can be found, they are easy to harvest in the nature. The net plankton used in this thesis was caught by net in the Fjord of Trondheim. The concentration of *Coscinodiscus sp.* was high in the seawater and hence a pure sample of *Coscinodiscus sp.* was collected. The sample was filtered such that water and diatoms separated, the frustules dried, and the diatoms were frozen down for later use. The sample was stored in a regular household freezer, keeping the samples fresh and without any external degradation from i.e. degradation of silica walls in water undersaturated with silica.

The diatoms were removed from the freezer and a few cubic millimeters (about the same amount as were centrifuged out of the cultivated diatom medium) of the material was placed in a tube for centrifugation. Centrifugation is necessary to remove any fixative and salts, the volume of these polluting materials are very small and was not taken into consideration when removing the sample from the frozen diatoms.

### 3.1.3 Cleaning of Diatoms

After centrifuging the diatoms 2-3 times a pipette were used to remove a few drops of the concentrated material from the test tube. The drops of material were transferred to a new test tube where 2 drops of  $\text{HNO}_3$  and 8 drops of  $\text{H}_2\text{SO}_4$  were added. The mixture was heated over an alcohol burner for a couple of minutes while shaking the tube. The surplus acid was removed by centrifugation with distilled water 7 times. The culture were centrifuged in 20 minutes at 100 G, so it formed a pellet. The pellet was resuspended in 40 ml of deionised water, centrifuged, and washed again two more times. The washed diatom cell pellet was resuspended in 40 ml of 50 g/l sodium dodecyl sulfate (SDS) this treatment was repeated two more times on 100 mM ethylene diamine tetraacetic acid (EDTA), stirred to a vortex formed in and kept the rpm for 1 minute, and then allowed to react for 20 minutes at room temperature without mixing. The SDS/EDTA treatment was repeated two times. The treated cell mass was washed three times in distilled and deionised water to remove the SDS, EDTA and any residual organic matter (40 ml, and 100 G for 20 minutes. The frustules were suspended in 5 ml of methanol for later use.

The reason the diatoms were cleansed this way is to remove any organic material which may prevent the following experiments. In experiments where detailed replicas are made of the surface of the diatom frustule a clean frustule surface without many particles are needed. The reason a single process is repeated is to remove any resin and assure there are reactants to dissolve all the organic material.

## **3.2 Part I: Characterisation of Diatom Frustules and Their Pore Structure**

To be able to get better insight in the internal structure of the diatom frustule and be able to measure how well the diatom frustules structure are reproduced, a thorough investigation of the diatom frustules must be conducted. By SEM and FIB the frustules are measured and cut through to obtain high quality images of the surface and internal structure of diatom frustules.

### **3.2.1 SEM-characterisation of Diatom Frustules**

Even though the diatom frustules are made of silicon dioxide, there was no need of any gold or carbon coating to increase the conductivity. This is a technique often used to remove and charge-up in the sample, as charge-up cause drift in the image and will eventually reduce the resolution of the SEM-images. The SEM-imaging was conducted to make measurements of the different pore structures of the frustule as a large amount of data would be necessary to be sure the replicas are of good quality.

The first step of the characterisation was to drip a few drops of the methanol suspension prepared in subsection 3.1.3 on an aluminum sample holder for use in SEM. The methanol evaporated off the sample holder, leaving many frustules across the surface of the holder. The sample holder was then inserted into the SEM for characterisation and imaging. The working distance was about the same for all images taken in the SEM as the frustules are very thin (a few microns), and the sample holders used all have the same height.

The pore size of the different pores was measured with the measuring software following the SEM. The accuracy of all the measurements is limited of the resolution in the image, which means the measurements will have very small deviations from the real dimension. Some hundred pores of each type and on each of the two sample types were measured giving a good basis of comparison.

Table 3.1: SEM settings used when investigating the pore size.

Hitachi S-5500 settings	
Acceleration voltage	30 kV
Working distance	0.9 mm
Filament current	7 $\mu$ A

### **3.2.2 FIB-characterisation of Diatom Frustules**

To obtain a good understanding of the internal structure of the diatom frustules a FIB has to cut through the frustule and SEM-images are to be taken at the cut. The internal structure could also be the reason for some of the light focusing properties of the diatoms. By mapping the structure, investigations of

how the diatom frustules are built up during diatom growth can be continued and possible alterations could be made to the pore structure in the frustule.

The methanol suspension containing a large amount of diatom frustules was dripped on an aluminum substrate and the methanol evaporated off the substrate. The aluminum substrate would give the conductive properties for FIB-characterisation, as FIB also cause charge-up of the sample if it would be insulating. The sample were placed in the FIB-vacuum chamber and pumped to a high vacuum before characterisation.

In the chamber the sample would be tilted to  $52^\circ$  as it is the angle between the gallium column and the electron column in the device. By tilting the sample to this angle, the gallium column would be normal to the surface of the aluminum, and the electron column would be inclined to the sample surface. The inclination rendered it possible to take SEM-images of the cross-section of the cut made by the gallium beam.

The difference between the regular SEM and the FIB is in how much current which is running through the sample. In the regular SEM the filament current is altered to an good picture is achieved, while in the dual-beam device an aperture is changed depending on purpose of the activation of the column, large aperture for cutting and small aperture for imaging. The aperture used for cutting were normally  $93 \mu\text{A}$ , while the current used for SEM-imaging were  $9.3 \mu\text{A}$ . There is another difference as well between cutting and imaging, and that is the medium which is accelerated by the column, namely electrons for imaging and gallium ions for cutting. It is possible to image samples with gallium ions as well, but that was not utilised in this project.

Table 3.2: FIB settings used when investigating the internal frustule structure.

FEI Helios Nanolab	
Acceleration voltage of Ga-beam	30 kV
Acceleration voltage of SEM-column	30 kV
Working distance	4.2 mm
Aperture used for cutting (FIB)	$93 \mu\text{A}$
Aperture used for imaging (SEM)	$9.3 \mu\text{A}$

### **3.3 Part II: Manufacturing and Characterisation of Gold for Use as Templates in Solar Cell Industry**

#### **3.3.1 Deposited Gold Film Characterised by FIB and SEM**

One of the simplest methods to replicate a surface structure is to deposit metal on the surface, and then separate the film from the original surface. By depositing gold on the diatom frustule it is possible to recreate the surface, and

gold is one of the materials often used to produce the first prototypes to see whether it is possible to recreate the surface at all. This subsection will focus on the sample preparation and the FIB- and SEM-characterisation.

### 3.3.1.1 Sample Preparation

A aluminum plate 1 mm thick is used as a substrate for the deposition to create a conductive contact towards the stage in the FIB. Multiple drops of diatom frustules suspended in methanol were dripped on the surface of the substrate. When the methanol was fully evaporated, diatoms were spread all over the substrate surface. This would give a large selection of frustules to choose from when later characterised. After the frustule deposition, the substrate was placed in an e-beam evaporator, and by using the device 500 nm of gold was deposited on top of the substrate. The interface between the gold film and the diatom frustule are the field of interest in the FIB investigation in the next paragraphs.

Table 3.3: Parameters used to deposit gold on the samples used to see how well a gold film follows the surface of a diatom frustule. Both the sample used in the cut-through and the lift-off of the gold film used these settings.

Electron beam evaporator settings	
Acceleration voltage	8 kV
Deposition rate	5 Å/s
Film thickness	500 nm
Material	Au

### 3.3.1.2 Cut-through with FIB

To get a preliminary result of how well the gold film follows the diatom frustule, a cut with FIB had to be made. Questions that had arisen before the FIB were; would there be voids, would the gold film follow the frustule, would the gold film have any cracks from stress that arose during cooling, and to what extent would the pore structure of the diatoms be replicated by the gold film. These questions motivated the characterisation with FIB.

Table 3.4: FIB settings used when investigating the internal frustule structure.

FEI Helios Nanolab	
Acceleration voltage of Ga-beam	30 kV
Acceleration voltage of SEM-column	30 kV
Working distance	4.2 mm
Aperture used for cutting (FIB)	93 µA
Aperture used for imaging (SEM)	9.3 µA

The sample was inclined to  $52^\circ$  and a FIB-cut through the gold film and frustule was done. The FIB cut were done normal to the substrate surface and with an acceleration voltage of 30 kV and current of  $93 \mu\text{A}$ . Afterwards the characterisation with SEM were performed at the same acceleration voltage as the FIB-characterisation, but with a current of  $9.3 \mu\text{A}$ . These settings gave the potential for high quality images of the cross-section of the interface between the gold film and the frustule.

### **3.3.1.3 Lift-off Gold Film with Tungsten Needle and FIB**

Although there have been attempts of removing gold films from diatom frustules before, there have been no experiments where microscale areas of gold film have been removed mechanically from the frustule. This experiment is an attempt to see how well an optimal replica of a diatom frustule can be made. The vibrations and distortions from a gold film separated from a frustule is difficult to control as the physical dimensions are so small. By using a tungsten needle in the FIB these vibrations can be reduced to a minimum, and a optimum replica obtained.

The sample were put into the vacuum chamber of a FIB and was not inclined. To get a cut which were accurate in depth, the sample were held normal to the electron column. This way the gallium beam would hit the sample with an angle of  $52^\circ$  from the normal vector to the sample, this would make it simpler to stop the sputtering in time to break through the gold film but not touch the surface of the frustule. By not breaking through the surface of the frustule it would retain enough strength to hold while the gold film were lifted of the frustule. As the sputtering in the FIB is optimised for silicon, all other materials would have different sputtering rates. Multiple trials gave eventually the correct depth set for sputtering.

An outline of a rectangle of the gold film was cut away from the rest of the gold film covering the surface of the frustule, apx.  $8 \times 8 \mu\text{m}$ . This was given with an angle of  $52^\circ$ , and due to the curvature of the frustule the rectangle might become disfigured. The curvature also might cause problems with the gold film becoming thicker or thinner in the direction which is parallel to the incident gallium beam. The problems would come in the form of not all the gold is sputtered away or too much is sputtered away by the gallium beam. If too much is sputtered away, the frustule might not be able to hold against the stress which is applied when trying to lift off the gold which is cut out from the rest of the gold film, and the frustule might break into pieces. If the sputtering is too shallow, the gold film will not be cut out from the rest of the gold, and they might be difficult to remove the gold rectangle from the frustule with the tungsten needle.

A rectangle-shaped trench  $0.07 \mu\text{m}$  deep and  $1 \mu\text{m}$  wide were cut out. The depth the sputtering were calibrated for silicon and other materials will have different sputtering rates. The rectangle shaped trench was about  $8 \times 8 \mu\text{m}$ . A tungsten needle was placed in contact with one of the edges of the gold square, and a layer of platinum  $2 \times 4 \mu\text{m}$  in height and width and  $2 \mu\text{m}$  thick was deposited, as seen in Figure 3.3. Afterwards the gold film was gently lifted from the frustule, the needle was then moved away from the frustule and rotated about  $180^\circ$ . This

Table 3.5: FIB settings used when lifting off the gold film. The depth of cut is calibrated for silicon

FEI Helios Nanolab	
Acceleration voltage of Ga-beam	30 kV
Acceleration voltage of SEM-column	30 kV
Working distance for FIB	16.5 mm
Working distance for SEM	4.1-4.2 mm
Aperture used for cutting (FIB)	93 $\mu\text{A}$
Aperture used for imaging (SEM)	9.3 $\mu\text{A}$
Depth of cut	0.07 $\mu\text{m}$

way the gold film was planted into the surface of the sample such that it stood out of the sample. The platinum glue was sputtered away by the gallium beam and the tungsten needle gently removed from the gold film. With the cut out gold film standing out of the sample, it was possible to take a look at the surface originally facing the frustule. The surface were investigated by SEM-imaging.

### **3.3.2 Manufacturing and Characterisation of Gold Film Templates**

One of the milestones that has to be reached before it is possible to use the diatoms to create texturation or diffraction grating is the ability to make templates from diatoms. By depositing a gold layer on diatom frustules and then removing the frustules a sample was made. The last step were to test and investigate to which degree a material can obtain the shape of the diatom by depositing a new material on the gold film shaped by the frustule. The investigations were done with a dual beam FIB.

#### **3.3.2.1 Sample Preparation and Gold Film Deposition**

Frustules were deposited on a glass substrate by evaporating off a methanol suspension with a high concentration of diatom frustules. The frustules were of the net plankton sampled from the Fjord of Trondheim. A microscope glass 3 mm thick and 2 cm in diameter was used as a substrate. Multiple drops of the suspension were dripped over the substrate to obtain a high concentration. On top of the microscope glass with frustules deposited on it, a 4.5  $\mu\text{m}$  thin film of gold were deposited by EBE. There is a chance that the frustules might be higher than the thickness of the gold film, a 4.5  $\mu\text{m}$  gold film might be sufficient thickness to cover all the frustules with gold.

After the gold was deposited, the gold film had to be removed from the substrate. Even though the gold film is not too good adhered to the surface of the gold it would be risky to separate those two mechanically, the gold film might tear and leave parts left on the glass substrate. To be sure the entire gold film is removed, the sample is placed in a HF solution. The film stayed in the HF solution

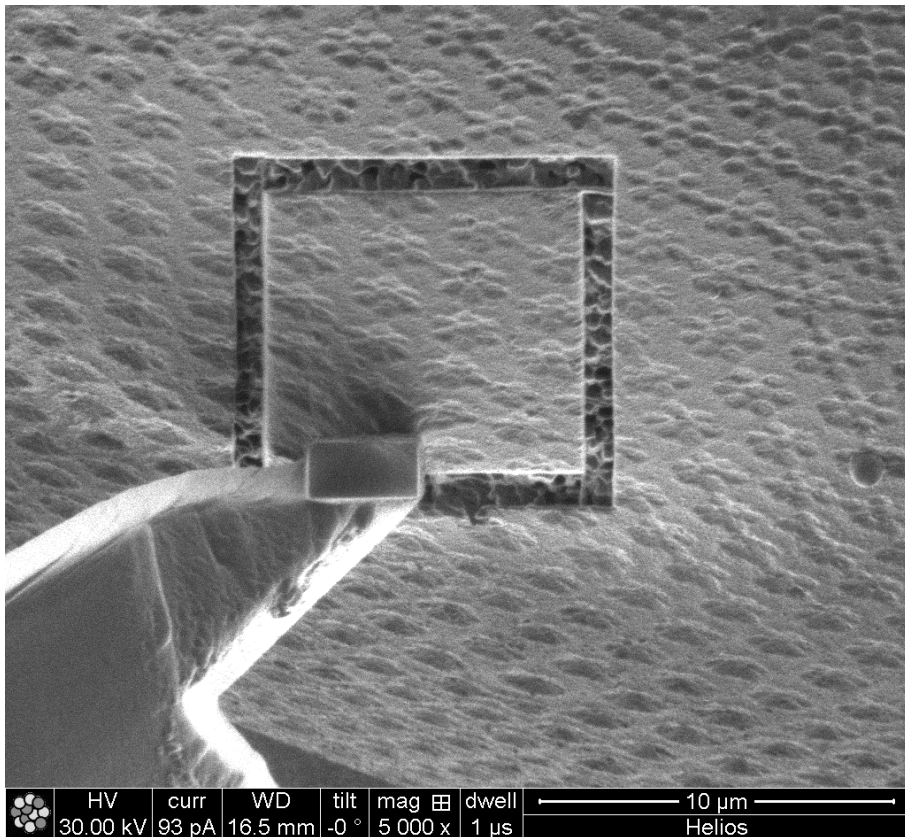


Figure 3.3: The trench sputtered away and the platinum square. The tungsten needle which will remove the gold film cut out of the rest of the gold film are entering through the lower left corner of the image. The part of the gold film chosen for removal is ‘glued’ to the tungsten needle by the platinum film.

until the glass was completely etched away. The gold film should now have the surface which faced towards the glass substrate completely free of glass, and the gold film should now be ready for further characterisation and processing.

### 3.3.2.2 Characterisation of Gold Film by SEM

The gold films were characterised by SEM and with a high acceleration voltage and aperture to ensure that any glass resin on the surface would charge-up and easy become visible. When no resin of glass was confirmed, the voltage and aperture were adjusted down to level where a high magnification and resolution of the SEM could be obtained. Images were taken at rather high magnifications to ensure that the gold film had replicated the diatom shapes, image magnification

Table 3.6: Parameters used to deposit gold on the glass substrates covered with frustules.

Electron beam evaporator settings	
Acceleration voltage	8 kV
Deposition rate	5 Å/s
Film thickness	4500 nm
Material	Au

Table 3.7: Parameters of the HF etch

HF etch	
Concentration	48 %
Time in etch	18 h

are given at every image taken. The working distance was short to gain a good signal and image, while the current were kept out of high current mode as there were none EDS characterisations done.

Table 3.8: SEM settings used when investigating the gold films.

Zeiss Ultra 55 and Zeiss Supra 55 VP settings	
Acceleration voltage	20-30 kV
Working distance	5 mm
Aperture size	30 µm
High current mode	Off

## 3.4 Part III: Deposition and Characterisation of Amorphous Silicon and Silicon Nitride on diatom frustules

### 3.4.1 Characterisation of Amorphous Silicon Film Deposited on Frustules by SEM and FIB

Silicon is a material very often used both for thin film solar cells and conventional silicon solar cells. In conventional silicon solar cells the wafers are cut out of a single ingot of silicon, and they are processed to become solar cells thereafter. For thin film solar cells based on silicon, the approach of manufacturing is different. Instead of cutting an ingot into slices and treat the wafers, a substrate is used as a foundation for depositing amorphous or nanocrystalline silicon to form a thin film solar cell. The silicon is deposited by PECVD on the substrate, and in

this way the solar cells become very thin and hence the cost of thin film solar cells might be reduced compared to conventional solar cells.

### 3.4.1.1 Sample Preparation

The samples prepared for this experiment were designed to have a simple structure. An aluminum substrate was used as foundation for the structure, with its conductive properties it would give potential for good images and no charge-up in the SEM or FIB modes. On the aluminum substrate there was dripped some drops of a methanol suspension containing cleaned diatom frustules from the net plankton. The methanol evaporated off the substrate, leaving the frustules spread across the aluminum plate.

Silicon and silicon dioxide have a very similar brightness in the SEM, to make those two materials easier to separate a 5 nm thick layer of gold was sputtered on top of the frustule and aluminum surface with a sputter coater. Gold have a high brightness and made the frustule and golf film easier to separate from each other. The sample was placed in a PECVD where 250 nm of amorphous silicon were sputtered on the substrate. The sample were then supposed to go to FIB-characterisation, but while investigating the sample charge-up was registred, and to prevent this a new 5 nm thick gold layer was sputtered on top of the silicon layer. The experimental details can be seen in Table 3.9.

Table 3.9: Parameters used to deposit amorphous silicon for preliminary results on how silicon and diatom frustules interact. The gas flow is measured in standard cubic centimeters per minute (sccm).

Plasma-Enhanced Chemical Vapour Deposition Device settings	
Chemical reaction	$\text{SiH}_{4(g)} \longrightarrow \text{Si}_{(s)} + 2\text{H}_{2(g)}$
Reaction product	Amorphous silicon
Gas flow of silane ( $\text{SiH}_4$ )	25 sccm
Gas flow of argon (AR)	475 sccm
Approximation deposition rate	25 nm/min
Total deposition time	10 min
Approximate thickness of film	250 nm

### 3.4.1.2 Cut-through with FIB

FIB-characterisation was performed to investigate how the silicon thin film interact with the diatoms frustule. By cutting through the silicon film and the diatom frustule images of the interface could be obtained. The sample were put into the vacuum chamber of the FIB, and the sample was tilted to 52° to cut normal to the sample surface. By removing a width of approximately 4 μm it was made possible to investigate the cross-section of the layered structure. A beam current of 93 μA was used to make the cut. The gallium ions have have so much energy when hitting the sample, that they sputter away the silicon and frustule

when hitting the surface. After the sputtering was done, the mode was changed to SEM and to a much lower current (9.3  $\mu\text{A}$ ), and images of the cross-section were obtained.

Table 3.10: FIB settings used when making a cut through the silicon film on the frustule surface.

FEI Helios Nanolab	
Acceleration voltage of Ga-beam	30 kV
Acceleration voltage of SEM-column	30 kV
Working distance	4.1 mm
Aperture used for cutting (FIB)	93 $\mu\text{A}$
Aperture used for imaging (SEM)	9.3 $\mu\text{A}$

### 3.4.2 SEM and FIB Characterisation of Silicon Nitride Film Deposited on Frustules

Silicon nitride is a material often used for anti-reflective coatings in solar cells. An imprint made by a mould of diatoms might prove effective for texturation for anti-reflective coatings. By depositing a thin layer of silicon nitride on diatom frustules the potential for replicate the diatom structure can be investigated. By cutting through the structure and investigating the cross-section of the diatom frustules and silicon nitride film, any sign of voids and gaps between the two materials can be detected.

### 3.4.3 Sample Preparation

An aluminum substrate 1 mm thick was prepared as the sample substrate. Diatoms from the net plankton were spread across the surface of the aluminum substrate by dripping a methanol suspension containing frustules, and then wait till the methanol evaporated off the substrate. In this way the frustules were left at the substrate surface for later processing. The next step was to coat the frustules and the rest of the exposed aluminum surface with 5 nm of gold to get a contrast layer between the frustules and and the silicon nitride film. Silicon nitride is very hard to investigate in SEM due to its low contrast to silicon dioxide, which is the material the diatom frustule consist of. The sample was placed in a PECVD-device where 250 nm of silicon nitride was deposited. To gain sufficient conductivity, the sample was put into a sputter coater after silicon nitride deposition to obtain a surface layer of gold. 5 nm of gold was deposited on the sample surface.

#### 3.4.3.1 Cut-through with FIB

To cut through the surface of a frustule with a thin film deposited upon is a rather straightforward task, but when the sample have a low conductivity the

Table 3.11: Parameters used to deposit silicon nitride to investigate how silicon nitride and diatom frustules interact. The gas flow is measured in standard cubic centimeters per minute (sccm).

Plasma-Enhanced Chemical Vapour Deposition Device settings	
Reaction product	Silicon nitride
Gas flow of silane (SiH <sub>4</sub> )	20 sccm
Gas flow of ammonium (NH <sub>3</sub> )	20 sccm
Gas flow of argon (Ar)	980 sccm
Approximation deposition rate	10 nm/min
Total deposition time	25 min
Approximate height of film	250 nm

charge-up can cause some problems, hence the extra gold layer on top. The layered structure was placed in a FIB and some frustules were chosen for characterisation, and the sample were tilted to 52° from the horizontal plane. Cuts 8–10 μm long and 3–4 μm wide were done by the gallium beam. The current was high, 93 mA, and a high acceleration voltage (30 kV) was used to cut through the frustule and silicon nitride thin film. After the cuts were made, the SEM column was engaged. The SEM-column operates at a much lower current than the FIB-column, 9.3 μA but the same acceleration voltage. The thought about using such a high acceleration voltage was that the electrons would pass through the nitride layer and settle into the silicon dioxide frustule and aluminum substrate underneath the silicon nitride film. Images were taken for investigation of the interface between the frustule and silicon nitride film. The experimental details for FIB characterisation can be seen in Table 3.12.

Table 3.12: FIB settings used when making a cut through the silicon nitride film and the frustule to investigate the interface region and cross-section between the two materials.

FEI Helios Nanolab	
Acceleration voltage of Ga-beam	30 kV
Acceleration voltage of SEM-column	30 kV
Working distance	4.2 mm
Aperture used for cutting (FIB)	93 mA
Aperture used for imaging (SEM)	9.3 μA

## **3.5 Part IV: Manufacturing and Characterisation of Structures similar to Solar Cells**

Analysis of the different structures with diatom frustules incorporated would be of great interest to any further research of diatoms for use as light harvesting materials in solar cells. To make a good and thorough survey of possible utilisation of diatom frustules in solar cells, the analysis of the structural properties is important. In this subsection the preparation of samples for reflection from the cell structure will be explained. Experimental details of the analysis of the given structures will also be presented in this subsection.

### **3.5.1 Sample Preparation**

Structural analyses are important to investigate the effect texturation by diatoms have for solar cells. Four samples, all with different structure, were assembled for reflectivity measurements. Two samples were manufactured to be examples of possible thin film structures. The two last samples were manufactured to be examples of crystalline silicon solar cells with texturation made by diatoms instead of an acidic mixture. The differences and objectives with all set-ups will be explained in detail in this subsection.

#### **3.5.1.1 Preparation of Thin Film Samples**

Glass substrates were prepared as the basic structures for the thin film measurements, the structure consisted of glass, aluminum, diatom frustules and amorphous silicon. The difference between the two samples prepared upon a glass substrate, is the sequence the materials is deposited in. The sequence could alter the objective of the experiments and investigate different effects from the cell structures.

For one of the samples, a thin aluminum film was deposited by EBE on the glass, and the methanol dispersion containing frustules were dripped on top of the aluminum. For the experimental details of EBE-deposition, see Table 3.13. The dispersion dried off and left a layer of randomly oriented frustules on the surface of the aluminum. On top of the frustules a layer of amorphous silicon was deposited by PECVD, making the layered structure seen in Figure 3.4(a). For the experimental details of the silicon deposition, see Table 3.14.

For the other sample, the aluminum layer was deposited directly on the glass substrate by EBE. On top of the aluminum the methanol dispersion containing diatom frustules was dripped, and the methanol evaporated leaving the frustules on the surface of the aluminum film. To finish the structure a layer of amorphous silicon was deposited by PECVD on top of the frustules. The resulting structure can be seen in Figure 3.4(b).

The objective of making a thin film structure with a layer of frustules between the glass and the thin film of aluminum is to transfer the porestructure over to the top of the aluminum. This way the light reflecting of the aluminum surface

Table 3.13: Parameters used to deposit aluminum during the manufacturing of the thin film samples. Both the glass-frustule-aluminum-silicon and the glass-aluminum-frustule-silicon set-up used these settings.

Electron beam evaporator settings	
Acceleration voltage	8 kV
Deposition rate	5 Å/s
Film thickness	50 nm
Material	Al

Table 3.14: Parameters used to deposit amorphous silicon during the manufacturing of the thin film samples. Both the glass-frustule-aluminum-silicon and the glass-aluminum-frustule-silicon set-up used these settings. The gas flow is measured in standard cubic centimeters per minute (sccm).

Plasma-Enhanced Chemical Vapour Deposition Device settings	
Chemical reaction	$\text{SiH}_{4(g)} \longrightarrow \text{Si}_{(s)} + 2 \text{H}_{2(g)}$
Reaction product	Amorphous silicon
Gas flow of silane ( $\text{SiH}_4$ )	25 sccm
Gas flow of argon (Ar)	475 sccm
Approximation deposition rate	25 nm/min
Total deposition time	200 min
Approximate height of film	5 $\mu\text{m}$

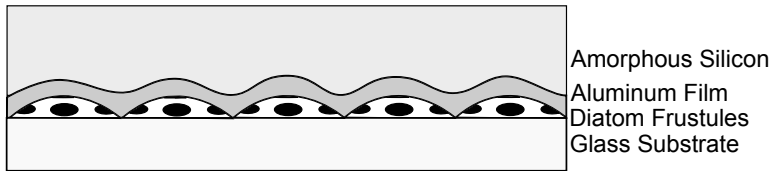
will gain a longer mean path through the cell, hence giving a higher absorbance in the entire part of the light spectrum in question.

The light-focusing properties shown for certain species of diatoms might be turned into light-scattering properties. The cell is far out the focus plane of the diatom frustule, and hence is the light scattering away from the focus point. Another possible effect is the principles of Snell's law, which will cause a light wave of bend when passing between two mediums with different refractive indices. The combination of these two effects can not be modelled easily, and further investigation of prepared samples are needed.

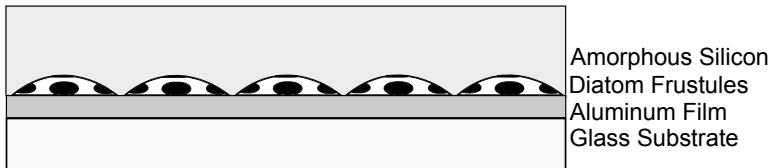
### 3.5.1.2 Preparation of Crystalline Silicon Samples

Silicon substrates were prepared from monocrystalline silicon wafers to be structural support for the layers which were deposited on top of the substrate. The samples had a simpler structure than the thin film samples prepared for similar analysis. The silicon wafers was deposited with silicon nitride and methanol dispersion. One of the samples was deposited with a single layer of diatoms between the wafer and the nitride layer, while the other had a nitride layer between the diatoms and the wafer as well.

The sample with a single silicon nitride layer started out as a silicon



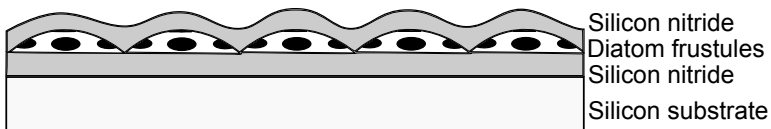
(a) Schematic of thin film cell. Glass substrate with frustules dried, and aluminum deposited on the frustules afterwards to attempt to transfer the surface structure of the frustules to the film. Amorphous silicon deposited on top of the cell structure.



(b) Schematic of thin film cell. Glass substrate with aluminum deposited on top. The diatom frustules were dried on the aluminum film on top of the glass substrate. The cell structure was rounded off with amorphous silicon deposited by PECVD.



(c) Schematic of silicon solar cell. A polished silicon substrate were used as the structural support. Methanol dispersion containing diatom frustules were dripped on the surface of the silicon, and after the dispersion was dried off, a thin film of silicon nitride were deposited on top of the frustules.



(d) Schematic of silicon solar cell. Polished silicon covered with silicon nitride at the bottom. Diatoms were dripped at the top of the silicon nitride, to give a texture to the last silicon nitride layer deposited on top of the structure.

Figure 3.4: Schematics of cross-sectional cut through the structures which were analysed with regards of light harvesting properties. The schematics are not in scale.

piece which were grinded. The silicon was grinded to remove any silicon dioxide which could have formed on the surface of the wafer, and this way obtain a reflective silicon surface. A methanol dispersion containing a high amount of diatom frustules was dripped on the wafer surface, the dispersion evaporated off, leaving the frustules on the surface of the wafer. More dispersion was then dripped on the surface of the wafer, and this was repeated 5-6 times to a high concentration of diatoms was gained. The Wafer with frustules on top was then placed in the PECVD for deposition of silicon nitride on the wafer. The resulting structure can be seen in Figure 3.4(c)

For the sample with two silicon nitride layers the silicon nitride wafer had to be grinded to remove the oxide. After grinding the wafer was placed in the PECVD to receive its first silicon nitride layer. After deposition the same process with dripping of methanol dispersion was done on this wafer, as with the sample with a single layer of nitride. After deposition of diatoms on the surface of the silicon nitride, a second layer of silicon nitride was deposited on the sample. The schematic of the double silicon nitride layer are seen in Figure 3.4(d)

The objective of making a sample with a single layer of silicon nitride is to see whether or not a texturation with the use of diatom frustules, or the surface of the frustules will have an effect on the light harvesting of silicon solar cells. A more textured surface will have less reflections, and the normal industrial procedure is to deposit a single layer of silicon nitride, hence the sample might gain similar properties as a solar cell produced by the industry.

With a single layer of silicon nitride, it is still possible for some light to pass through the diatom, hit the surface of the wafer and be reflected from the wafer, some of the photons reflected from the wafer will leave the cell and might cause suboptimal light harvesting properties. This is where the second layer of silicon nitride comes into the picture. By placing a second layer of silicon nitride between the diatom frustules and the wafer some of the photons which were lost with a single layer would be absorbed by the wafer instead, and might cause better light harvesting properties than the single layer set-up.

Table 3.15: Parameters used to deposit the different layers of the crystalline silicon structure. The gas flow is measured in standard cubic centimeters per minute (sccm).

Plasma-Enhanced Chemical Vapour Deposition Device settings	
Chemical reaction	$\text{SiH}_4(\text{g}) + \text{NH}_3(\text{g}) \longrightarrow \text{Si}_3\text{N}_4(\text{s}) + 2\text{H}_2(\text{g})$
Reaction product	Amorphous silicon
Gas flow of silane ( $\text{SiH}_4$ )	20 sccm
Gas flow ammonium ( $\text{NH}_3$ )	20 sccm
Gas flow argon (Ar)	980 sccm
Approximation deposition rate	10 nm/min
Total deposition time	7 min
Approximate heigth of film	5 $\mu\text{m}$

### **3.5.2 Analysis of Solar Cell Structures**

The analysis of the different structures of silicon and silicon nitride was necessary to investigate how the deposited materials behave around the frustules. Frustules with no metal coating on top will have an electric field which may cause the silicon and silicon nitride to be deposited uneven across the sample surface. With this motivation cuts with FIB and investigation in SEM were done.

In addition of the SEM and FIB investigations, there were also performed investigations in light microscope to see how the light behaved in the structures made. Interesting features were how the frustules and the area between the frustules reflected the light, and if the frustules would adhere to the surface just by drying them, or if any fixative has to be used for future experiments.

#### **3.5.2.1 Characterisation of the Structures by Light Microscope**

An optical investigation of the solar cell structures would reveal if much light escape from the, more absorbing structures would be darker in a light microscope. This is why light microscopy were preferred to SEM for this purpose. The two types of cells will have different ways of reflecting light. The crystalline solar cells an antireflective coating, while the thin film cells have not. This means that light emitted from the crystalline solar cells would be of the colour the antireflective coating are. The thin film cells does not have diatoms on top, but on the bottom. These are supposed to diffract light and cause a longer mean pathlength of the light in the solar cells. Any structural flaws were also imaged for later characterisation in SEM and FIB.

The thin film samples were investigated with both bright field and dark field settings on the microscope. Dark field images the rays which are deflected by the sample, while bright field images the light waves returning from the sample close to the center line of the microscope. This will give information whether or not the light have been deflected by the diatom frustules.

For the crystalline silicon samples a check of how the light behaved through the antireflective coating were performed. By checking how the light reflected from the diatom frustules, if any diffraction patterns arose, the potential for antireflective texturation could be evaluated from the images. both the silicon piece with a single and two layers of silicon nitride were investigated by this method.

#### **3.5.2.2 Characterisation of the Structures by FIB**

Around the diatom frustules during deposition there will be an electric field which is not normal to the substrate. As one of the controlling parameters during deposition is this electric field, the film thickness can be lower or higher in the area close to frustules. The thickness of both the amorphous silicon and the silicon nitride is important for solar cell manufacturing, and how the diatom structure influence the deposition would be of great interest. Around the diatom frustules there was made cut to measure the thickness, both the amorphous silicon and silicon nitride layers were cut to investigate how the thickness of the deposited films changed across the surface of the diatom.

Table 3.16: FIB settings used when investigating solar cell structures.

FEI FIB-200 settings	
Acceleration voltage of Ga-beam	30 kV
Acceleration voltage of SEM-column	30 kV
Working distance	4.2 mm
Aperture used for cutting (FIB)	93 $\mu\text{m}$
Aperture used for imaging (SEM)	9.3 $\mu\text{m}$

---

## 4. Results

In this chapter the experimental results and facts will be presented. SEM and FIB pictures important to the following discussion and conclusion will be presented in this chapter as well. Every experimental result from characterisation of diatoms to the preparation and analysis of thin film samples will be presented thoroughly here. Due to the large span in different samples and tests conducted on the samples, a survey of the results obtained will be presented.

To attain the results, the different characterisation techniques presented in section 2.4 were utilised. By SEM, FIB and light microscopy the diatoms and their potential to use in solar cells were investigated. The results will form the base for which the remaining part of the thesis was built, namely the discussion and conclusion.

### 4.1 Part I: Characterisation of Diatom Frustules and Their Pore Structure

The diatoms that were cleaned were of two different samples, and images done by SEM revealed different structures in the net plankton and the sample cultivated in the lab. For diatoms a species is defined by the same shape and pore structure of the diatom frustule. Even a small difference of the structure between two specimens is enough to characterise them as two different species. It is important to know that different species also might have different surface properties even though they are structurally closely related.

#### 4.1.1 SEM-characterisation of *Coscinodiscus walesii*

The cultivated species was characterised as the diatom *Coscinodiscus walesii*, while the species in the net plankton remained unidentified, and will be denoted *Coscinodiscus sp.* in this thesis. The different structures in the two samples are different in not only the surface layer but also further into the frustule as well.

The *Coscinodiscus walesii* was imaged to obtain good references for its structure, and the images of the pore structure can be seen in Figure 4.2. With the foramen in the surface, there is no layer of pores at the inner surface of the frustule different from the outer layers.

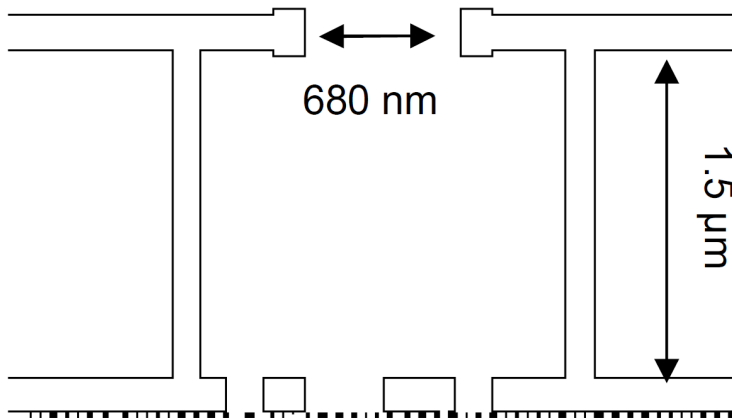


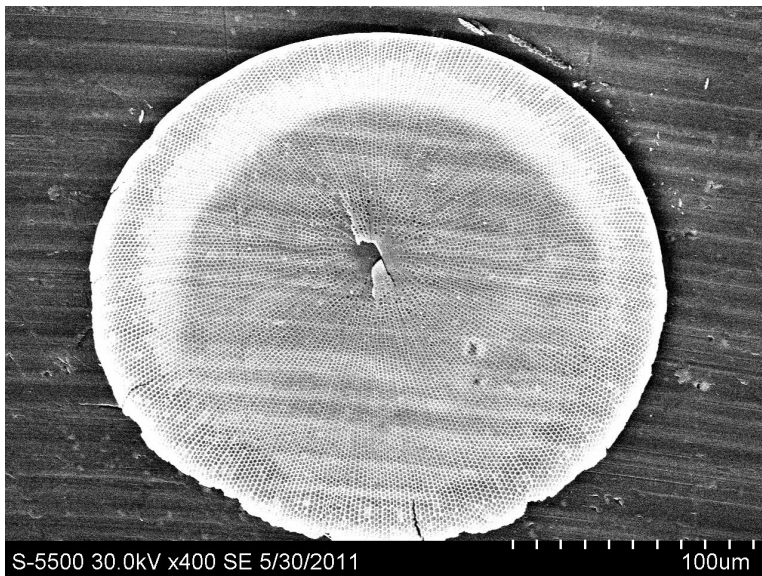
Figure 4.1: Schematic of the pore structure of *Coscinodiscus walesii*. The outside of the frustule is towards the bottom of the schematic. [Ottesen et al., 2011]

Another issue that is revealed by the SEM images is the quality of the acidic wash. Small amounts of material was cleaned in every batch, as all the material is washed in one batch, the quality will be more or less equal between every diatom. Figure 4.2(b) revealed a reduced quality of cleaning. The surface and insides of the diatoms are well cleaned, but the pore structure is not that well cleaned. The cribellum are worst cleaned, and the pore structure which should have clear pores with a diameter of 40 nm have more material present than what has been washed away.

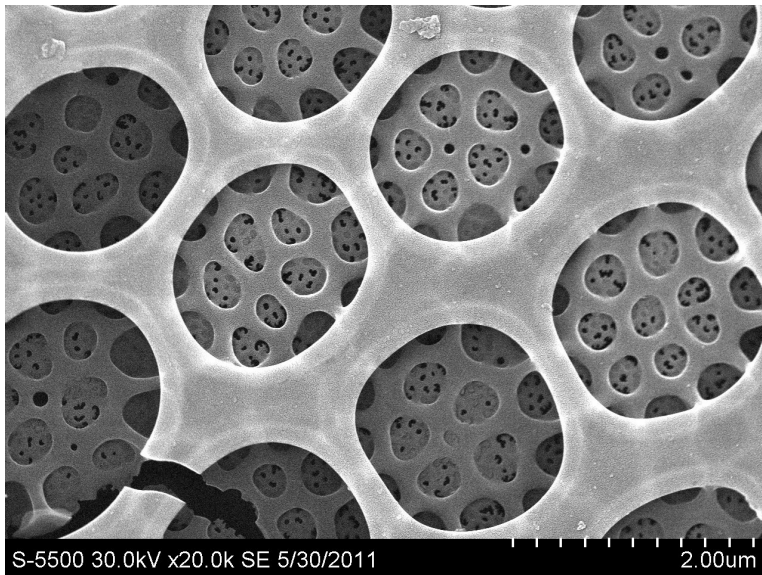
#### 4.1.2 SEM-Characterisation of the *Coscinodiscus sp.*

For the net plankton, the situation was different. By investigating the frustules in SEM it was decided the structure were different from the *Coscinodiscus walesii* and had a layer of pores at the inside of the areola. The SEM images revealed both a pore structure very similar to the cultivated diatoms at the outside of the frustule, while the inner side of the frustule had circular pores. The inner layer is very similar to the foramen, and the wall between them are present in both diatoms. The wall is to work as a beam for structural support.

The quality of the washing was also evaluated for the *Coscinodiscus sp.*, for this batch there clear signs of very well washed frustules. Most of the cribellum were washed away, leaving the cribrum standing alone as a pore in the nano-range. The SEM-images from the SEM-session are Figure 4.3–4.4. While the low magnification images show that the large majority of the organic material is dissolved, the high magnification images show that the structure of the smallest pores have been etched away during cleaning.

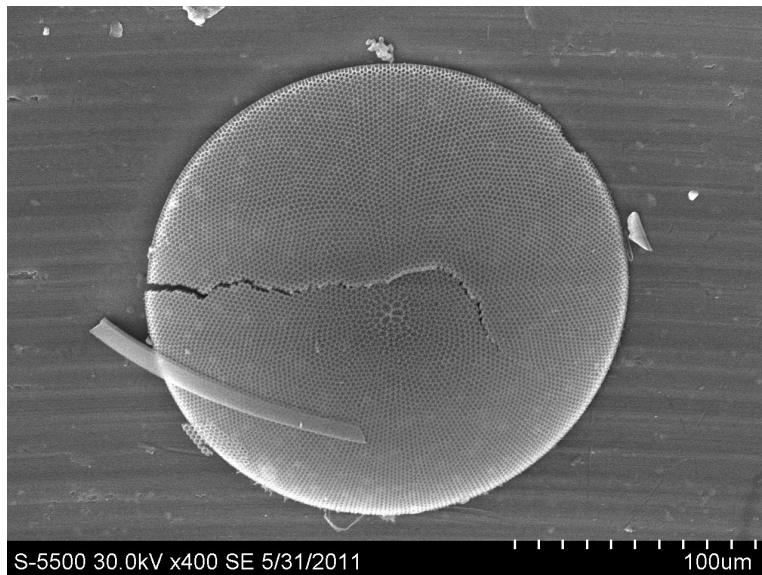


(a) An entire thecae dried on an aluminum substrate. Some cracks and structural faults are visible.

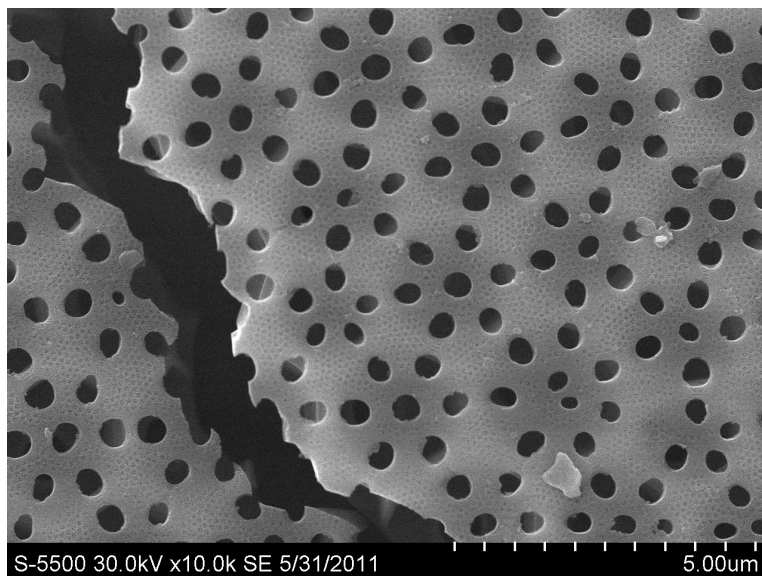


(b) A closer view of the hexagonal structure the foramen and foramen make up in the surface of the frustule.

Figure 4.2: Images with magnification of the structure of *Coscinodiscus walesii*

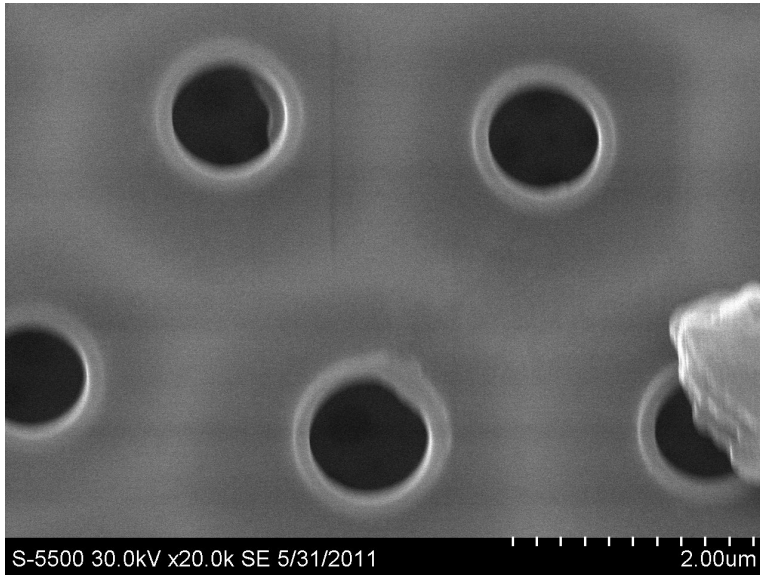


(a) A diatom frustule of the net plankton with the outer pore structures facing away from the substrate.

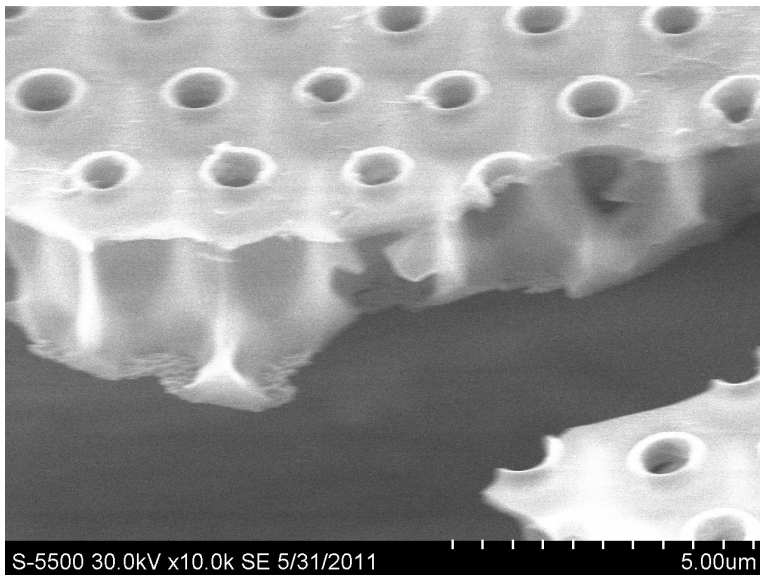


(b) SEM-image that show the clear pore pattern for the cribrum, and also the missing cribellum of the frustule.

Figure 4.3: SEM-images with low magnification of *Coscinodiscus sp.* Showing the complexity of the pore structure.



(a) High magnification image of the diatom's formamen, even the walls of the areola is visible through the inner surface of the frustule.



(b) SEM-image of cross-section of a frustule with all the types of pores visible. On top the foramen, in the middle the areola and at the bottom the cribrum and cribellum.

Figure 4.4: SEM-images with of the *Coscinodiscus sp.* areola structure.

The holes on the inside of the net plankton's frustule are circular holes with an edge which is elevated from the inner surface. A hexagonal pattern is made out of the holes which are very uniform in size and distribution across the surface. The foramens are about 680 nm in diameter and placed 1.8  $\mu\text{m}$  apart. Every areola contains a cluster of cribrum on the outer surface and a foramen at the inner surface.

In Figure 4.4(b) it is possible to see the cross-section of the diatom frustule from the inside. The foramen and areola are easy to distinguish, while the outer layer can be seen at the bottom of the cross-section. The outer pore structure seems to be more complete on the frustule captured in Figure 4.4(b) than in Figure 4.3. This difference will be discussed further in the chapter about discussion.

## 4.2 Part II: Manufacturing and Characterisation of Gold for Use as Templates in Solar Cell Industry

### 4.2.1 Deposited Gold Film Characterised by FIB and SEM

There were several experiments with gold film and different characterisations. Several cuts by FIB were performed to check the conformity and quality of the gold film. In addition it was made attempts of removing parts of the gold film in the FIB.

#### 4.2.1.1 Cross-sectional Cuts by FIB on Gold Film

The gold film deposited by EBE was going to be cut by FIB and investigated by the electron column in the dual-beam FIB. The cultivated plankton were chosen for FIB, and both the inside and outside of the diatom frustule were sampled to test to what extent it is possible to template a frustule surface.

The cross-section images of the gold film reveal how the gold film and diatom frustule follow each other. There were made cut on several places on the outside of diatom frustules and of the inside, including the girdle band. The EBE gives a very conformal layer of gold, and all surfaces facing towards the target will be covered in gold.

The gold film appear to a have covered the top as well as the sides of the diatom frustule in Figure 4.5(a), and no large uncovered areas of frustule. The 500 nm of gold has made a conformal layer over the entire frustule. Figure 4.5(b) give an overview of a cut with FIB, and the pore structure that lays beneath the gold film. The gold film appear to follow the frustule very well, and Figure 4.6 clearly show that there are no inner pore layer as in the *Coscinodiscus sp.*

Figure 4.6 give a good sight of the cross-section and how the pore structure and gold film separates over the pore. And this rise the question whether or not the surface of the frustule is replicated by the gold film. An issue which may

arise is how well the gold follow the vertical walls down towards the pores in the surface.

In addition to the outer surface of the diatom, the cultivated diatoms are lacking the inner foramen as the net plankton have. Instead at the inner surface there are a rough porous structure which acts as structural support. Figure 4.7 shows the inside of a *Coscinodiscus walesii* frustule. The foramen goes radially out of the center of the thecae, and when the distance between two pores have grown sufficiently, a new row of foramen appears between two existing rows.

In Figure 4.7 it is easy to distinguish the gold film on top of the frustule and the frustule beneath it. Each foramen contain many cribrum, and it also appear the gold penetrates deep into the pore structure, leaving deep pits in the surface of the gold film. In Figure 4.7 it is easy to see the gaps in the structure between the gold and frustule. The black pores in the surface runs the entire depth from the top of the film into the deep pores of the frustule, where the gold have not been able to form a film in the entire frustule.

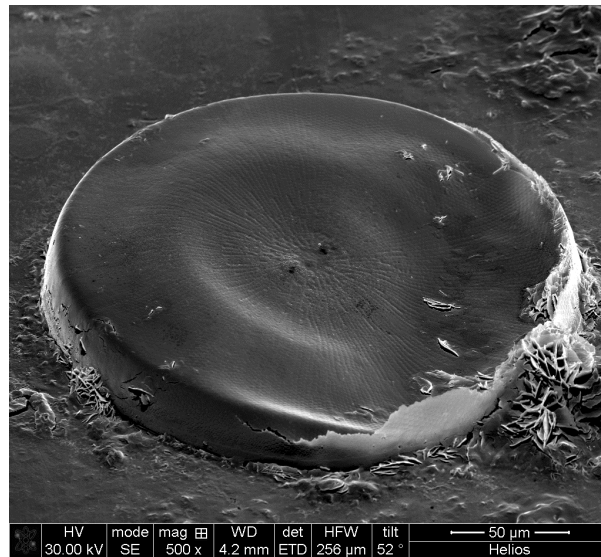
#### 4.2.1.2 Removal of Micrometer Sized Sheet of Gold from Diatom Frustules

Even though it has been papers describing separation of a gold film mechanically from frustules, it has been no attempts of removing parts of the gold film with a tungsten needle. A tungsten needle would be great to check what the optimum template would look like. A tungsten needle does not vibrate much, and that would eliminate the risk of the gold film's structure being reduced by a shaky hand or other possible vibrations.

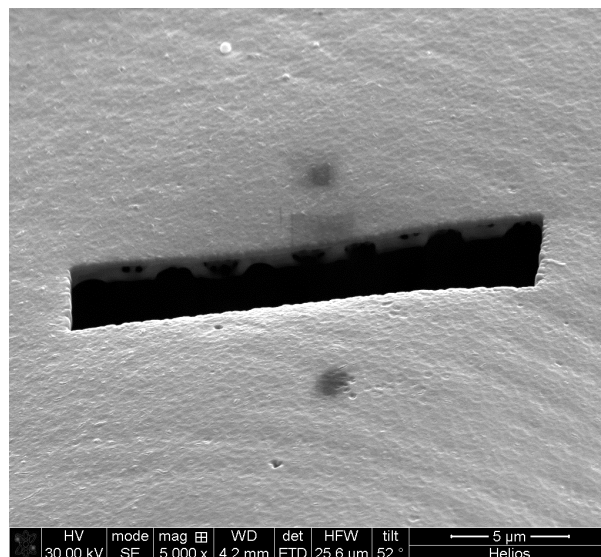
Figure 4.8(a) shows a rectangle cut out of the gold film. The tungsten needle comes into the image from the left and is connected with the gold film with a deposited platinum film. The rectangle is removed and the frustule laying beneath the gold film rectangle is in Figure 4.8(b). It is easy to see that there are a thin layer of gold left where the cut have been made, but the rectangle came of gently anyhow. In the upper right of the image, a dust grain is laying in the middle of a cribrum. It is also possible to see some faults in the cribrum. The image also reveals that the cribellum is present over the entire surface of the frustule, and in some of the cribrum the cribellum is missing. Another feature in the image is small gold dots spread across the surface of the frustule.

Figure 4.9 are SEM-images of the gold film which was removed from the frustule. A cribrum in Figure 4.8(b) had a dust grain on top of itself, and the mould after it can be observed in Figure 4.9(a). In Figure 4.9(a) prints after the cribrum can be seen in the gold film. They are easy to identify as the clusters in the gold film are identical to the clusters in the frustule. Some places it is possible to see the parts of the cribellum, which have been torn off the frustule as the gold film were lifted off the structure. The cribellum are easy to see in the area surrounding the cribrum clusters, while very few signs of the cribellum is visible in the cribrum clusters.

In difference from other cribrums, there is a cribrum in Figure 4.9(a) which have a very well defined pore structure. In Figure 4.9(b) this cribrum is the



(a) Overview of the a diatom frustule covered with 500 nm of gold, it was later cut by the gallium beam to give a view of the interface between the gold film and diatom frustule.



(b) SEM-image showing area where the cut were made. The cross-section of the diatom thecae and gold film are visible. The gold film is the light layer on top, while the frustule is the dark shade below.

Figure 4.5: Images captured during the FIB-session to cut through the goldfilm and look at the interface between the two materials.

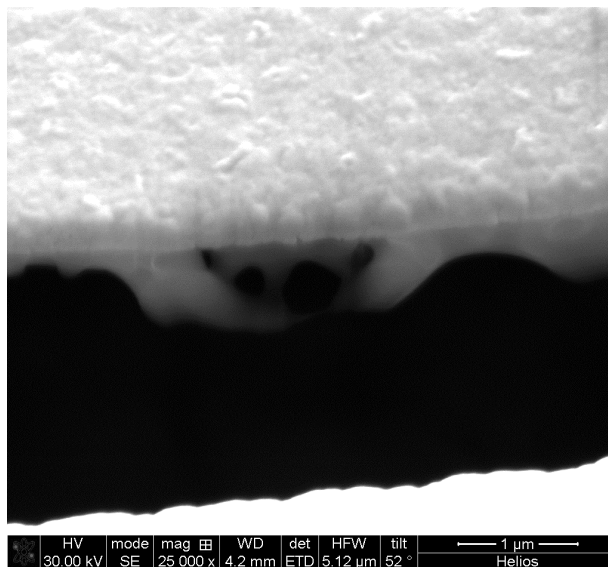


Figure 4.6: High magnification image of the cross-section revealing that the gold film is following the surface of the diatom, but not down in the pores.

focus. A very well defined cribellum mould was defined, and at the same place in Figure 4.8(b) the cribellum structure is missing. In the area outside the cribrum cluster, the cribellum is still easy to see, with a pore size around 40 nm.

Figure 4.10 is SEM-images of the same gold film, but those images are taken with an angle nearly parallel with the surface of the gold film. The moulds of the clusters of cribrum are visible on the surface which faced the frustule. The aim of investigating the profile of such a structure is to find out how the mould would be after a separation from the frustule. In Figure 4.10(a) it is easy to see that every cribrum cluster is about equally in topography, and the area outside the clusters is completely flat if the cribellum structure is ignored.

Figure 4.10(b) is a higher magnification of the same area as in Figure 4.10(a). The cribellums outside the cribrum cluster moulds are easy to see, but it is also possible to see the cribellums in the cribrum moulds. The cribellum replicas are not very good, but they are clearly there. The quality of the cribellum moulds are also varying, the highest quality of replicas are along the edges of the cribrums, while the replica quality is reduced along the edges. Whether or not this is an important feature will be discussed later.

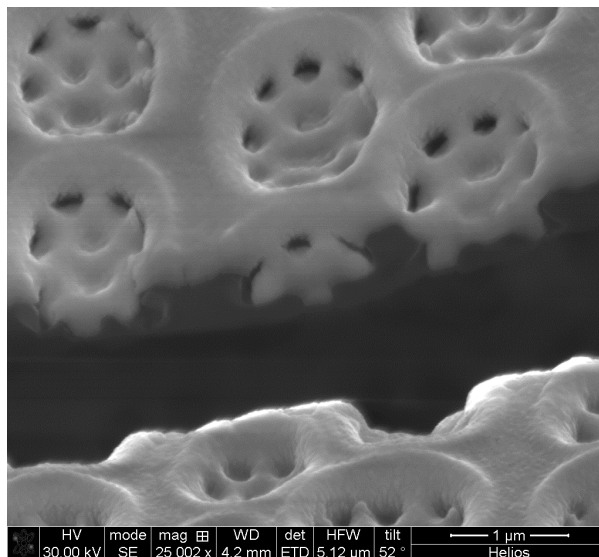


Figure 4.7: SEM-image of the inner side of a diatom frustule covered in gold. The gold is shown to penetrate the frustule, but also leaves some empty room where the gold has not been able to form a film.

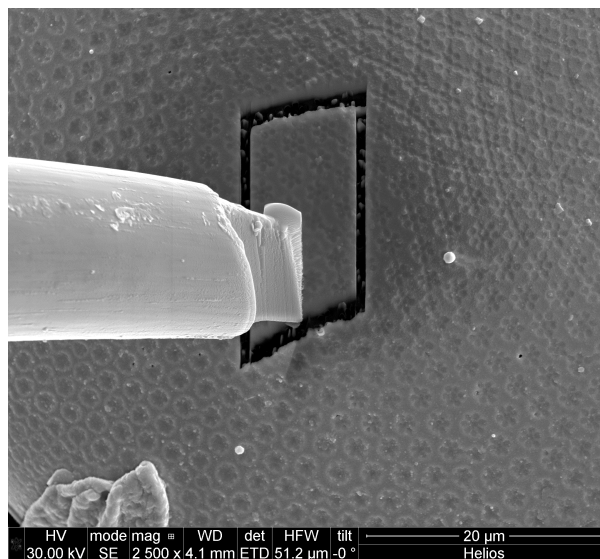
## 4.2.2 Manufacturing and Characterisation of Gold Film Templates

Cleaned diatom frustules were dried on a glass substrate. Gold was evaporated onto the substrate to try to make a print of the diatom frustules. The glass substrate and most of the diatom frustules were dissolved by the HF etching, and the gold film were put in SEM for characterisation.

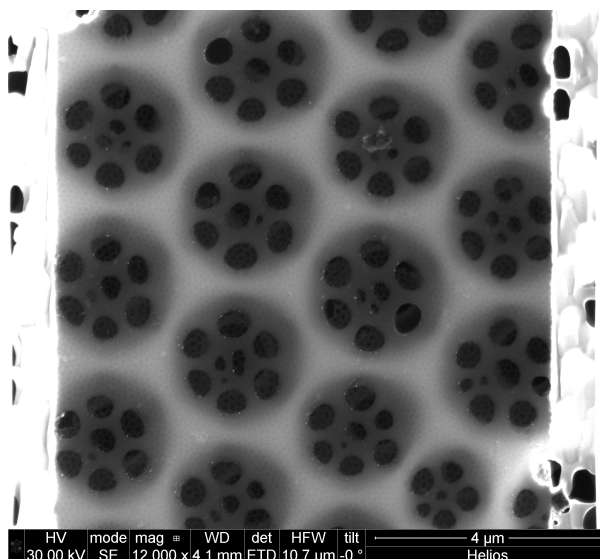
### 4.2.2.1 Characterisation by SEM after Etching

The diatom frustule were etched away by the HF etch. In the gold film there was many holes of the same size as the diatom frustule, a clear sign of diatom frustules have come loose from the gold film. In Figure 4.11(a) it is possible to see that the areola have been replicated over the entire surface of the diatom frustule. A crack in the surface of the frustule has made a wedge from the edge of the print and towards the middle of the print. There are also some holes in the print, this might be from pieces of broken frustules which have been laying on the frustule surface during deposition of gold.

Figure 4.11(b) is a higher magnification image of the same frustule as in Figure 4.11(a), the areola and cribrum are replicated with a high quality. The periodic pore pattern of the areola are replicated all the way from the centre of the valve to the edges. In the cribrum there are no signs of the cribellum.

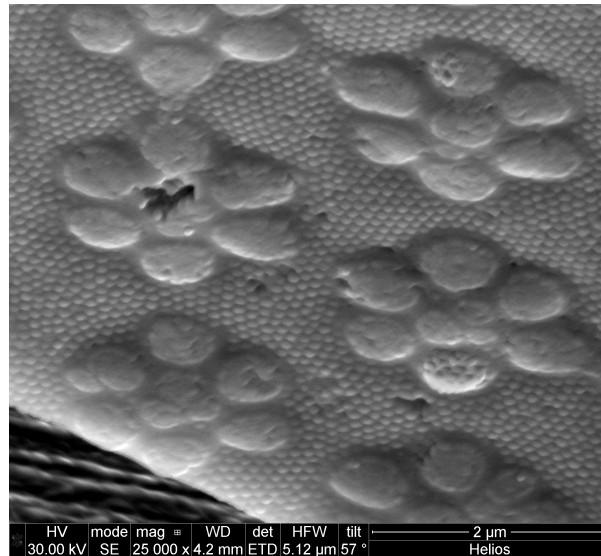


(a) SEM-image of the rectangle cut out for removal. The tungsten needle used for removal of the film is entering through the left edge of the image.

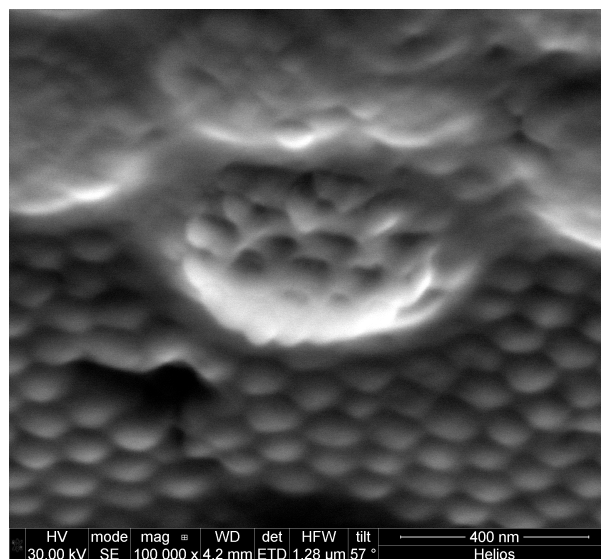


(b) A view of the pore pattern beneath the part of the gold film which were removed. A dust grain is visible, and it is clear that there are a thin layer of gold left where the cut were made.

Figure 4.8: SEM-images of the gold rectangle cut out of the gold film and the frustule beneath it.

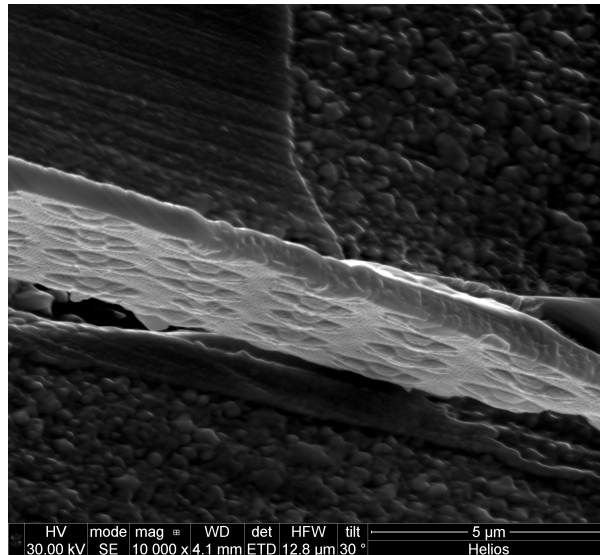


(a) Gold film showing the optimum replica of a *Coscinodiscus sp.* Some of the frustule is still stuck to the gold film. The cribellums are visible outside the cribrum clusters, and the dust grain have left a print in the gold film.

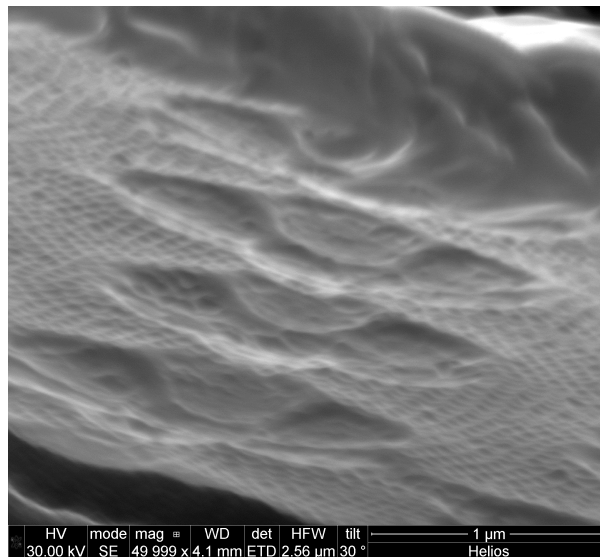


(b) A piece of the frustule gives a very good replica as it is still stuck to the gold film.

Figure 4.9: SEM-images of the surface of the gold film which was cut away from the frustule.

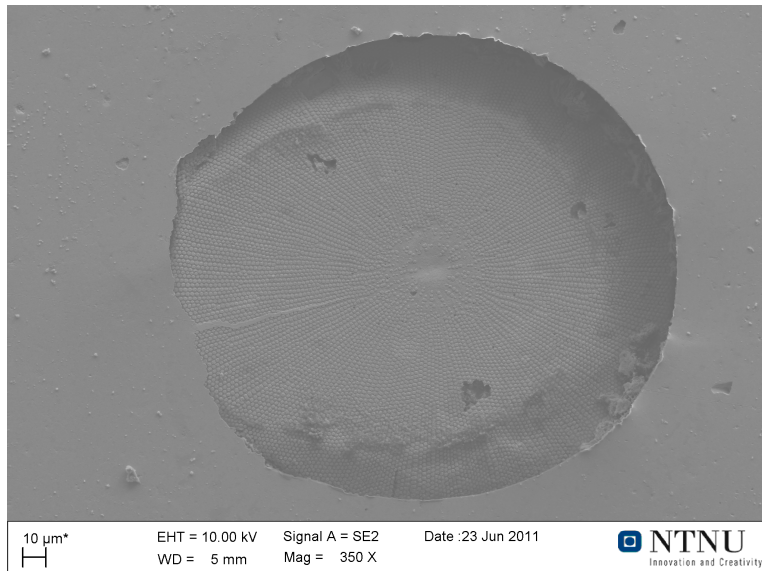


(a) The cut away gold rectangle stand at one side down in the substrate, making it possible to characterise it.

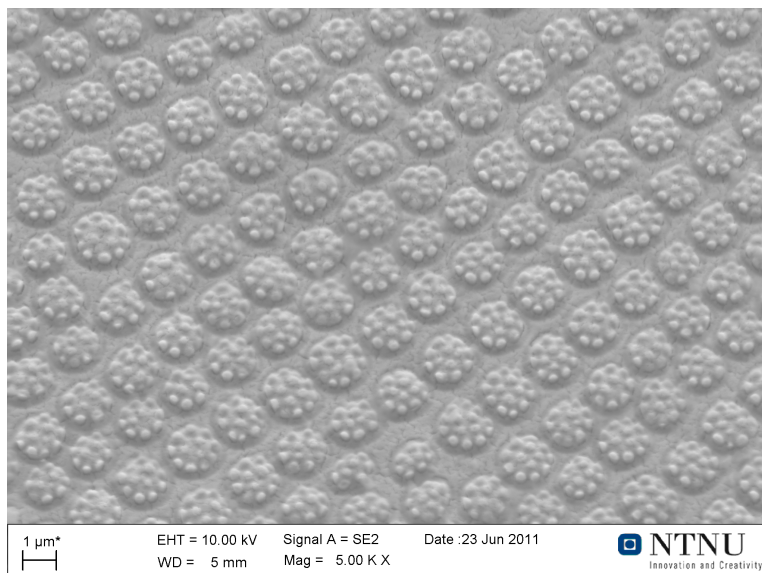


(b) Closer view of the side profile and topography of the gold film. It is clear that all the replicas of cribrum clusters follow the topography of the original structure.

Figure 4.10: Low angle profile of the gold film which was cut away from the frustule.



(a) Image of a diatom frustule which have been etched away. The print have been partially loosened from the gold film deposited over the diatom.



(b) The porestructure of a diatom frustule print in the gold film. The areola in the surface is replicated with high precision and also the bribrum, while the cribellum are not visible.

Figure 4.11: SEM-images of a diatom frustule print in the gold film.

## **4.3 Part III: Deposition and Characterisation of Amorphous Silicon and Silicon Nitride on diatom frustules**

### **4.3.1 Characterisation of Amorphous Silicon Film Deposited on Frustules by SEM and FIB**

Diatom frustules of the net plankton were used as a substrate for deposition of amorphous silicon. In Figure 4.12(a) and 4.12 the images taken during the FIB-session are presented. The gold deposited between the two layers are not visible in any of the images. The gold films only function were to act as a conductive layer and prohibit any charge-up in the sample.

Figure 4.12(a) shows a cut into the frustule and the amorphous silicon film. The cross-section between those two layers appear clear, but the contrast between the amorphous silicon and diatom frustule is very low, but it is possible to differ them on the little difference in contrast and the dark line on the interface between the two layers. The flower pattern the cribrum clusters make up on top of the frustule are visible through the silicon layer.

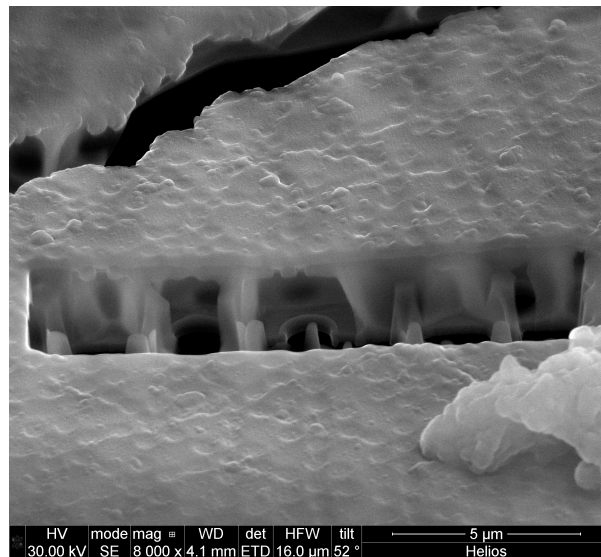
At a higher magnification than in Figure 4.12(a), the Figure 4.12 show how the silicon film follow the diatom frustule. In the cribrum the amorphous silicon forms a zigzag shaped surface. There is no signs of the gold layer in the image, but there is no charge-up in the sample. It is also possible to see material deposited along the vertical walls of the cribrum. The amorphous silicon can during deposition diffuse on the surface and settle on areas which are not on the top surface of the frustule.

The gold layer on top of the frustule have a well defined topography, this can be seen in Figure 4.12(b). There are small features visible on the surface, this might be the shape of the cribellums in the frustule. Both cribnums in Figure 4.12(b) have this structure which have the same size as the cribellum. What this good replica of the frustule indicates will be discussed further in the discussion in this thesis.

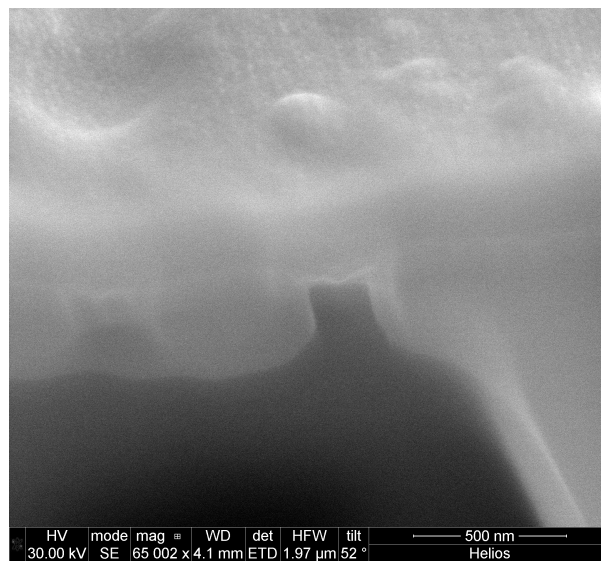
### **4.3.2 SEM and FIB Characterisation of Silicon Nitride Film Deposited on Frustules**

A similar sample as the amorphous silicon samples was created, just by adding ammonia in the gas mixture, and by that composition depositing silicon nitride instead of amorphous silicon. The procedures in the FIB-session were very similar to the session investigating amorphous silicon, cuts were made to investigate the cross-section and interface between the silicon nitride and diatom frustule. In advance a gold layer was deposited on top of the silicon nitride to conduct electrons away from the sample.

In Figure 4.13(a) it is possible to see the cribrum through the silicon nitride layer on top of them. Silicon nitride is clearly a very electron transparent



(a) SEM-image of a cut made in a diatom frustule covered with amorphous silicon. There is only a small difference in contrast between the silicon layer and the silicon dioxide layer.



(b) High magnification image of a cribellum which is covered in silicon.

Figure 4.12: SEM-images of a cross-section of a silicon covered diatom frustule.

material, this can cause resolution issues in the SEM as less electrons returns to the sensor. The contrast between the silicon nitride layer and the diatom frustule is very low. This is expected as silicon dioxide and silicon nitride have very similar densities.

A closer view of the cross-section, as seen in Figure 4.13(b), reveals how the silicon nitride interacts with the frustule. Due to the electron transparency of silicon nitride it is hard to define the precise interface between the two materials. Even though the thin film is semi-transparent it is possible to see a thin layer of silicon nitride follow the cribrum and also have a topography from the cribellum. The resolution of the SEM-images from the silicon nitride cover is lower, but it is still possible to see the smallest features of the diatom frustule and the thin film on top of the frustule.

## **4.4 Part IV: Manufacturing and Characterisation of Structures similar to Solar Cells**

There were manufactured structures very similar to solar cells, the only real difference were the lack of dopants in the structures and also that there were no metallic contacts connected. Both light microscope and a dual-beam SEM were used to test the structures, and the interesting features and structures from those characterisation sessions would be investigated.

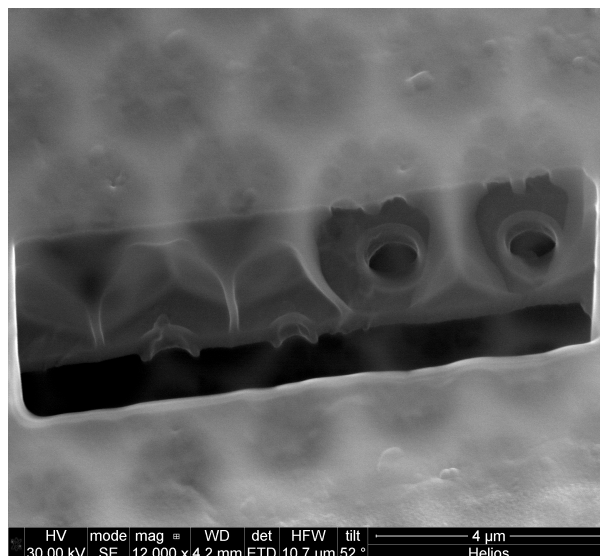
### **4.4.1 Characterisation by Light Microscope**

The light microscope images presented here are of interest to the properties of the film. The results will try to explain how light interact when reflected by and around diatom frustules in the manufactured solar cell structures. All four different samples were investigated to see how they behave in light microscope.

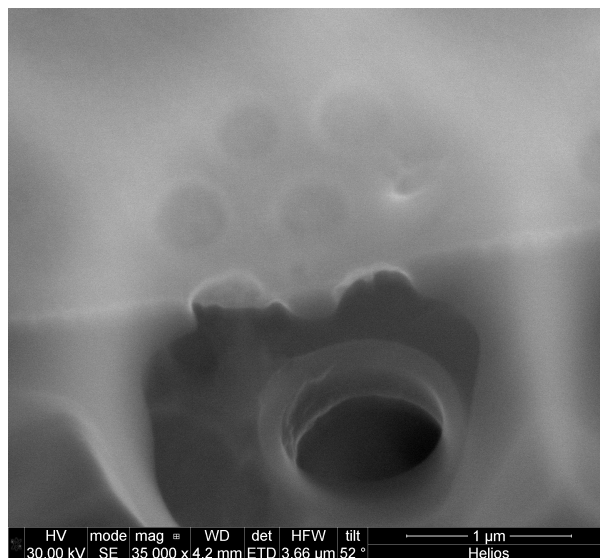
Figure 4.14 is the sample where there are two layers of silicon nitride. As expected from the two layers of silicon nitride, the surface is yellow. Figure 4.14(a) shows several frustules laying around on the silicon dioxide surface, and also have some blue circles. These circles are diatoms that have moved or fallen off the substrate surface.

Figure 4.14(b) is a higher magnification image of a selected area of Figure 4.14(a). It is clear that there are no other structure in the blue circles than the substrate, and it is uncertain whether or not there are any silicon nitride on the diatom frustules at all. Even the light microscopy image with the highest magnification, Figure 4.14(b), there is no silicon nitride layer visible on the diatom frustule. Due to the thickness of the silicon nitride, a light microscope can not be used to see the isicon nitride if it does not give any colour change. Hence SEM and FIB must be used to check whether or not there are silicon nitride on the diatom frustules.

The silicon sample with a single layer of silicon nitride, were much darker than the one with a double layer, just as expected. In Figure 4.15(a) some

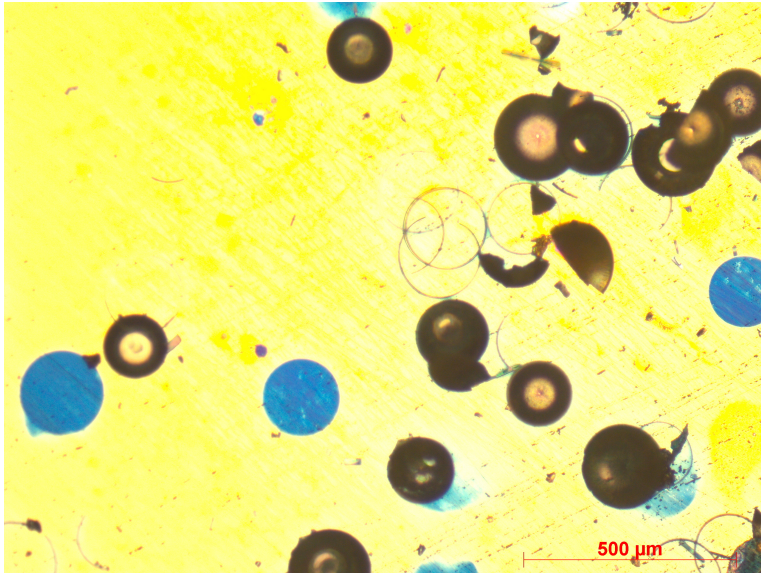


(a) A semi-transparent silicon nitride layer on top of the diatom frustule. A cut is made to investigate the cross-section between the two materials.

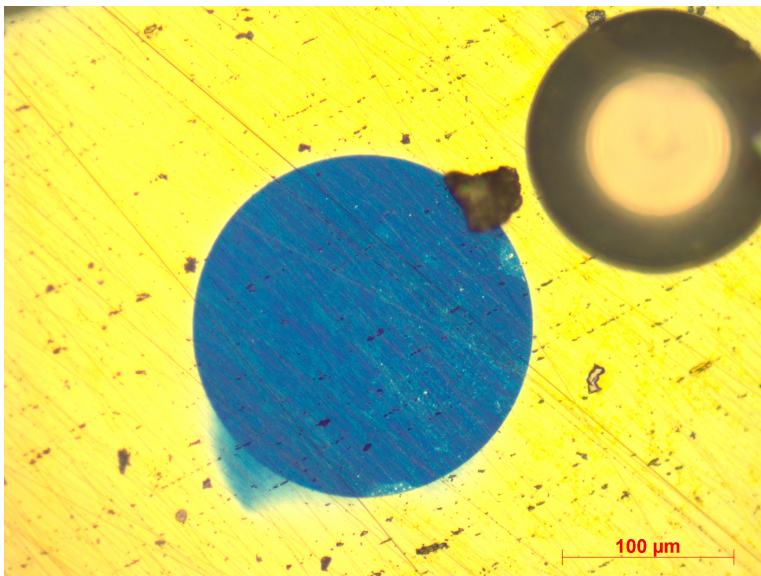


(b) The interface between the silicon nitride film and the diatom frustule.

Figure 4.13: SEM-images of a cross-section of a silicon nitride covered diatom frustule

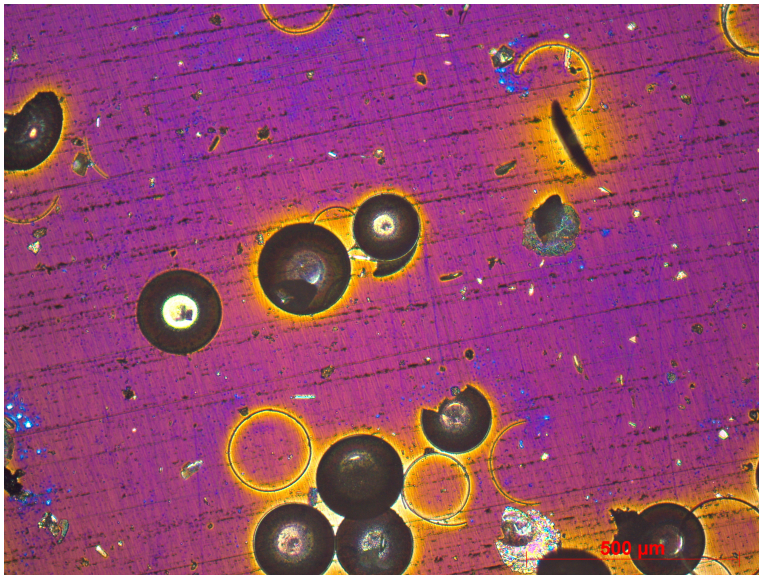


(a) Image of diatom frustules on a silicon substrate, different shapes are shown. There is no sign of the silicon nitride layer becoming thinner around the pores.

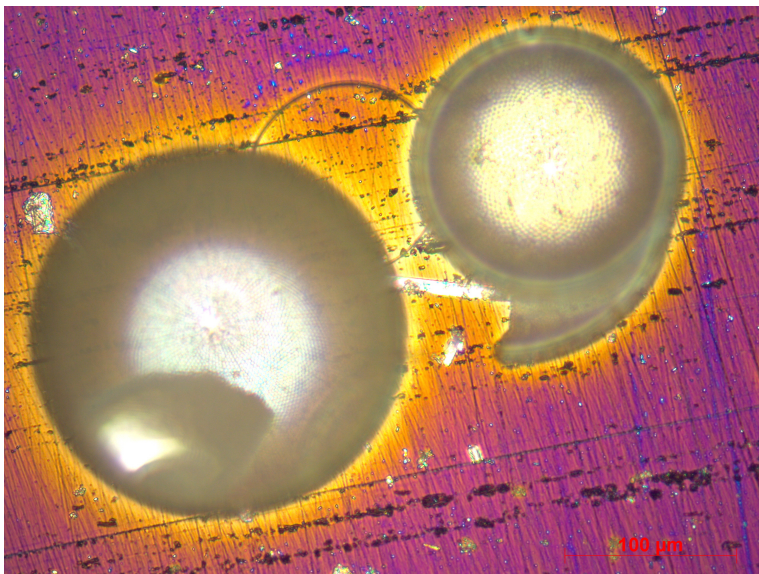


(b) A large magnification of one of the missing frustules. The diatom frustule up to the right is very bright compared to the single silicon nitride layer.

Figure 4.14: Light microscopy images of the crystalline solar cell structure with two layers of silicon nitride.



(a) Image of the silicon antireflection coating textured with silicon dioxide. Diatom frustules are spread across the surface.



(b) Image of two frustules. A yellow colour is emitted from the diatom to the upper right, while a more blue colour in the frustule to the left.

Figure 4.15: Light microscopy images of the crystalline solar cell structure with a single layer of silicon nitride.

frustules on the surface of the crystalline silicon sample are imaged, it is clear that there are yellow rings round all frustules. The diatoms are dark, while the top of some of the diatoms emit some light. There are some diatom frustules which have been partly crushed or broken during cleaning, which have only a single layer of the frustule left. Those have a light emission/reflection of many different colours, and those can be seen in the lower right of the image.

In Figure 4.15(b) some of the diatom frustules are magnified further than in Figure 4.15(a). It is possible to see that the transition between the silicon substrate and the diatom frustule have a yellow tint. There is no or little colour change on the diatom frustules, whether or not this means there is no silicon nitride on top of the frustules will be investigated further by FIB. It is also possible to see the orientation of the thecae on the substrate, and while the yellow borderline is wider for those thecae with the outside facing towards the substrate, the thecae with the outer surface facing away from the substrate have a smaller.

An iridescence occur in both diatoms in Figure 4.15(b). While in the frustule to the left there is a blue tint to the color, it is in the smaller to the right a yellow tint. In small pieces of frustules laying around these two frustules there are even more colours present. Up to the left in Figure 4.15(b) there are a small piece of frustule, which the light reflects in all colours.

Figure 4.16 are light microscope images of a glass substrate where diatom frustules are dried on top, and the substrate is then covered in aluminum. This make up the substrate for the amorphous silicon. It is easy to see in the images that there are many different shapes made by the diatom frustules. Some frustules are easy to see, while others are more difficult to see.

In Figure 4.16(a) three diatom frustules are placed so they for a smiley face in the middle of the image. Two girdle bands a visible through the silicon, while the frustule which is completely covered with silicon. This structure might have interesting light reflective properties and must be investigated further. The other diatoms in Figure 4.16(a) are visible, and this difference will be the focus for further characterisation.

Figure 4.16(b) is a higher magnification image of the same area as in Figure 4.16(a). At this higher magnification, it is possible to see more features of the silicon covered diatom frustules. The girdle bands of the structure have such a large height difference that they are out of focus when focusing on the silicon surface. There is some iridescence present in the silicon covered diatom frustule, and in the diatom frustule visible through the silicon a yellow tint is visible, showing that there is silicon present on top of the frustule here as well.

Figure 4.16(b) is an image of the silicon covered frustule with a clear iridescence on top of the frustule. A phenomenon called Newton's rings explain this experiment, Newton's rings occur when two surfaces, a flat and a spherical surface reflects light and an interference pattern occur. It appears that there have been none cracks or gaps in the silicon deposition over the entire diatom, and hence it will be a very good contact between the aluminum and silicon layers in the solar cell structure.

Figure 4.17 are light microscopy images of the sample where the struc-

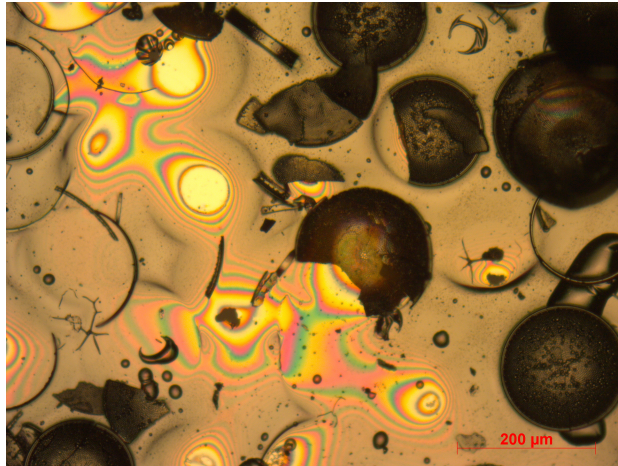


(a) Diatom frustules laying spread on the substrate surface. A smiley face consisting of two whole thecae and one broken is easy to distinguish from the other frustules.

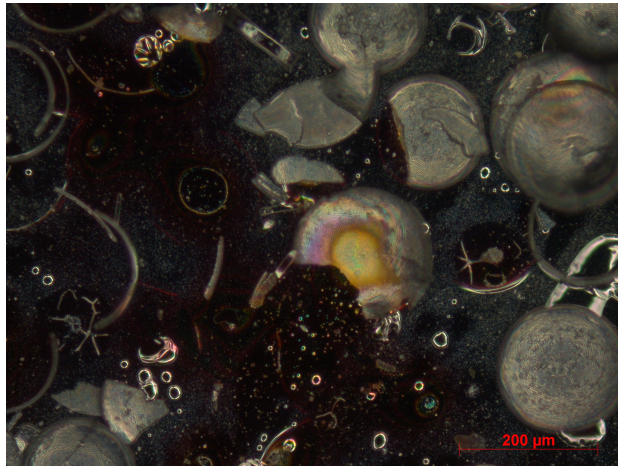


(b) The silicon have covered the entire frustule. Iridescence is visible on top of the silicon structure, and debris is laying around on the substrate beneath the silicon.

Figure 4.16: Light microscopy images of the amorphous silicon sample with an aluminum layer between the frustules and silicon.



(a) Image showing the interference patterns which occur in the bright field image of the sample. Both visible frustules and frustules not visible gives these patterns.



(b) The dark field image of the sample. Only the visible frustule in the middle of the image give any strong reflections in this mode. A number of defects in the thin film also are visible. For the circle up to the left of the frustule with bright interference patterns, this area is the center of the thecae.

Figure 4.17: Light microscopy images of the thin film sample with the aluminum layer between the glass and frustules. The silicon was deposited on top of the frustules, after they were dried on the aluminum film.

ture is a glass substrate with an aluminum coating, and with diatom frustules dried on top of the coating before silicon deposition was performed. Figure 4.17(a) was captured in bright field, while Figure 4.17(b) was captured with dark field imaging of the same area.

Diatoms underneath the surface of the amorphous silicon are not visible through the silicon in Figure 4.17(a), but Newton's rings appear in the surface of this sample as well. Some of the silicon frustules are visible on the sample, it will be decided by FIB whether or not these structures are covered with silicon.

In Figure 4.17(b) the diatoms giving the Newton's rings are not visible at all. The diatom frustules visible in the Figure 4.17(a) are also visible in the dark field image. In the middle of the image a diatom is emitting an iridescence, in difference from Newton's Rings this iridescence does not disappear in the dark field image.

#### 4.4.2 Characterisation by FIB and SEM

The silicon structures had the same structure with the exception of the double silicon. For that reason only one of those samples was investigated, as the silicon nitride do not have problems depositing on silicon. The silicon nitride showed a conformal thickness over the entire frustule, and at the surface of the thin film deposited it is easy to observe the cribellum even with 70 nm of silicon nitride over the frustule. Figure 4.18 reveal more information than the conformity of the silicon nitride thin film. The low resolution obtained in silicon nitride is an obstacle for further magnification.

In the thin film structure with the aluminum coating between the glass and the frustule much drift was caused by attempts to cut into it with the gallium beam of the FIB. The drift made it impossible to make a proper cut into the structur, so a broken diatom frustule was searched for. Broken diatom frustules are possible to tilt with the sample in a such manner that their profile is revealed. Figure 4.19(a) is an image of a such structure, the 5  $\mu\text{m}$  thick silicon layer covers the outer surface of the frustule, while the fracture surface is with out any coating. There are some voids and gaps observable between the silicon film and the diatom frustule. In addition there is charge-up in the image. The charge-up in this image is so low it is still possible to gain a good image quality.

In Figure 4.19(b) there are three different structures of interest. Up to the right a frustule oriented with the outer surface towards the substrate, down to the left a frustule oriented with the outer surface away from the substrate, and down in the middle the outermost layer have loosened from a diatom frustule and adhered to the substrate. It is possible to see that all three structures have been coated with amorphous silicon. In the frustule having the outside facing the substrate, the small pores have been covered up with silicon but are still observable through the film. The features along the edge of the frustule are not covered up that well, if they are covered up at all.

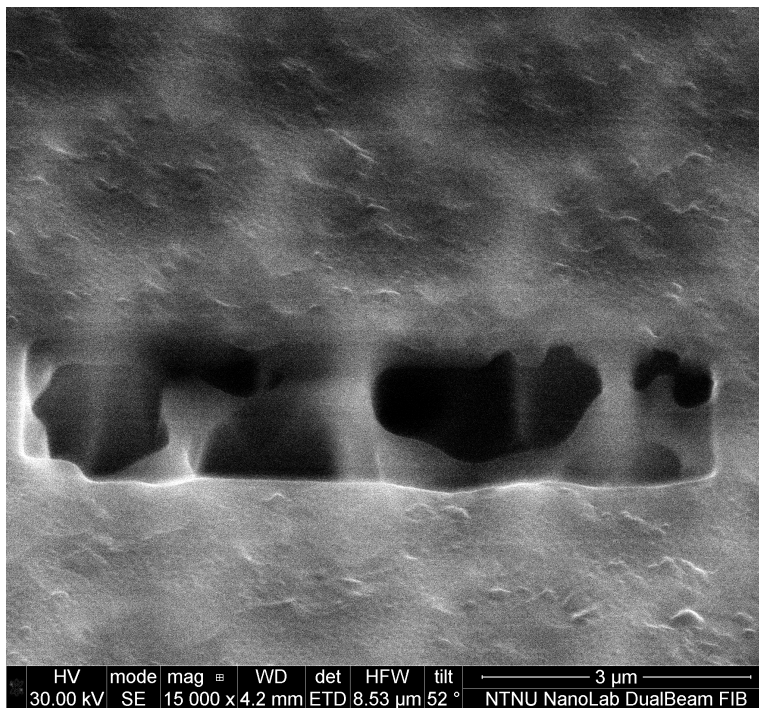
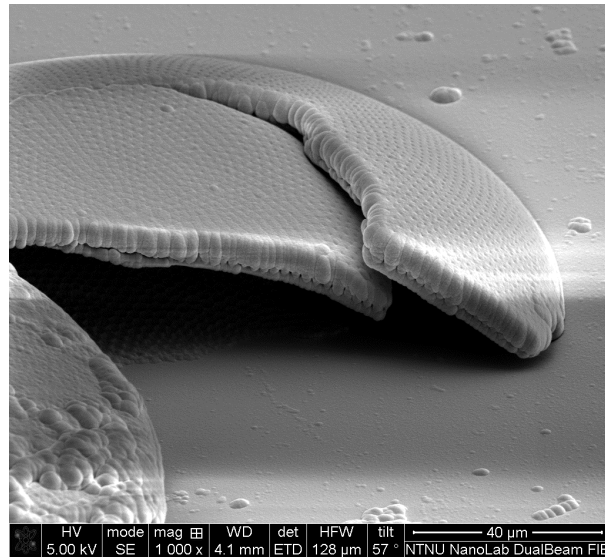
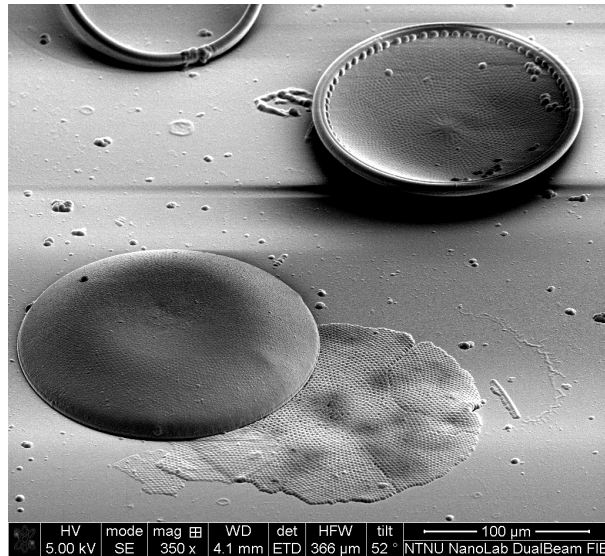


Figure 4.18: Solar cell structure with texturation of silicon nitride and diatom frustules. There is a low contrast between the silicon nitride thin film and silicon dioxide diatom frustule.



(a) A broken frustule show a cross-section of a amorphous silicon covered diatom frustule. The silicon film is on top and the diatom frustule beneath it.



(b) Three possible structures obtainable from diatom frustules. All three structures are covered in amorphous silicon.

Figure 4.19: SEM images of solar cell structures with a layer of aluminum between the frustule and amorphous silicon.

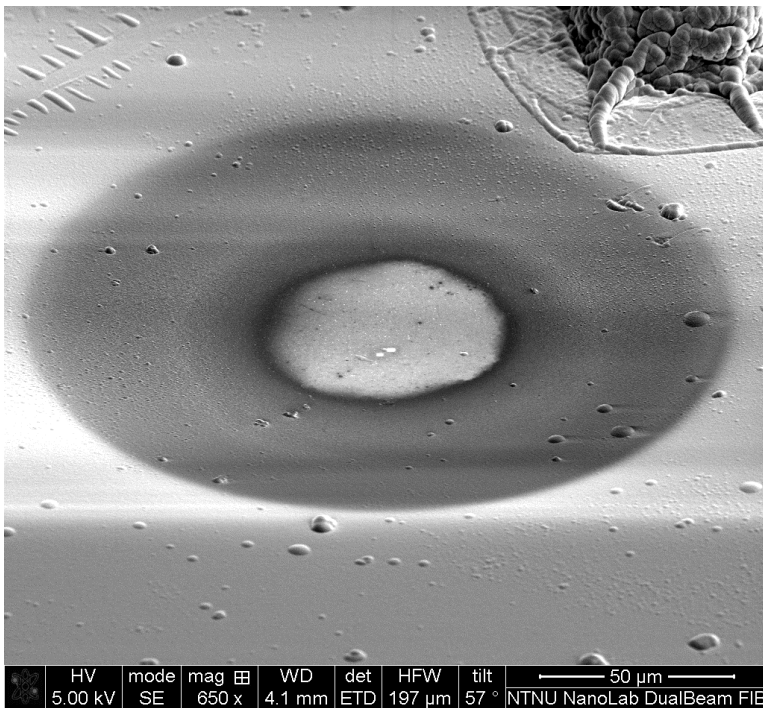


Figure 4.20: The pit in the solar cell structure where there is a missing diatom frustule.



---

## 5. Discussion

This chapter will discuss what the different results indicate. Arguments leading to the conclusions of this thesis will be revised and discussed. In addition of the gold templates, deposition of silicon and silicon nitride directly on the diatom frustules will be investigated. The last feature which will be discussed is the possibility to incorporate diatom frustules directly into solar cells.

### 5.1 Part I: Characterisation of Diatom Frustules and Their Pore Structure

There are certain specifications that are needed to be met for antireflective texturation and back-surface diffraction grating. A highly repetitive structure and large topographical differences would be preferable. There are some differences between the antireflective texturation and the back-surface diffraction grating. A antireflective texturation would need to be transparent for letting the light through but need a high refractive index to stop the light from exiting front surface of the cell. The back-surface diffraction grating would need to be diffracting and reflective at the same time. In this subsection the different structures of the diatom will be discussed to obtain a sense of which of the structures that can be utilised as either antireflective texturation or back-surface diffraction grating.

When investigating the diatom frustules it is one tendency that appear, the frustules have tendency to break and to get cracks from the edges and far into middle of the frustule. Cracks are structural weaknesses which may cause harm to any diffraction pattern and may cause structural failures in the cell. There are also signs that in some of the frustules the layers have separated from each other. Such structural failures in the cell have to be investigated to give more information about what is causing these separations and if any single layer can be used as antireflective texturation or back-surface diffraction grating.

The diatom frustules are highly repetitive structures, the cribellum of the cultivated diatoms are the least repetitive layer, as they are only present in the cribrum. The side walls of the cribrum are also very steep. If a surface should have any reflective properties, it must have a surface directed partially towards the incident light. The side walls down to the cribrum are perpendicular to the outer surface, too steep for any reflective purposes. The cribellum of the net

plankton are spread all across the surface of the frustule, while the cribellum of the cultivated plankton only exist in the cribrums. The question whether this structure is necessary for antireflective texturation and back-surface diffraction grating is still to be answered, but diffraction of light waves occur at the same dimensions as the wavelength of light. The cribrum are about 200 nm in diameter of both diatom species, and photons with a high energy might have get diffraction effects from the diatoms pore structure. The cribrum pore of the *Coscinodiscus walesii* is placed in the areola, which makes the distance between the cribrum small. In the *Coscinodiscus sp.* the cribrum in an areola are farther from each other, but the distance between them are also more even. For the areola, they are about 1.5  $\mu\text{m}$  in diameter for both. . And they could act as diffraction pattern for photons with low energy, typically photons in the infrared part of the spectrum. For the foramen, the pore into the areola of the net plankton, the mean pore size was about 680 nm, which is in the same magnitude as visible light. These pore dimensions are promising for diffraction and also reflection properties.

Another feature of the diatom frustules are the shape of each thecae, the side walls of the thecae are steep, but due to the thickness of the silicon dioxide, the structure is possible to bend and deform some. It is possible other diatom species could be more suitable for the use as antireflective texturation in solar cells. On the other side it might give some positive advantages to have this height differences with regards of antireflective purposes or back-surface diffraction grating, only in-depth tests of different diatom structures will give an answer to that.

The inside of the frustule of the cultivated diatoms have an interesting structure, as there is no unique pore structure on the inside as it is in the net plankton. The areola give a regular hexagonal structure of 1.5  $\mu\text{m}$ , which might be used as a texturation for solar cells, or even might be used a structure for a diffraction grating.

As the structure is consisting of multiple layers it might cause problems during characterisation if one or more of the layers have loosened from the remaining diatom frustule. The number of diatom frustules per sample makes it rather easy to make up an image of how the diatom frustule structure is. For an increased resolution of diatom frustules a thin gold layer could be sputter coated onto the surface. The gold layer would give high contrast and a strong signal of secondary electrons, in addition it would remove any charge-up in the sample during characterisation.

When diatom frustules break in pieces, the frustule get a fracture surface revealing the

## **5.2 Part II: Manufacturing and Characterisation of Gold for Use as Templates in Solar Cell Industry**

### **5.2.1 Deposited Gold Film Characterised by FIB and SEM**

In the author's specialisation project it was proven that the gold film contracted and withdrew from the surface of the diatom, the same appear to have happened in Figure 4.6. On the other side, in Figure 4.7 it appear that the gold film follow the inside of the valve very well. Exactly why there is such a large difference between the inside and outside of the frustule is unknown, but there is a possibility that due to the large height difference between the middle of the pores and between the pores, the gold film is actually stuck to the frustule. The gold film in this experiment is very thin, only 500 nm thick, hence there might be no contact between the gold film on the inside of the frustule and the film on the substrate surface. A piece of gold film separated from the rest of the deposited material will contract towards a central point in the film, and the gold film would then stay in the pores or at least not be pulled out of the pores. The importance of Figure 4.7 can not be underestimated, the gold film show a clear and good tendency to follow the topography of the diatom frustule, and by comparing it to Figure 4.6 it is clear that the gold itself does not have any material properties incompatible with the silicon dioxide in the diatom frustule. These properties are important of gold films are to be used as a material for templating of solar cells.

By comparing the film thickness of Figure 4.6 and Figure 4.7, it is seen that it is very similar, an accurate measurement was not conducted, but there are no visible differences with regards of thickness of the film. EBE is a technique which is supposed to give very conformal films. Due to this observation and by evaluating the EBE technique used to deposit it is rather safe to assume that the thickness of the gold film is the same all over the sample. In addition to the even conformity of the film, there are no cracks visible on the film surface. These results give the indication of a high quality film is obtainable from a diatom frustule on a glass substrate.

The images of the gold-frustule interface only give this much information, to get more and better results a small square of the gold film was cut out and removed from the frustule surface. Due to the topography and size of the frustules it is not possible to get the tungsten needle down in the frustules where gold have been deposited on the inside of the frustule, this limited the experiment to the outside of the frustules. The gold film interesting features with regards of the pores and topography of the outside of diatom frustules were revealed by this experiment. The cut from the FIB did not go all the way through the gold film which made it easier to separate the gold film from the frustule, as a frustule cut by the gallium beam would be weakened and break of when trying to remove the piece of gold from the frustule.

By comparison of Figure 4.9(b) and Figure 4.10(a), the highest obtain-

able quality of a gold film replica is obtainable this way. In Figure 4.10(a) it is easier to see all the features of the frustule in the replica than in the image of the original structure in Figure 4.9(b). Due to the low thickness of the cribellum layer of the diatom frustule, there are a low contrast between that layer and the layer beneath in the diatom frustule. The regular pore pattern spread all over the surface of the gold film in Figure 4.10(a) shows that nanometer precision of diatom replication can be achieved with a controlled experiment.

The dust grain visible in Figure 4.9(b) is replicated by the gold film and the shape is visible in Figure 4.10(a) as well. The dust grain show the importance of having a clean frustule surface, as all observable features will be replicated by the gold film. In addition to the dust grain there are another important feature in the gold film in Figure 4.10(b). Namely a high detailed replication of the diatoms cribellum over a cribrum, this particular cribrum distinguish itself from the other cribrum due to this difference. The other cribrum do not have replicas of the cribellum, even though in Figure 4.9(b) it is possible to see the cribellum of the frustule. For the cribellum replicated with a high precision, there is no pore layer present over the cribrum, this might be due to the pore layer have actually broken af from the frustule and followed the gold film when that was removed. In Figure 4.10(b) the brightness is high, very similar to a local charge-up due to the bombardment of electrons and low conductivity of the frustule material. This support the hypothesis of the diatom cribrum is partially stuck to the gold film.

One important feature of the gold as a material is the potential to follow the sample also in height differences across the surface. This is easy to observe on the inside of the *Coscinodiscus walesii* in Figure 4.7, but the question is still how well it follows the outside of the frustule. Figure 4.10 are low angle images of the gold film removed from the diatom frustule. Although it is not possible to distinguish the height difference in Figure 4.9, it is easy to see in Figure 4.10. This height difference gives the potential for antireflective purposes and diffraction grating. The size of the cribrum are around 200 nm in diameter, while the cribrum clusters are larger, closer to 1.5  $\mu\text{m}$ .

The smallest pore structure of the diatom frustule, the cribellum are around 40 nm, this dimension is the same as a very high energy photon. There are no photons with such a high energy entering our atmosphere, and there would be no effect from pores with that size. The template do not lose any potential from the result that the cribellum have not been replicated by the gold film when separated from the frustule. The optical properties of such small features as the cribrum needs to be investigated further to see what potential these have to affect the incident light in solar cells.

## 5.2.2 Characterisation of Gold Film Templates

To be able to make a template of gold or any other metal there are certain properties which must be accomplished; the pores must be conserved in the print, materials used in solar cells must be possible to deposit in the template, the film must have the potential of being reused over and over again, an efficient etching technique for the substrate must be found, a more suitable substrate material might

be found, and a film thickness sufficient to contain all the frustules adhered to the film. This section will discuss which of these parameters the gold film fulfills.

Due to the diatoms which have loosened together with a piece of gold film, it comes natural to assume that the film is too thin for the gold film to be properly coherent between the area around the frustule and over the frustule. In addition to the prints there is also a number of diatoms which have been partially loosened due to the thickness of the gold film, the print seen in Figure 4.11 is one of them, these also have to be taken care of if a template is to be made. A thicker film might be one way to reduce the number of loosened frustules, but a thicker film also requires a longer process time and more material, both of these parameters increase cost of production. By controlling the height of a valve from the edges to the middle it is possible to see that it is close to 35–40  $\mu\text{m}$  in difference in height between those two points on the frustule, a film that thick will take some time to manufacture by EBE. Due to the structural differences between diatoms there might be species better suited for the industrial use as templates for the solar cell industry, with regards to frustule shape, curvature, size and pore structure. As the gold film was not tested as a substrate with removal of a deposited material, it is not possible to anticipate to what extent the gold film will deteriorate for each texture produced by it. Another material might be chosen, in theory any material with the possibility to recreate nanoscale features by a deposition technique might be used instead of gold.

To remove the glass substrate and the diatom frustules from the gold film was done with HF with a concentration of 48 %, HF is corrosive and hazardous material to work with, and it should be avoided. Other materials which can be etched by weaker acids should be chosen as substrate to reduce the amount of HF used. On the other side HF had to be used to remove the diatom frustules chemically from the gold film. The use of HF can only be eliminated if an adhesive agent is placed between the substrate and the diatom frustules, in addition an antisticking agent is sprayed on the sample after drying of the frustules to the surface.

The antisticking and adhesive agents are versatile, as they can be used regardless of what technique chosen for separation of substrate and template. There are other methods of separation of the substrate and template. One of them is mechanical separation. The gold film could be pulled off the surface by an adhesive tape or by a pair of tweezers. This is possible for gold, but for other materials removal from a substrate by mechanical means are not necessarily possible. Another aspect of mechanical removal of the gold is the vibrations from an unsteady hand which pulls off the film. Vibrations are non-existent with chemical removal of the substrate, and these vibrations must be compared with the HF etch or other acidic etches which might be used.

In addition to the change of substrate material, the thickness of the substrate could also be changed. A thicker substrate requires a larger amount of acids to be etched away, the glass substrate was 3 mm thick but still took 18 h to be etched away completely. To reduce the preparation time for the sample and increase the productivity in an industrial manufacturing process, a thinner substrate

should be used instead. Of course, if another material is chosen as a substrate, its mechanical properties must be taken into account to decide the thickness of the substrate.

In Figure 4.11(b) the intricate pore structure of the areola and cribrum are replicated, while the cribellum are not replicated by the gold film. There are two possible reasons for the cribellum not being replicated. One of them are the poor cleaning of the diatoms are making the gold replica impossible due to small or non-existing pores. Another possible reason for the non-present cribellum are the heat during deposition. As the 4.5  $\mu\text{m}$  of gold are deposited, the heat which are transferred to the sample is removed slowly on a glass substrate, as glass is a thermal insulator. As heat builds up in the thin gold film the smallest nanoscale features tend to disappear due to Ostwald ripening, which is a phenomenon where large particles grow on the expense of smaller particles. [L.Ratke and Voorhees, 2002] One possible solution is to deposit the film in multiple steps and lay in cool down periods for the sample so the heat can dissipate and Ostwald ripening reduced. If the cleaning is the reason for the poor reproduction of the cribellum, a more thorough cleaning process must be used, an increase in the number of repeated cleaning steps would be possible without damaging the structure of the diatom frustules.

## **5.3 Part III: Deposition and Characterisation of Amorphous Silicon and Silicon Nitride on diatom frustules**

### **5.3.1 Characterisation of Amorphous Silicon Film Deposited on Frustules by SEM and FIB**

The FIB cut made in the amorphous silicon sample was only to give an image of the cross-section to see how the interface between silicon nitride. Figure 4.12(a) shows the pore pattern is still visible through 250 nm of amorphous silicon, this give a good foundation for a high quality replication of the pores. It appear to be none or very few cracks in the film, to such conformity over large surfaces like solar cells are, good process control is needed. The film thickness appears to be conformal over the sample, and there is no difference in thickness between the middle of the frustules to the edges of the frustule and the substrate.

In Figure 4.12(b) the deposited silicon film follows the pore such that a pit is made in the surface even after 250 nm is deposited on top of the frustule. As the cribrum are followed this well, it is safe to assume that the cribrum clusters are replicated in height, just as the gold film. The important features for usage as template is there, and the results reveal no limitation to the use as a antireflective or diffraction grating.

### **5.3.2 SEM and FIB Characterisation of Silicon Nitride Film Deposited on Frustules**

The silicon nitride deposited on the frustule before FIB in Figure 4.13 is only 70 nm thick. This thin layer is semi-transparent and hard to characterise by SEM and FIB due to the transparency. The pores are easy to observe in Figure 4.13(a), and very similar to the amorphous silicon sample, the cribrum are also visible on the surface of the silicon nitride. In Figure 4.13(b) it is possible to see that the silicon nitride goes down on the cribrum, while it is not possible to detect any cracks in the surface in the silicon nitride.

To be able to make antireflective coatings directly by depositing silicon nitride on diatom frustules, the angles and topography of the silicon nitride layer have to be correct. In a solar cell these features are made periodic by etching, frustules do not have the possibility to be etched into the correct topography. Silicon nitride appear to follow the frustule well enough to act as a antireflective coating with frustules as a texturation instead of an etched structure of silicon coated with silicon nitride.

## **5.4 Part IV: Manufacturing and Characterisation of Structures similar to Solar Cells**

By having a curvature on the surface of a diatom frustule, a material would be suitable as an antireflective texturation, any incident light will hit the surface and will either be diffracted into the materials, or be reflected and hit an adjacent antireflective structure and be diffracted into the material by that structure instead. The structures will interact stronger with waves if the dimensions are in the same magnitude. Light with wavelengths down to 200 nm are let through the atmosphere of the Earth, and hence the structures might have a potential as antireflective texture.

A diffraction grating at the back of a solar cell must have many of the same feature as a antireflective texturation and coating, the three real differences are which material used with regards of conductivity and transparency, and the refractive index. While a antireflective coating have to be transparent, there is no need for the diffraction grating to be transparent. It might as well be reflective, or at least reflect light in one way or another. The front side of a solar cell has either a transparent conductive oxide to work as a contact for the cell, or a metallic fingers spread across the surface to collect charge carriers. At the back-surface there is either another transparent conductive oxide or an aluminum layer over the entire surface to work as a back-surface collector. The aluminum surface have to be in contact with the solar cell, and hence a diffraction grating should be conductive, this can be achieved by coating an insulating structure with a conductive layer, or placing the diffraction grating behind the metallic contact. If the metallic layer is placed between the cell and the diffraction grating, the diffraction grating does not have to be reflective or transparent itself as the metallic layer will reflect light.

---

### 5.4.1 Crystalline Silicon Solar Cell Samples

The solar cell structures manufactured were basic structures to give an example of how the diatoms could be used directly into solar cells of different kind. In the crystalline silicon samples there were signs of diatoms loosened during manufacturing.

The blue circles in the sample with the double layer are spots where there are only one layer of silicon nitride present, an example of these blue circles are Figure 4.14. By the size and shape of the circles it is possible to say that these are made of diatom frustules which have loosened from the sample. The top of the diatom frustules on the surface are tinted yellow, this is a clear sign of the double layer of the silicon nitride does not give the wanted effect. Two single layers of silicon nitride give the same effect one layer with the same thickness as two single layers combined. A double layer of silicon nitride is therefore not to be desired.

The crystalline silicon sample with a single layer of silicon nitride on top of the diatom frustules is seen in Figure 4.15. The silicon nitride confer a deep blue antireflective coating even on a flat substrate, around the frustules there are yellow circles, this is probably due to the thickness changes as the silicon nitride. In the light microscope image in it appear that there are no or little silicon nitride on top of the frustules Figure 4.15, while in the SEM image from the FIB of the same sample there are clear that there are a layer of silicon nitride on top of the frustules (Figure 4.18). Why the color have not changed to purple for the frustules might be to the electric field which occur along the edges of samples with different electric conductivity. PECVD is a deposition technique which is driven by an electric field, and the thickness might be different from the substrate to the frustule, giving different diffraction colours.

### 5.4.2 Thin Film Cell Samples

In the thin film samples where an entire thin film solar cell was manufactured, other uses of the frustules were intended. Instead of working as an antireflective texturation they would work as a back surface diffraction grating. In Figure 4.16(b) the Newton's rings are a proof of the light being spread by the interaction of the two surfaces. Newton's rings occur as an interference pattern from the interaction of a flat and a curved surface, and are directly dependent how the light interacts with the silicon and the aluminum coating beneath it. [Goodwin and Wyant, 2006] Although how much increase of light harvesting this cause are not clear, and new and more through investigations are needed to be done. A production of a new cell and efficiency measurements could also be performed to investigate the effect of diatom frustules in this kind of frustules.

It is also difficult to see in the light microscope whether or not the diatom frustules are covered in silicon, but Figure 4.19(a) is revealing that the frustules are covered with silicon. A conformal silicon layer is present on the frustule, which means that PECVD do not have any issues regarding deposition of silicon on diatom frustules. In Figure 4.19(b) two frustules with different orientation is imaged. The interesting feature here is the silicon deposited on the frustule

with the outer surface faced towards the substrate. Along the edges of the frustule there appear to be very little silicon compared with the middle, in addition it does not appear that that silicon is in direct contact with the rest of the silicon thin film. To gain a layer of silicon which is thick enough, a total of 30–40  $\mu\text{m}$  have to be deposited in addition to the 5  $\mu\text{m}$  which already have been deposited.

In the sample where the aluminum was beneath the layer of diatom frustules it is possible to see more Newton's rings than in the sample where aluminum was between the frustules and the silicon deposited on top of the frustules, Figure 4.17 are examples of that. By comparison of Figure 4.17(a) and Figure 4.17(b) it is possible to see that the only frustule reflecting light out to the sides are the one in the middle. If the only light scattering is from single diatoms, diatoms can only be used as back-surface diffraction grating when gently placed on a substrate.

The aluminum in the thin film cells can in addition to work as a reflector of light work as the rear contact of a solar cell, this means that by placing an diatom frustule between the contact and the cell would reduce the contact area and cause ohmic losses. To avoid ohmic losses some adaption of the frustules must be done.

The potential for the use of diatom frustules in solar cells are not dismissed completely, but to be able to have cheap, quick and efficient solar cell production the number of process steps have to be kept to a minimum. To include diatom frustules in solar cells have large challenges which have to be overcome. If the frustules are to be utilised in dry solar cells it is probably indirectly as use as templates for further production of intricate structures. So far the only kind of cells where diatom frustules have been used with success is dye-sensitised solar cells where the titanium dioxide electrode have been substituted with diatom frustules.

In this part of the thesis there have been used two different deposition methods; namely EBE and PECVD. For both of these deposition methods require a vacuum chamber for processing a sample. Samples going into a vacuum chamber have to enter through a load-lock chamber, and the load-lock chamber has to be pumped to the same pressure as the process chamber before the sample can enter the processing chamber. This is a time consuming process, and increased time for processing means a higher cost.

For EBE there are other techniques like sputter coating which might be used instead. Sputter coating is a low pressure process where an argon plasma sputter metallic atoms from the target to the sample. The film quality would be poorer, but the process time would be shorter. The process temperature for sputter coating is lower as it is kinetic energy which makes the sputter effect, and not the temperature as in EBE.

The PECVD process have in the later years been partially replaced with the HDPCVD as a deposition technique used where there are large step heights in a substrate. HDPCVD is a process which requires many of the same properties of the process chamber and control as the PECVD. For a sample containing diatom frustules HDPCVD could be used as well as PECVD.

Both EBE and PECVD give very conformal films, and that is a feature which is important when the dimensions of a sample increase and a texturation coating of silicon nitride is applied. The colour of silicon nitride is very dependent

of the thickness of the coating, and the desired thickness is highly wanted.

For the characterisation techniques used. Both SEM and FIB require a conductive sample, for SEM this is rarely a problem. Either a conductive coating can be sputtered on top or a low acceleration voltage can be used, this way charge-up in the sample can be avoided and the resolution increased. For FIB it is not that easy. With FIB cutting of structures are often done, during cutting the current is higher than during regular imaging. If there is poor conductivity in the sample the charge-up would increase during cutting, causing the cutting beam to move over the sample surface. This would make it difficult to cut in the sample, and other methods would have to be used.

---

## 6. Conclusion

Templates has been a part of material science the last fifty years, but it is only with an increasing understanding of nanotechnology diatoms have been the focus of new templates. The first part of this thesis investigated how gold and diatom frustules interacted with regards of topography and prints of pore structures. The second part is testing of deposition of two different materials used for solar cells onto diatom frustules, while the last part were manufacturing and characterisation of structures similar to solar cells where diatom frustules have been incorporated directly into the structure.

### 6.1 Part I: Characterisation of Diatom Frustules and Their Pore Structure

- Cultivated diatoms and net plankton were investigated with regard to their pore structure. Their pore structure are very similar, but there were some differences. Cultivated diatoms lack the inner pore structure which is found in net plankton. The side walls of the pore structure in cultivated diatoms are too steep to act as reflective surfaces.
- In the net plankton the smallest pores are spread across the surface of the diatom, while the nanoscaled pores of the cultivated diatom are only present in the mesoscaled pores.
- The microsized pores of the two different samples is about the same size but placed differently. The microsized pores of the cultivated diatoms are placed at the outer surface, while the microsized pores of the net plankton are placed along the inner surface.
- The mesosized pores of the net plankton are spread evenly over the surface in pore clusters with a flower shaped symmetry.

## **6.2 Part II: Manufacturing and Characterisation of Gold for Use as Templates in Solar Cell Industry**

- In this part two successful experiments of templating were done. A thin gold film was deposited on a frustule and a small piece of the gold film was cut and lifted off the frustule and further investigated with FIB. For the second experiment the substrate and frustules were etched away, leaving a self supported gold film with good imprints of the diatom frustules.
- The gold film follow the inner structure of the cultivated diatom, even the mesosized pores are followed deeply.
- Removal of a piece of gold film give a good replication of the pore structure. The mesosized pores are replicated very well, while the nanosized is not replicated due to the lacking nanosized pores in the diatom frustule. Outside the mesosized pores the nanosized pores are replicated very well.
- The gold film should be thicker than 5  $\mu\text{m}$  to gain an optimal film, as diatoms loosened from the film during storage between the different processes.

## **6.3 Part III: Deposition and Characterisation of Amorphous Silicon and Silicon Nitride on diatom frustules**

- The thin films deposited on diatom frustules followed the frustules very well. A conformal film of both materials is confirmed.

## **6.4 Part IV: Manufacturing and Characterisation of Structures similar to Solar Cells**

- The two crystalline solar cell samples manufactured gave clear and different results. Silicon nitride should only be applied in a single layer. A double layer of silicon nitride will confer a yellow reflection, even when those two layers are split across a diatom frustule. A single layer of silicon nitride gives a blue coating, which is more optimal for the antireflective coating in the front of solar cells.
- The thin film samples clearly show that the diatom frustules are spreading the incident light. Diatom frustules give diffraction patterns in the thin film samples due to the curvature in the surface.

---

## 7. Future Work

As a main goal for further work has to be to incorporate the diatoms into thin film solar cells. To obtain good properties from the frustules a monolayer of frustules are necessary. To control both the cleaning process and the deposition of diatom frustules onto a substrate, further research is required. Incorporation of an insulating material in a solar cell could also be potential harmful to any solar cell characteristics, and that effect has not been investigated yet.

To be able to utilise the diatom frustules in solar cells, a dense monolayer must be made. There have been reports of how diatoms have been grown in self assembled monolayers, these must be kept stuck to the substrate at the same time as the diatoms are cleaned and processed for templating. In addition, a high density of diatoms must also be achieved to make a good antireflective coating or back-surface diffraction grating.

To be able to figure out which pore structures which have an effect and which do not, a more in-depth modeling and testing of the diffraction properties are needed. Just as the pore structure, the diatoms have to be tested in solar cell structures with efficiency measurements. A light spectrum analysis of the solar cell structures is also needed to see which wavelengths which are reflected and which are absorbed by the structure.

The cribellum of the diatom frustules were not replicated in this thesis. The reasons for this might be the aggressive cleaning the frustules were exposed to removed the cribellum. Cleaning methods which is less aggressive to the structure might be tested for the same purpose.

For the gold film templates, the film should be thicker. Any kind of metal plating or other deposition methods could be attempted to make thicker film on shorter time. A combination of EBE, sputter coating and metal plating could be used to gain films with high precision and also a thickness large enough to make the metal film sturdy enough to hold on to the frustules.

New solar cell structures should be made with frustules incorporated into them. Hopefully a monolayer of diatom frustules can be achieved by functionalising the frustules and the substrate, and then conduct efficiency measurements on them. Another issue which must be investigated is the contact placements on the frustules when they are placed on the back-surface electrode, as they might cause ohmic losses in the cell.



---

# Bibliography

- Armin G. Aberle. Surface passivation of crystalline silicon solar cells: A review. *Progress in Photovoltaics: Research and Applications*, 8(5):473–487, 2000.
- P.M. Ajayan and L.D. Marks. Quasimelting and phases of small particles. *Physical Review Letters*, 60(7):585–587, 1988.
- Michael W. Anderson, Stuart M. Holmes, Noreen Hanif, and Colin S. Cundy. Hierarchical pore structures through diatom zeolitization. *Angewandte Chemie*, 112(15):2819–2822, 2000.
- Jorge A. Ascencio, Mario Pérez, and Miguel José-Yacamán. A truncated icosahedral structure observed in gold nanoparticles. *Surface Sciences*, 447(1–3):73–80, 2000.
- Zhihao Bao, Michael R. Weatherspoon, Samuel Shian, Ye Cai, Phillip D. Graham, Shawn M. Allan, Gul Ahmad, Matthew B. Dickerson, Benjamin C. Church, Zhitao Kang, Harry W. Abernathy III, Christopher J. Summers, Meilin Liu, and Kenneth H. Sandhage. Chemical reduction of three-dimensional silica microassemblies into microporous silicon replicas. *Nature*, (446):172–175, 2007.
- J.-C. Bertolini and J.-L. Rousset. *Nanomaterials and Nanochemistry*, chapter 10 Reactivity of Metal Nanoparticles, pages 281–304. Springer, 2006.
- M. Brust, Y.-P. Liu, and T. O. Hutchinson. Templates for metal nanowire self-assembly. In E. Buzaneva and Peter Scharff, editors, *Frontiers of Multifunctional Nanosystems*, volume 57 of *NATO Science Series II. Mathematics, Physics and Chemistry*, 2002.
- Ph. Buffat and J.P. Borel. Size effect on the melting temperature of gold particles. *Physical Review A*, 13(6):2287–2298, June 1976.
- Sindre Bunkholt. Effect of small nickel and vanadium additions on microstructure and mechanical properties of al-mg-si alloys. Master’s thesis, Norwegian University of Science and Technology, 2010.
- Ye Cai and Kenneth H. Sandhage. Zn<sub>2</sub>SiO<sub>4</sub>-coated microparticles with biologically-controlled 3d shapes. *physica status solidi (a)*, 202(10):R105–R107, 2005.
-

- Ryan W. Drum and J. Trevor Hopkins. Diatom locomotion: An explanation. *Protoplasma*, 62(1):1–33, 1966.
- L. A. Edgar and J. D. Pickett-Heaps. The mechanism of diatom locomotion. i. an ultrastructural study of the motility apparatus. In *Proceedings of the Royal Society of London. Series B, Biological Sciences*, pages Vol. 218, No. 1212 (Jun. 22) 331–343. The Royal Society, 1983.
- T. Fuhrmann, S. Landwehr, M. El Rharbi-Kucki, and M. Sumper. Diatoms as living photonic crystals. *Applied Physics B*, 78(3–4):257–260, 2004.
- Jo Gjessing, Erik Stensrud Marstein, and Aasmund Sudbø. 2d back-side diffraction grating for improved light trapping in thin silicon solar cells. *Optics Express*, 18: 5481–5495, 2010.
- Eric P. Goodwin and James C. Wyant. *Field Guide to Interferometric Optical testing*. SPIE, 2006.
- Richard Gordon, Dusan Losic, Mary Ann Tiffany, Stephen S. Nagy, and Frithjof A.S. Sterrenburg. The glass menagerie: diatoms for novel applications in nanotechnology. *Trends in Biotechnology*, 27(2):116–127, 2008.
- Edward B. Graper. Evaporation characteristics of materials from an electron beam gun ii. *Journal of Vacuum Science & Technology A*, 5(4):2718–2723, 1987.
- M. A. Green. Crystalline silicon solar cells. e-book, 2004. [http://www.icpress.co.uk/etextbook/p139/p139\\_chap4.pdf](http://www.icpress.co.uk/etextbook/p139/p139_chap4.pdf).
- R. Van Hardeveld and F. Hartog. The statistics of surface atoms and surface sites on metal crystals. *Surface Science*, 15(2):189–230, 1969.
- M. Hildebrand, G. Holton, D.C. Joy, M.J. Doktycz, and D.P. Allison. Diverse and conserved nano- and mesoscale structures of diatom silica revealed by atomic force microscopy. *Journal of Microscopy*, 235(Pt 2):172–187, 2009.
- Jarle Hjelen. *Scanning elektron-mikroskopi*. Norges Tekniske Høyskole, 1989.
- S. M. Holmes, B. E. Graniel-Garcia, P. Foran, P. Hill, E. P. L. Roberts, B. H. Sakakini, and J. M. Newton. A novel porous carbon based on diatomaceous earth. *Chemical Communications*, (25):2662–2664, 2006.
- Sumio Iijima and Toshinari Ichihashi. Structural instability of ultrafine particles of metals. *Physical Review Letters*, 56(6):616–619, 1986.
- Nils Kröger and Nicole Poulsen. Diatoms—from cell wall biogenesis to nanotechnology. *Annual Review of Genesis*, (42):83–107, 2008.
- M. Lipinski, P. Panek, S. Kluska, P. Zieba, A. Szyszka, and B. Paszkiewicz. Defect passivation of multicrystalline silicon solar cells by silicon nitride coatings. *Materials Science-Poland*, 24(4):1003–1007, 2006.

- Dusan Losic, James G. Mitchell, and Nicolas H. Voelcker. Complex gold nanostructures derived by templating from diatom frustules. *Chemical Communications*, (39):4908–4910, 2005.
- Dusan Losic, James G. Mitchell, and Nicolas H. Voelcker. Fabrication of gold nanostructures by templating from porous diatom frustules. *New Journal of Chemistry*, 30(6):4908–4910, 2006a.
- Dusan Losic, Gerry Triani, Peter J. Evans, Armand Atanacio, James G. Mitchell, and Nicolas H. Voelcker. Controlled pore structure modification of diatoms by atomic layer deposition of TiO<sub>2</sub>. *Journal of Materials Chemistry*, 16(41):4029–4034, 2006b.
- Dusan Losic, James G. Mitchell, and Nicolas H. Voelcker. Diatomaceous lessons in nanotechnology and advanced materials. *Advanced Materials*, 21(29):2947–2958, 2009.
- L.Ratke and Peter W. Voorhees. *Growth and coarsening: Ostwald ripening in material processing*. Springer, 2002.
- E. Lugschreider, C. Barimani, C. Wolff, S. Guerreiro, and G. Doepper. Comparison of the structure of pvd-thin films deposited with different deposition energies. *Surface and Coatings Technology*, 86–87:177–183, 1996.
- D. H. MacDonald, A. Cuevas, M.J. Kerr, C. Samundsett, D. Ruby amd S. Winderbaum, and A. Leo. Texturing indutrial multicrystalline silicon solar cells. *Solar Energy*, 76(1–3):277–283, 2003.
- M. Meyyappan, Lance Delzeit, Alan Cassell, and David Hash. Carbon nanotube growth by pecvd: a review. *Plasma Sources Science and Technology*, 12:205–216, 2003.
- Allen J. Milligan and François M. M. Morel. A proton buffering role for silica in diatoms. *Science*, 297(5588):1848–1850, 2002.
- Petter Ottesen. Processing and characterisation of diatoms for use as light harvesting materials in solar cells. Specialisation project, Norwegian University of Science and Technology, 2010.
- Petter Ottesen, Anne Kirsti Noren, Gabriella Tranell, Arne Røyset, Ingeborg Kaus, and Mari Juel. Processing and characterisation of diatoms for enhanced efficiency in solar cells. In *Photovoltaic Technical Conference*, 2011.
- Janice L. Pappas. Geometry and topology of diatom shape and surface morphogenesis for use in applications of nanotechnology. *Journal of Nanoscience and Nanotechnology*, 5(1):120–130, 2005.
- Song Peike, Zeng Xiangbin, Wang Huijuan, and Zhang Rui. Research of the amorphous silicon layers in hit solar cells. In *Proceedings of ISES World Congress 2007*, volume 4, pages 1206–1209, 2009.

- Olga Leticia Pérez, David Romeu, and Miguel José Yacamán. Distribution of surface sites on small metallic particles. *Application of Surface Science*, 13(3–4): 402–413, 1982.
- Michael Quirk and Julian Serda. *Semiconductor Manufacturing Technology*. Pearson Education International, 2001.
- F. Roca, G. Sinno, G. Di Francia, P. Prosini, G. Fameli, P. Grillo, A. Citarella, F. Pascarella, and D. della Sala. Process development of amorphous silicon/crystalline silicon solar cells. *Solar Energy Materials and Solar Cells*, 48: 15–24, 1997.
- K.H. Sandhage, M.B. Dickerson, P.M. Huseman, M.A. Caranna, J.D. Clifton, T.A. Bull, T.J. Heibel, W.R. Overton, and M.E.A. Schoenwaelder. Novel, bioclastic route to self-assembled, 3d, chemically tailored meso/nanostructures: Shape-preserving reactive conversion of biosilica (diatom) microshells. *Advanced Materials*, 14(6):429–433, 2002.
- C. Solliard. Debye-waller factor and melting temperature in small gold particles: Related size effects. *Solid State Communications*, 51(12):947–949, 1984.
- L. De Stefano, A. Lamberti, L. Rotiroti, and M. De Stefano. Interfacing the nanostructured biosilica microshells of the marine diatom *Coscinodiscus wailesii* with biological matter. *Acta Biomaterialia*, (4):126–130, 2008.
- Raymond R. Unocic, Frank M. Zalar, Peter M. Sarosi, Ye Cai, and Kenneth H. Sandhage. Anatase assemblies from algae: coupling biological self-assembly of 3-d nanoparticle structures with synthetic reaction chemistry. *Chemical Communications*, (7):796–797, 2004.
- C. A. Volkert and A. M. Minor. Focused ion beam microscopy and micromachining. *MRS Bulletin*, 32:389–395, 2007.
- Yajun Wang, Yi Tang, Angang Dong, Xingdong Wang, Nan Ren, and Zi Gao. Zeolitization of diatomite to prepare hierarchical porous zeolite materials through a vapor-phase transport process. *Journal of Materials Chemistry*, 12(6):1812–1818, 2002.
- Anthony R. West. *Basic Solid State Chemistry*. John Wiley & Sons, LTD, 1999.
- Aud Wærnes, Ola Raanes, Eivind Øvrelid, Bart Geerligs, Paul Wyers, Sven Santen, and Benno Wiersma. New feedstock materials. In *Freiberg Solartage*. ECN Solar Energy, 2005.
- Yang Yu, Jonas Addai-Mensah, and Dusan Losic. Synthesis of self-supporting gold microstructures with three-dimensional morphologies by direct replication of diatom templates. *Langmuir*, Submitted:–, 2010.
- N. Yuge, M. Abe, K. Hanazawa, H. Baba, N. Nakamura, Y. Kato, Y. Sakaguchi, S. Hiwasa, and F. Aratani. Purification of metallurgical-grade silicon up to solar grade. *Progress in Photovoltaics: Research and Applications*, 9(3):203–209, 2001.